BNWL-1379
UC-80

[redacted]

EXPERIMENTAL AND CALCULATED RESULTS FOR UO_2 AND UO_2-PuO_2 FUELED H_2O-MODERATED LOADINGS

August 1970

[redacted]

AEC RESEARCH & DEVELOPMENT REPORT

BNWL-1379

BATTELLE NORTHWEST
BATTELLE MEMORIAL INSTITUTE PACIFIC NORTHWEST LABORATORIES
3000 STEVENS DRIVE, P. O. BOX 999, RICHLAND, WASHINGTON 99352

LEGAL NOTICE

PACIFIC NORTHWEST LABORATORY
RICHLAND, WASHINGTON
operated by
BATTELLE MEMORIAL INSTITUTE
for the
UNITED STATES ATOMIC ENERGY COMMISSION UNDER CONTRACT AT(45-1)-1830

AEC-RL RICHLAND, WASH

BNWL-1379
UC-80, Reactor
Technology

EXPERIMENTAL AND CALCULATED RESULTS FOR UO_2 AND UO_2-PuO_2 FUELED H_2O-MODERATED LOADINGS

P. Loizzo,* R. Martinelli,* N. Pacilio,*

L. D. Williams

Reactor Physics Department
Physics and Engineering Division

J. B. Edgar

Nuclear Safety Department
Safety and Standards Division

August 1970

BATTELLE MEMORIAL INSTITUTE
PACIFIC NORTHWEST LABORATORIES
RICHLAND, WASHINGTON 99352

---

* *On assignment from Italian Comitato Nazionale Per L'Energia Nucleare (CNEN), Rome, Italy.*

Printed in the United States of America
Available from
Clearinghouse for Federal Scientific and Technical Information
National Bureau of Standards, U.S. Department of Commerce
Springfield, Virginia 22151
Price: Printed Copy $3.00; Microfiche $0.65

EXPERIMENTAL AND CALCULATED RESULTS FOR UO_2 AND UO_2-PuO_2 FUELED H_2O-MODERATED LOADINGS

P. Loizzo, R. Martinelli, N. Pacilio,
L. D. Williams, J. B. Edgar

ABSTRACT

This report contains data collected during a series of experiments in the Plutonium Recycle Critical Facility (PRCF) using plutonium and uranium enriched fuel. The experiments were designed to provide a base for assessing the accuracy of calculational techniques used for designing plutonium enriched cores in Boiling Water Reactors with regard to predicting core reactivities, power distributions, and control system worths. Reactivity and power distribution measurements were made in both single region and multiregion loadings. Calorimetric techniques were used to intercalibrate the different fuel types for the multiregion loadings. The reactivity effect of various control blade materials was determined as a function of the prompt neutron decay rate (Rossi-Alpha). Theory-experimental comparisons are based primarily on CNEN developed theoretical models.

TABLE OF CONTENTS

LIST OF FIGURES

LIST OF TABLES

EXPERIMENTAL AND CALCULATED RESULTS FOR UO_2 AND UO_2-PuO_2 FUELED H_2O-MODERATED LOADINGS

P. Loizzo, R. Martinelli, N. Pacilio,
L. D. Williams, J. B. Edgar

INTRODUCTION

A cooperative program between USAEC and Italian Comitato Nazionale Per L'Energia Nucleare (CNEN) was conducted at Argonne National Laboratory (ANL) and at Pacific Northwest Laboratory (PNL) under the auspices of the Plutonium Utilization Program. The purpose of this program was to obtain experimental information on the neutronic characteristics of plutonium fuel in prototypical boiling water reactor (BWR) systems. The program consisted of two separate but related areas of effort. One was to obtain information on the neutronic characteristics of fuels irradiated in the Experimental Boiling Water Reactor (EBWR) at ANL during the joint ANL-PNL plutonium demonstration experiment.[1-3] The results of these studies are reported elsewhere.[4-9] The other area of effort which is the essence of this report was to conduct critical experiments at Pacific Northwest Laboratory (PNL) in the Plutonium Recycle Critical Facility (PRCF) to obtain information on the neutronic characteristics of plutonium and uranium enriched fuels in various prototypical BWR loading schemes. These data provide a base for assessing the accuracy of calculational techniques used in reactor design in regard to predicting core reactivities, power distributions, and control system worth.

The physical arrangement of fuel and control rods coupled with coolant voiding in a BWR lead to problems in predicting power distributions and control system worths. In this regard, the two main neutronic parameters investigated were the determination of local power peaking factors and the worth of reactor control systems. The calculation of

reactivity changes due to coolant voiding is also important; this parameter was measured in both the plutonium and uranium enriched systems.

The experiments described by this report were designed in such a way as to acquire solutions of how best to describe mathematical models for the BWR. During the investigation of the mathematical models, the following questions were asked:

- Is a simple cell calculation adequate, or is it necessary to allow for the interaction of surrounding cells?
- What kind of energy group structure should be used in the calculation? What is the effect of the spectral variations from element to water gap to a different element?
- Are diffusion calculations fully adequate for these conditions?
- What kind of model is to be used for a fuel element to obtain the radial power shape within the fuel bundle when large water gaps surround it and a different type of fuel is coupled with the one being investigated?
- What model should be used to calculate the transparency of control rods to neutrons of different energies? Is the model adequate for both uranium and plutonium systems?

Answers to these questions require experimental information of the types reported here.

SUMMARY

The general experimental program was as follows:

- Single region UO_2 and UO_2-PuO_2 uniform lattice criticals and power distribution measurements in varying degrees of loading nonuniformity; i.e., water holes, water slabs, water crosses, etc.
- Multiregion criticals and power distribution measurements with typical fuel element arrangements surrounded by UO_2 and UO_2-PuO_2 driver regions.
- Control blade measurements using a variety of absorbing materials in single region UO_2 and UO_2-PuO_2 loadings.

The following items were emphasized during the experiments:

- Power distributions in single and multiregion loadings. (Five different types of fuels were investigated.)
- Control rod deformation of power shapes in UO_2 and UO_2-PuO_2 loadings.
- Direct correlation between prompt neutron decay rate (Rossi alpha) and control rod worth.

Power distributions were deduced from fission product gross gamma activity; different fuel types were intercalibrated by calorimetric measurements. Rossi alpha measurements were made in critical and subcritical loadings using the endogenous pulsed source method.[10,11] The calculations are based primarily on CNEN developed theoretical models.[12-15] The reliability of the various models and the validity of the approximations were checked by comparison with experiments and with other more sophisticated calculational schemes.

The theory-experiment comparisons demonstrated that the CNEN models can predict local power peaking within 1 to 2%. Development of the theoretical aspects of the Rossi alpha method

revealed a method of calculating this parameter as an eigenvalue of the diffusion equations thereby permitting a direct comparison between alpha measurements and calculations.

DESCRIPTION OF FACILITY

The Plutonium Recycle Critical Facility (PRCF) is an H_2O-moderated, low power reactor designed for the purpose of making critical measurements with various types of plutonium and uranium fuels. The reactor is contained in a right cylindrical tank 9 ft. high by 6 ft. in diameter. Since the fuel for this experiment was in the form of rods of different diameters and lengths, two aluminum templates and an aluminum support plate were used to position and support the fuel at the upper and lower ends. The larger diameter, shorter fuel rods were both positioned and supported by the two templates, while the smaller diameter, longer rods, equipped with spacers to center them in the upper template, were supported by the plate below the lower template. See Figure 1 for an elevation view of the reactor.

The fuel rods were positioned on a 0.75 in. square lattice pitch. Cruciform slots enclose a central nine by nine (9 x 9) hole zone. The slots allowed for installation of typical BWR cruciform (cross-shaped) control blades. Additional holes between lattice positions in the central zone were provided for aluminum thimbles used in the void experiments. Oversized holes were also included at specific points in the lattice to accomodate thermally insulated fuel rods during calorimetric measurements. The lattice template details are shown in Figure 2.

Shutdown and control of the reactor was maintained by two control rods and four reflector sheets. Each control rod consisted of a cluster of four Zircaloy-2 clad cadmium cylinders with interchangeable fuel elements (followers) attached to the bottom. The fuel followers were matched to the type of fuel in the reactor. Each of the rods in a control cluster occupied a lattice position as shown in Figure 2. The reflector sheets were each 8 1/4 in. wide and 1/4 in. thick made entirely of Lexan except for the encased cadmium (7.5 x 36 x 0.030 in.).

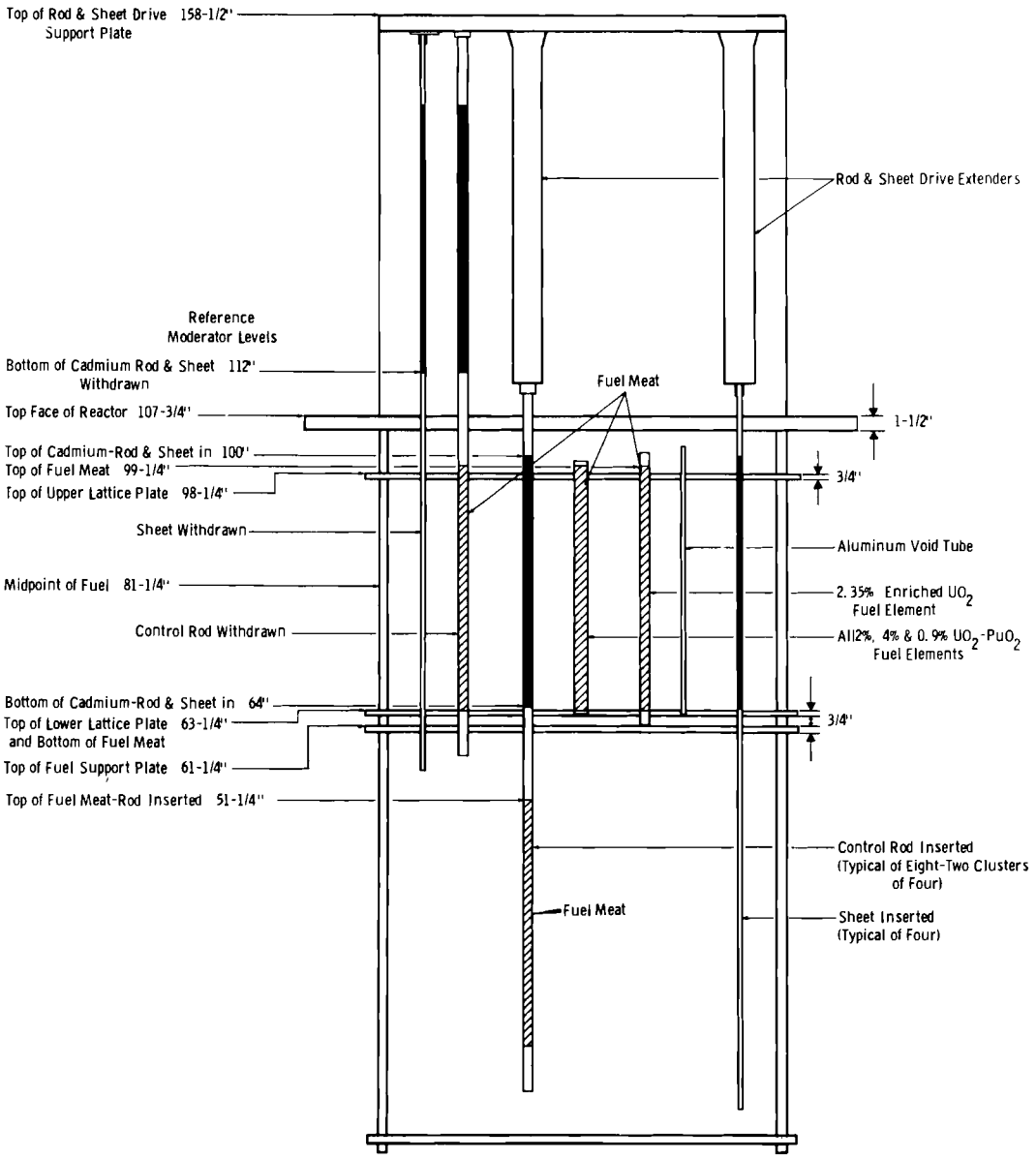

FIGURE 1. ELEVATION DRAWING

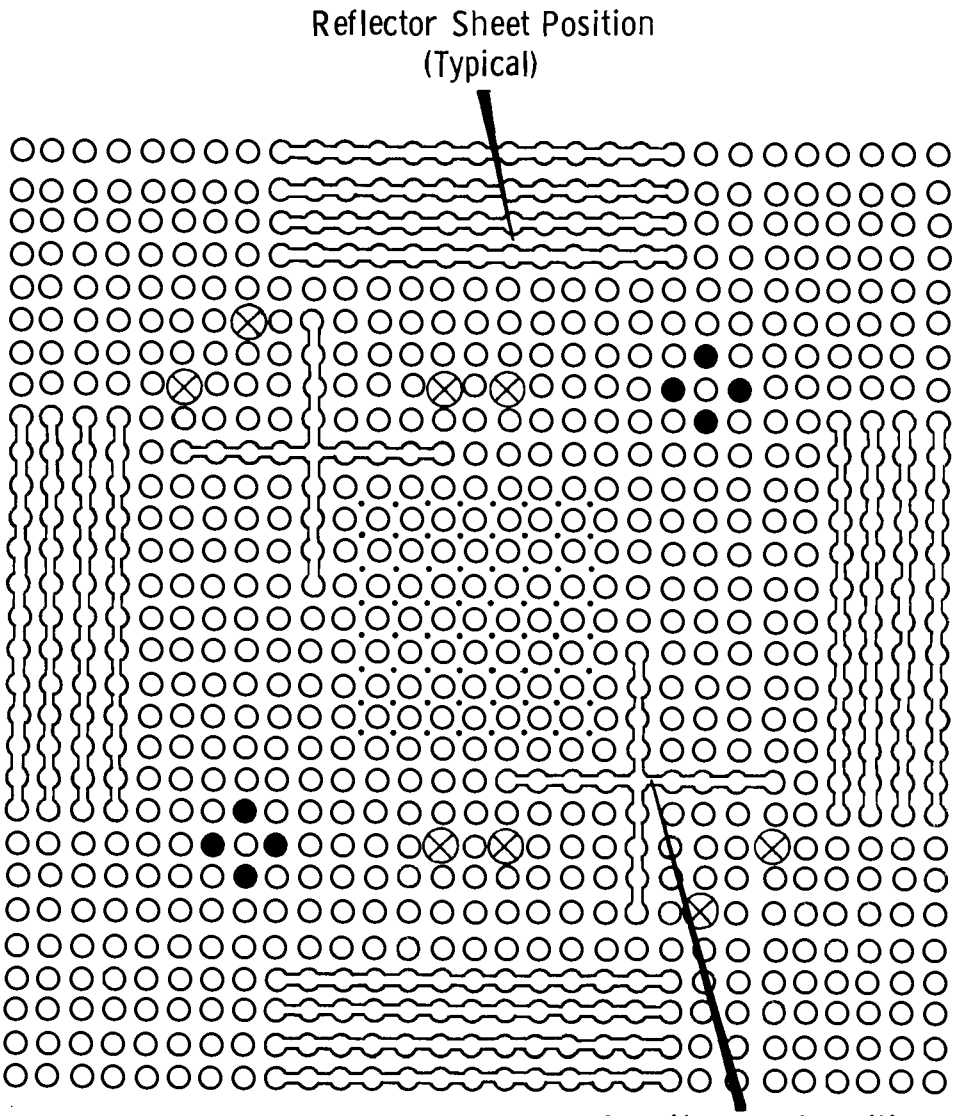

FIGURE 2. LATTICE TEMPLATE

There were four sheet slots at the middle of each side of the template so that the sheet position could be changed depending upon the size of the fuel loading. The elevation of the control devices relative to the fuel can be seen in Figure 1.

Core reactivity was also adjusted by moderator height. The liquid level was remotely adjusted by means of a weir which has a range from 3 in. below the bottom of the fuel meat to 7 in. above the top of the fuel meat. The weir has a measured reproducibility of ± 0.01 in. Water was continually pumped over the weir maintaining a constant moderator level in the reactor tank during the experimental measurements. The reactor tank and a simplified view of the moderator system are shown in Figure 3.

A typical plutonium fueled loading is shown in Figure 4. The control devices are shown in their least reactive positions. Figure 5 illustrates a typical uranium loading with the cruciform control blade installed.

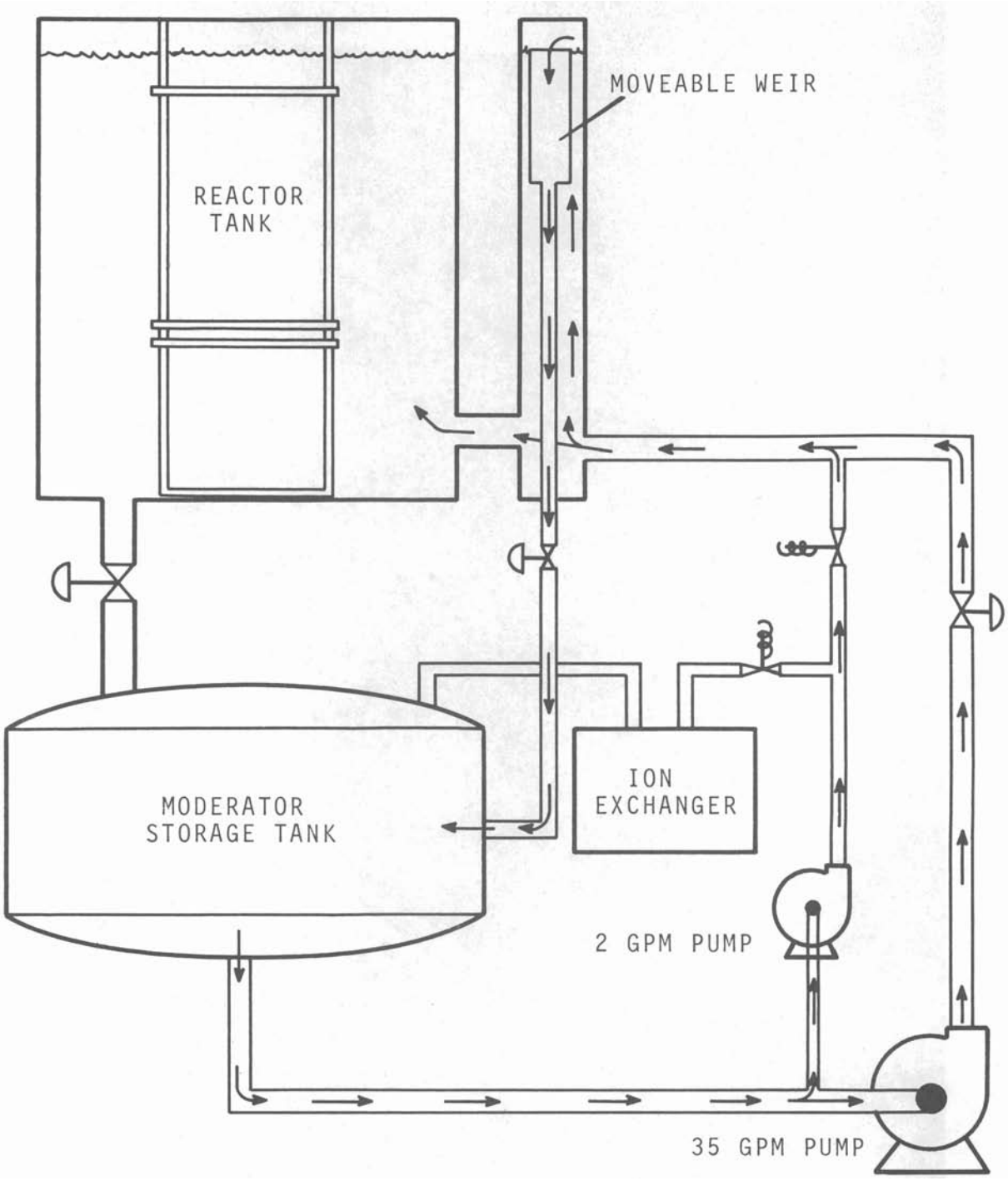

FIGURE 3. SIMPLIFIED MODERATOR SYSTEM

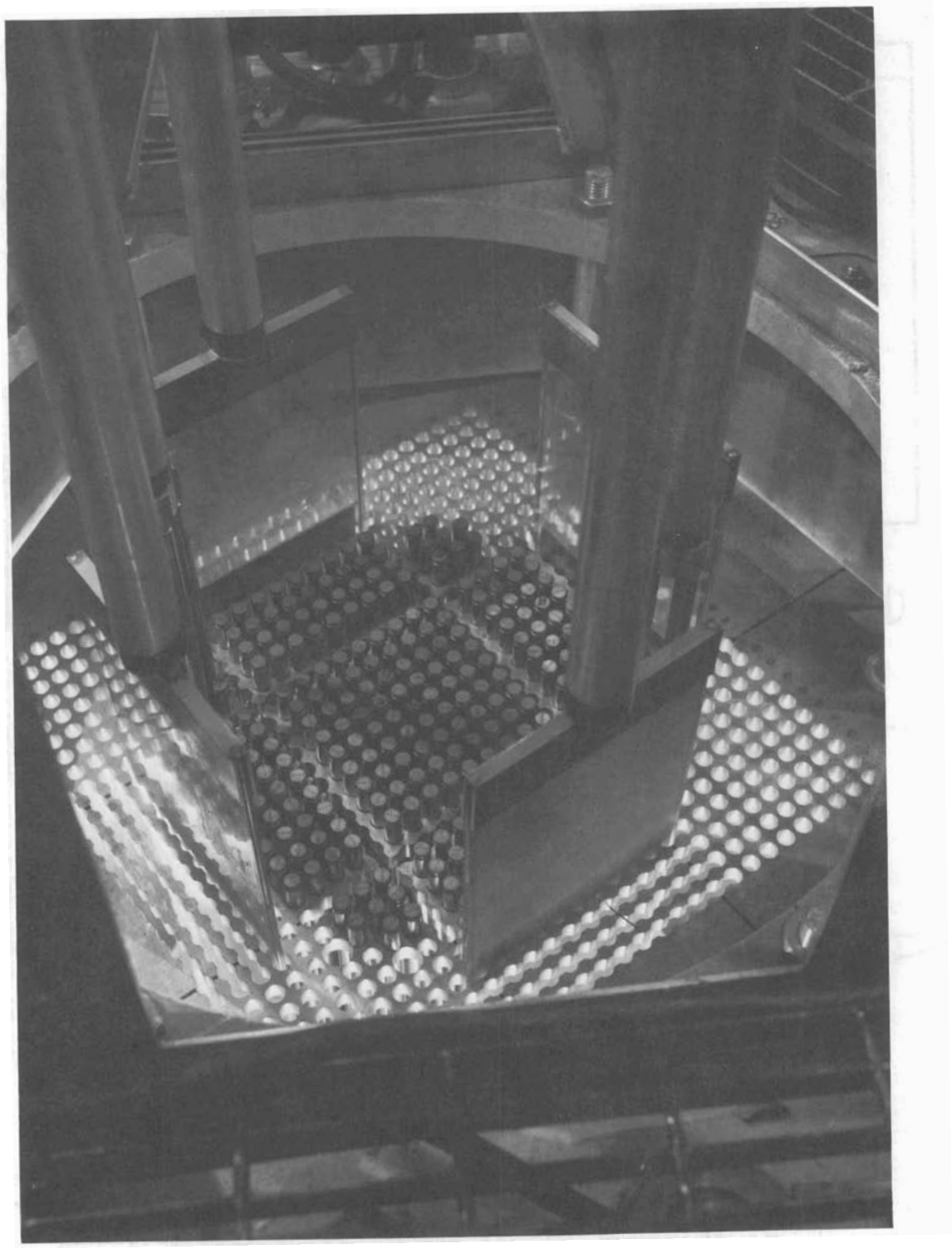

FIGURE 4. TYPICAL UO_2-2 WT% PuO_2 LOADING

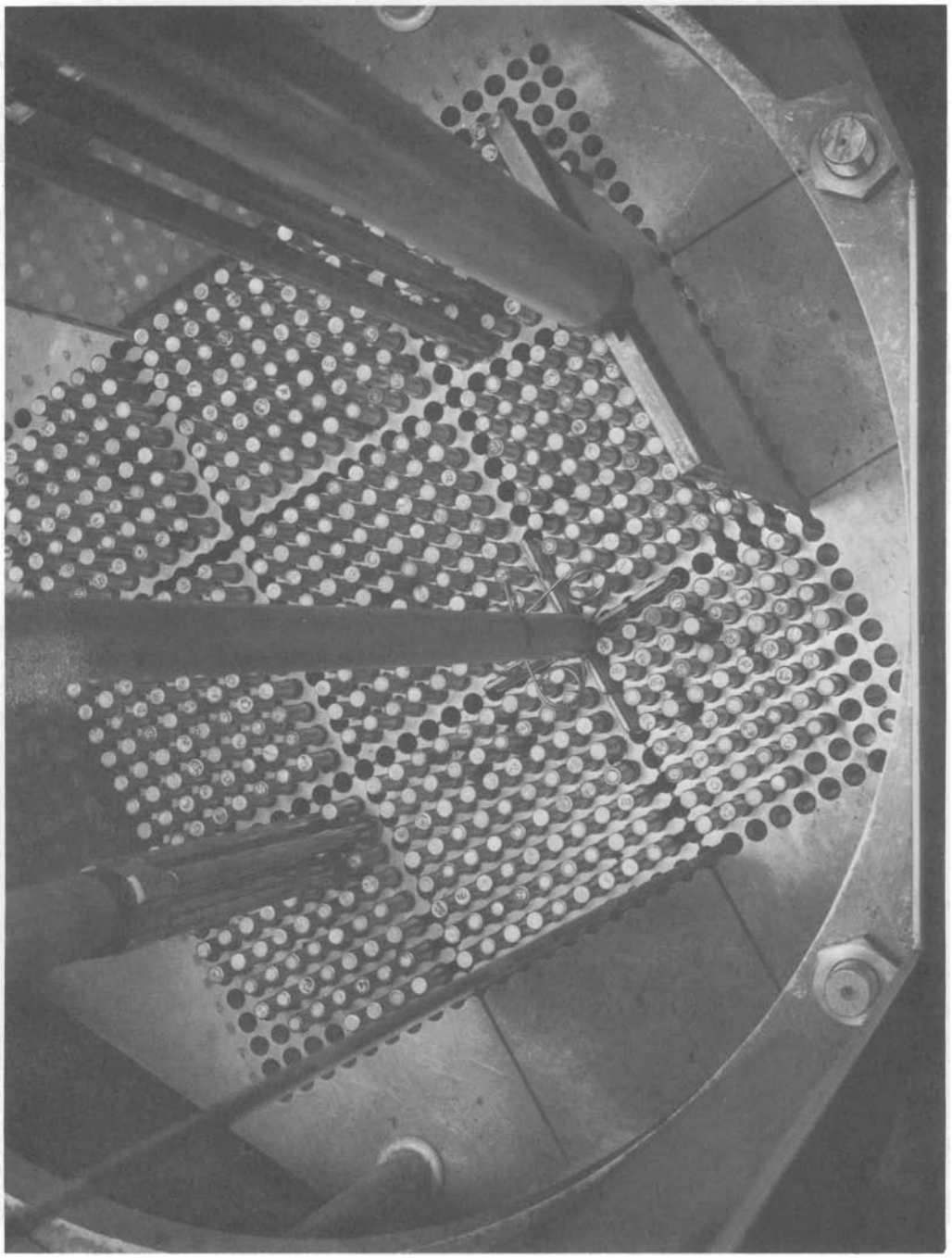

FIGURE 5. TYPICAL UO_2-2.35% ^{235}U WITH TEST CRUCIFORM BLADE

CRITICAL EXPERIMENTS

The measurements made during the critical experiments were aimed specifically at reactivity determinations and power distributions for single and multiregion loadings. The loadings investigated were directed toward determining the effect of water gaps, voids, control blade materials, and various types of fuels on reactivity and power shapes.

The critical experiments were divided into four parts: single and multiregion loadings using 2.35 wt% UO_2 and UO_2-2 wt% PuO_2 (8% ^{240}Pu) fuel rods. Three other types of fuel were used during the multiregion measurements; UO_2-4 wt% PuO_2, UO_2-0.9 wt% PuO_2, and UO_2-2 wt% PuO_2 (24% ^{240}Pu). The specifications for these fuels can be found in Appendix A.

Voids were produced in the central element zone by using aluminum (6061-T6) thimbles extending over the full length of the core. A total of 64 thimbles (5/16 in. OD x 0.020 in. wall) were placed in the holes shown in the lattice template in Figure 2 to simulate an approximate 25% moderator void in the central element. The axial position of the thimbles is illustrated in Figure 1.

REACTIVITY MEASUREMENTS

The excess reactivity of the investigated loading was determined by measurement of the critical moderator level with the reactor control system in the most reactive position. The worth of the moderator level from the critical height to an infinite top reflector was the excess reactivity for the loadings.

The moderator level worth was calibrated differentially using positive period measurements from an infinite top reflector to below the top of the fuel meat. The calibration curve is shown in Figure A-1.

The followers on the reflector sheets complicated clean reactivity measurements. The presence of the followers, in all

cases, increased the core reactivity. This effect was measured for the regular* UO_2-2 wt% PuO_2 fuel loading and the basic** 9 x 9 UO_2 loading. From these measurements, the effect on the other loadings was inferred.

POWER DISTRIBUTION MEASUREMENTS

Selected fuel rods were removed from each loading following reactor operation and gamma counted at their axial mid-plane. This gamma activity reflected the relative fuel rod power in the single region loadings and was related to rod power in multiregion loadings by application of gamma to power conversion ratios for the various fuel types. The gamma activity measured from each rod was automatically corrected for fission product decay by using a dual system preset count technique. The system employed two matched counting systems--one measured the rods of interest (called the traverse system), and another provided a means of correcting the measurements for radioactive decay during counting (called the decay system). A fuel rod of similar exposure history to those being measured was placed in the decay system at the start of the measurement and left there for the duration of the measurements. The decay system was electronically arranged to stop the traverse system after a preset number of count has been obtained from the decay rod, thereby correcting for decay. Both systems were matched according to gain and energy discrimination. An integral counting method was used; only gammas with energies greater than 0.5 MeV were counted.

The fuel rods were rotated about their longitudinal axis in the traverse system during the counting periods in order to average the circumferential fuel rod activity. The decay rod

---

* *Regular loading - a uniform loading.*

** *Basic loading - a fuel loading where columns of fuel rods were removed to isolate a central fuel rod array by water slabs (7 × 7 and 9 × 9 fuel rod arrays were studied in this program.)*

was not rotated. Figure 6 shows the traverse system with a UO_2 fuel rod in counting position. A variable speed electric drill, mounted to a movable arm, was used for rotating the fuel rods.

Items which had to be taken into consideration during counting were electronic drift, variation in the backgrounds of the two systems, counting dead time, and the difference in fuel rod irradiation histories. Dissimilar gain drift between systems was the primary problem. The setting of the energy cutoff on the single channel analyzer was not felt to be a problem. The baseline was set on the ^{22}Na 0.511 MeV positron annihilation peak using a coincidence circuit in conjunction with a multichannel analyzer. The system electronic drift was observed and corrected for by using one rod as a drift monitor; counting it periodically in the traverse system throughout the gamma measurements. In most cases, the irradiation time of the fuel and the decay time before counting were adjusted to avoid excessive counting rates where dead time corrections would need to be applied. However, where applicable, corrections were made using an experimentally measured dead time.

Corrections were also made for differences in the background activity of the fuel rods used in the measurements. In most cases, the background contribution was insignificant compared to that from the irradiation. However, to minimize this effect, rods with similar irradiation histories were selected for the measurement. For very long counting periods (up to 5 hr), the counting rates from the fuel rods sometimes dropped below 500 counts/sec. When this occurred, the difference in the backgrounds of the two systems became significant. Normal background counting rates in the traverse-system was 1 to 2 counts/sec compared to 6 to 10 counts/sec in the decay system. Corrections were applied to the data when appropriate.

As previously mentioned, in multiregion loading, the gamma activity for different types of fuel was converted to relative

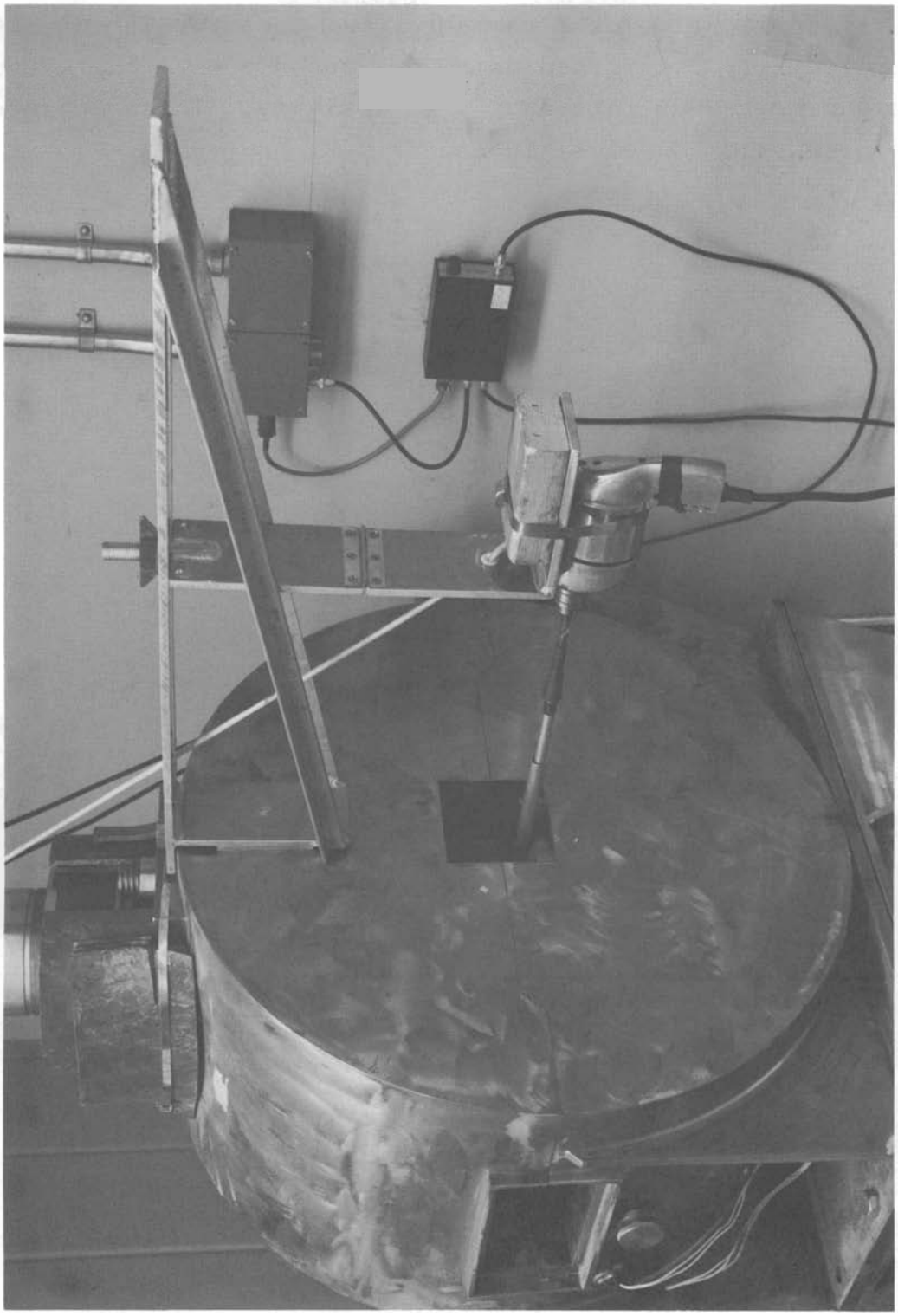

FIGURE 6. TRAVERSE GAMMA COUNTING SYSTEM

rod power by application of a gamma to power factor. These factors were experimentally determined using two techniques: the measurement of cladding heatup rate and ^{140}La activity. These measurements are discussed in detail in Appendix C.

CONTROL BLADE WORTH MEASUREMENTS

Measurements of the worth of different materials loaded in a test cruciform blade were made in UO_2-235% ^{235}U (Configuations A, B and C) and in UO_2-2 wt% PuO_2 (8% ^{240}Pu) (Configurations D, E, and F) cores. Details of these configurations are given in Figures 7 through 10, respectively. A total of ten loadings containing the test cruciform blade were investigated, covering a wide range of materials (boral, boron-carbide, hafnium metal and oxide, rare-earth-pyrohafnate), thicknesses and shapes (cylindrical and flat tubes).

Rod-worths were obtained by critical experiment and by measurement of the decay of the prompt-neutron-density following a spontaneous burst of fissions. A detailed discussion of the theory of these measurements is given in Appendix E, together with descriptions of the test blade and materials, and a description of the electronic system used to measure the decay of the prompt neutron bursts.

Typically in critical experiments, the focal point is the correlation between measurements and calculations. The procedure is normally as follows:

- A clean core is first loaded to critical. The nuclear constants in a calculation of that core are adjusted in order to give k = 1.
- After a control rod has been placed in the reactor, a new critical loading is reached by increasing the number of fuel elements. The nuclear constants of the former case are used in a calculation of the new core and only control rod constants are adjusted in order to obtain the desired k = 1.

Although reliable, accurate, and widely used, this type of reactivity determination may suffer from serious systematic errors in the basic terms of the balance (Production = Absorption + Leakage) equation, which cancel each other in the summation

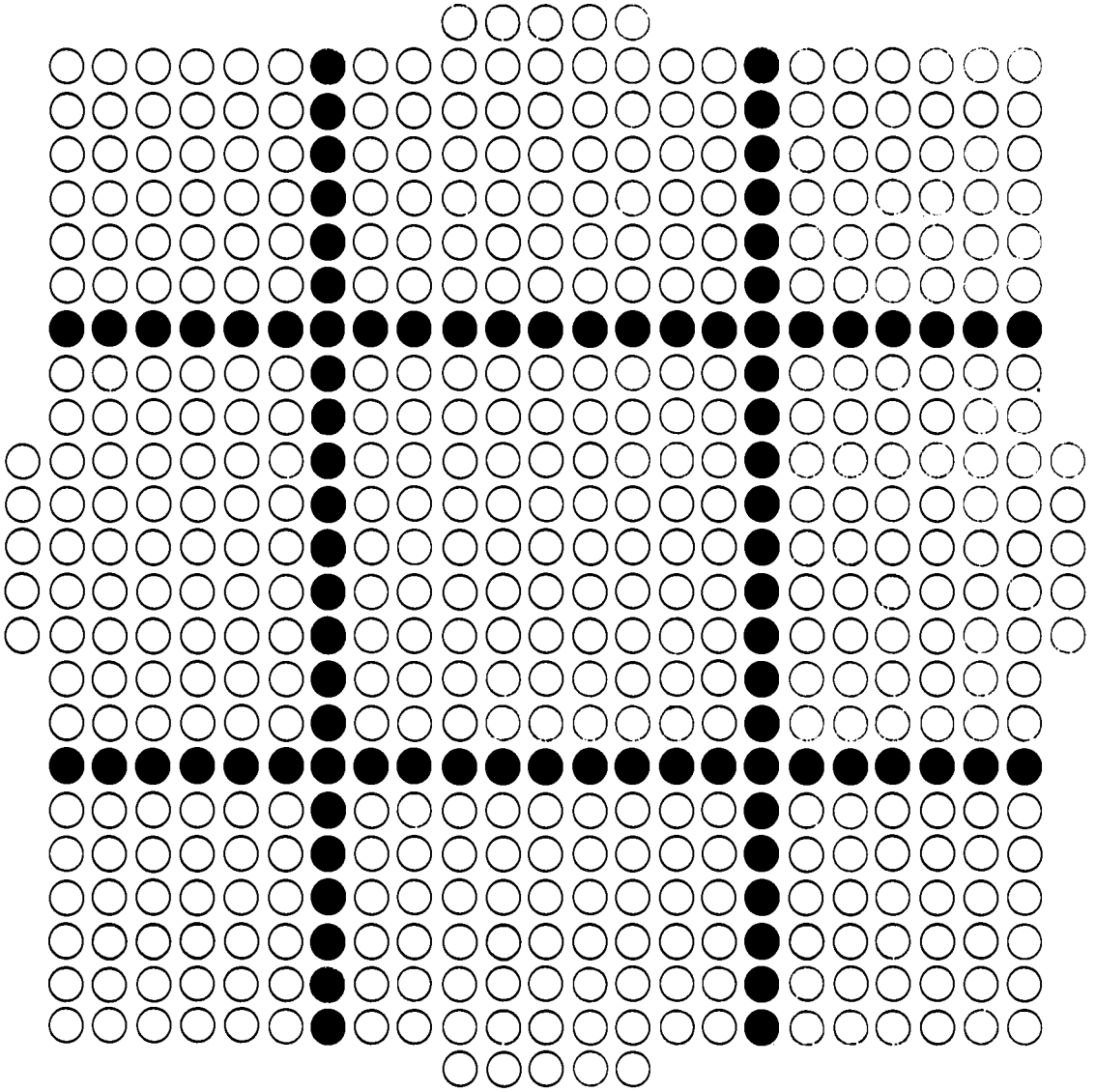

Configuration A

Basic 9x9, UO_2 - 2.35% ^{235}U

461 Elements

Moderator Level 94.68"

FIGURE 7

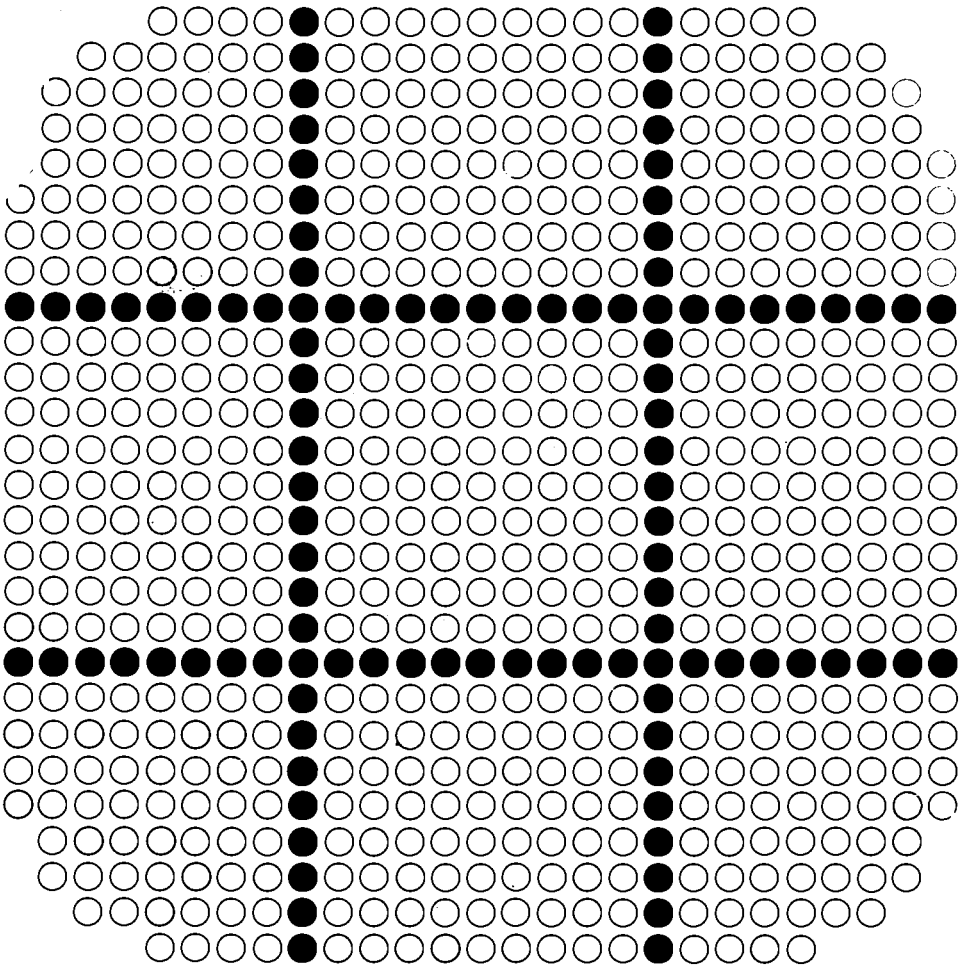

Configuration B and C

Basic 9x9, UO_2 - 2.35% ^{235}U

593 Elements

Moderator Level 94.81" and 95.66"

FIGURE 8

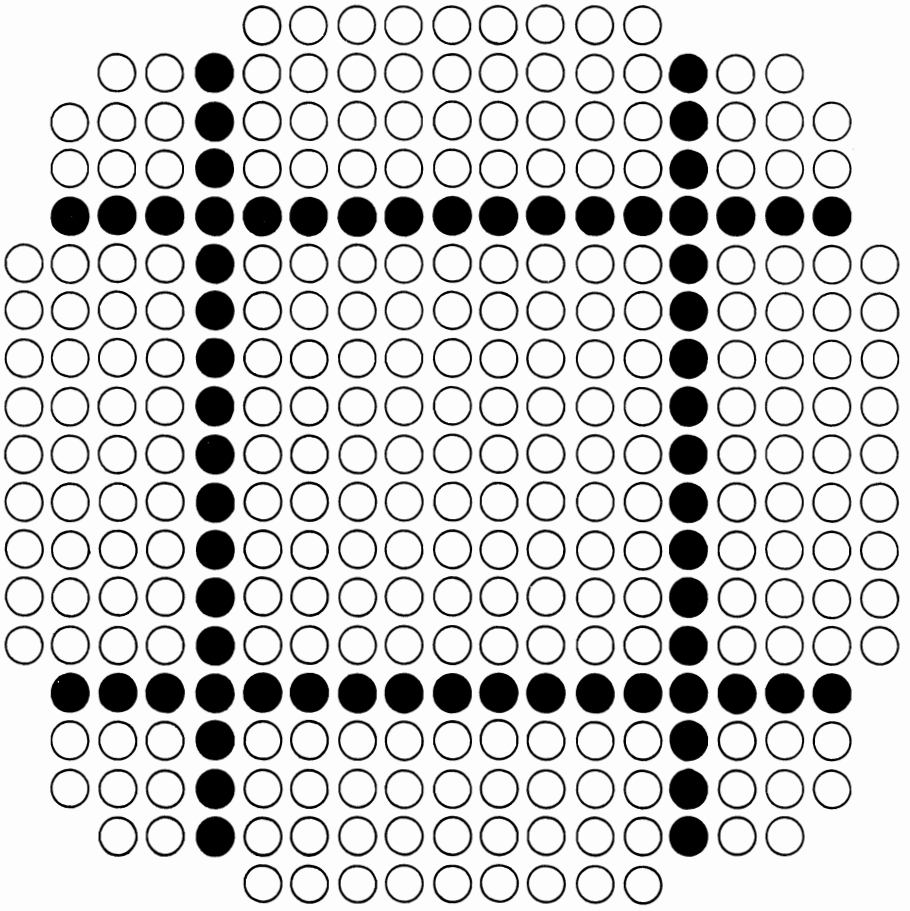

Configuration D

Basic 9x9, UO_2 - 2 wt% PuO_2 (8% ^{240}Pu)

257 Elements

Moderator Level 95.00"

FIGURE 9

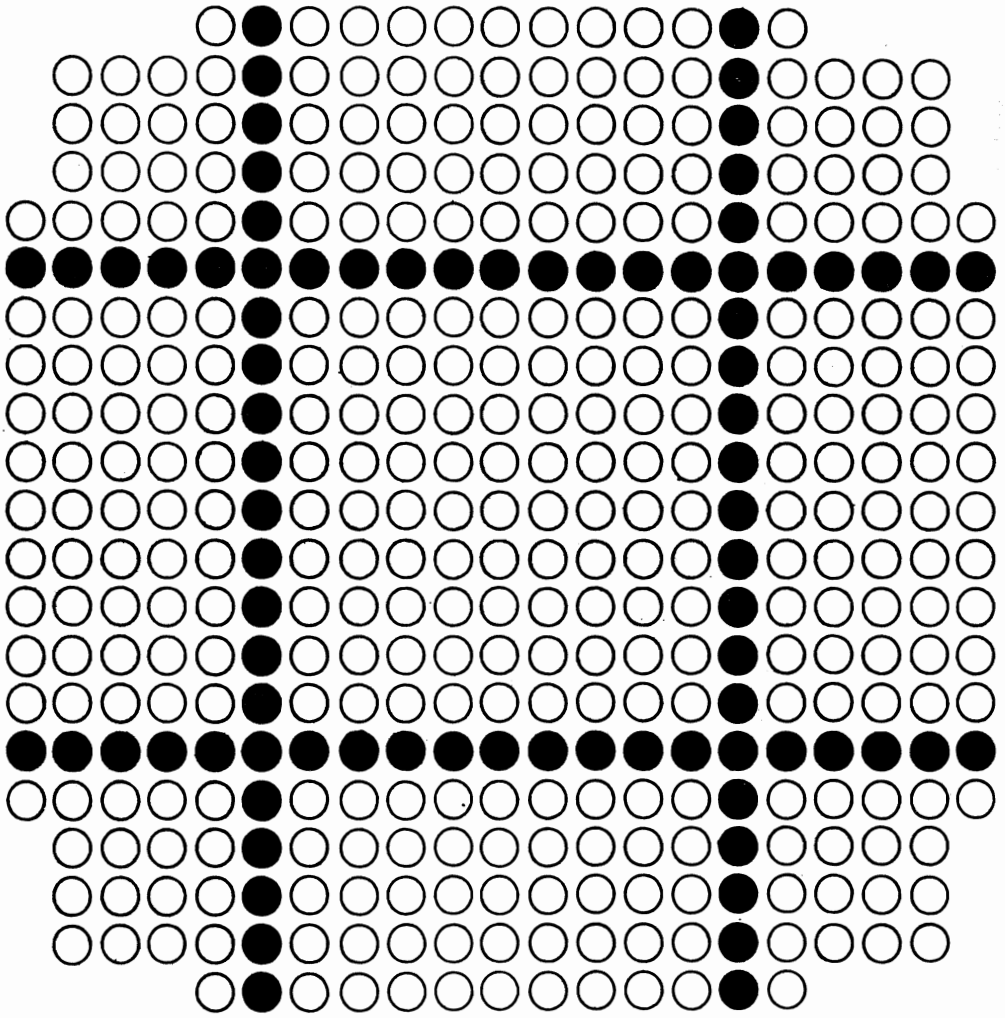

Configuration E and F

Basic 9x9, UO_2 - 2 wt% PuO_2 (8% ^{240}Pu)

333 Elements

Moderator Level 94.78" and 95.31"

FIGURE 10

and do not affect the equality k = 1. This way one may be led to strongly erroneous rod constants and there is no practical way to avoid such a circumstance unless one is no longer tied only to critical measurements, viz. to the same leakage to absorption ratio.

The measuring of the prompt neutron density decay constant, α, offers an alternative to the above mentioned situation and leads to a control rod-worth determination of the following kind:

- A clean core is made critical (or subcritical). The value of α is measured and compared to the one calculated via code: nuclear constants are adjusted in order to obtain the desired coincidence in terms of α;
- A control rod is placed in the reactor and the value of α is measured for the subcritical system. The comparison between calculated and measured values of α allows rod-constants in the calculation to be adjusted in order to obtain a successful matching.

The measurement of α is equivalent to a reactivity determination, although α may not be directly convertible in reactivity units. This way one never introduces reactivity and actually adopts α as a rod-worth parameter. This rod worth parameter is sensitive to rod-constants, cross-section sets, neutron energy spectrum and discreteness of energy groups, effective total fraction of delayed neutrons, etc. When compared to the conventional critical experiment for measuring rod-worths, the α-oriented procedure is characterized by the following facts:

- Rod-worths are not counterbalanced by fuel-additions; their reactivity effect is measured by the degree of subcriticality from the initial clean core.
- An opportunity is available for measuring rod-worths in rather different leakage to absorption ratios which is very helpful in giving code calculations more significance and confidence.

- A better economy can be realized in terms of fuel elements since very large rod-worths can be measured with no additional fuel elements required beyond those required for a clean core criticality.

Among the various alternatives of pulsed neutron and reactor-noise time-analysis experiments, the endogenous pulsed source method has been chosen because of its straightforward relationship to α, the economy of its application, and the relatively fast execution and data reduction. The technique[16] does not require any external input of reactivity of neutron wave form but instead it is based on observing the time decay of spontaneous bursts of neutrons, due to positive fluctuations of the instantaneous power level above the long-time-averaged level. The parameter α is derived by a least-square fit of experimental data to the following formula:[17]

$$n(t) = N\varepsilon\Delta t\ (\Delta F e^{-\alpha t} + \langle F \rangle)$$

where the symbols represent,

$n(t)$	neutron density at time t
N	total number of bursts analyzed
ε	detection efficiency (counts/fission)
Δt	sampling time-interval
$\langle F \rangle$	mean fission rate
ΔF	amplitude of the spontaneous burst

The value of α, together with its standard deviation, was obtained by fitting prompt neutron decay data to the exponential plus background formula using program LEARN.[18]

Since only a few of the experiments were actually compared with calculations, the significance of the measurements has been checked against critical loading data. In fact, α and the critical number of fuel elements are compatible reactivity indexes. Alpha is proportional to the amount of poison to be removed from the reactor to reach prompt-criticality. On the other hand, the

number of elements is related to the amount of multiplication needed to restore criticality, i.e., to compensate the rod absorption with a diminished leakage.

EXPERIMENTS IN UO_2-2.35% ^{235}U CORES

The parameter α was measured for a basic 9 x 9 core at critical and in configurations made subcritical by insertion of the test cruciform blade containing various neutron absorbing materials. Critical alpha (α_c)* was measured for a clean (no blade in) core and for two blade containing cores. A wide range of subcritical conditions was this way explored under the particular viewpoint of the leakage of absorption ratio.

The survey of the performed experiments is given in Tables I through III. A graphical comparison of the cruciform blade measurements in Configuration A can be seen in Figure 11. From the Tables one can see that the measurements and critical experiments are consistant, since they lead to the same order of importance for the reactivity-worth of the rods under investigation. It is interesting to note that no appreciable change appears in the value of critical alpha when one goes from a clean core to a core with a control blade and additional fuel elements.

A strong difference in critical alpha was observed when loading nonuniformities were eliminated, i.e., a regular core was loaded. A value of $\alpha_c = 165.7 \pm 1.8$ sec^{-1} (1.1%) was found for a 385 fuel element regular core (see Figure 12 for Configuration R) as compared with a value of $\alpha_c = 134.0 \pm 1.1$ sec^{-1} (0.8%) for the basic 9 x 9 core seen in Figure 10. The more conspicuously thermal characteristics of the latter configuration are well expressed by the value of α, which here plays the role of an integral spectrum parameter. Results from 4- and 5-energy group calculations of α_c for the regular configuration are shown in Table IV and can be seen to be consistant with the experimentally determined value.

---

* *Critical alpha (α_c) - value of β/ℓ for a critical assembly.*

TABLE I. Values of α in Configuration A (461 UO_2-2.35 wt % ^{235}U Fuel Elements, Moderator level at 94.68 in.) and Criti-Loadings for Different Control Blade Materials

Control Blade Material	Measured Alpha in Configuration A, sec^{-1}	Critical Loading	
		No. of Elements	Moderator Level, in.
No Blade in Core	134.0 ± 1.1 (0.8%)*	461	94.68
HfO_2 Cylinders	606 ± 10 (1.6%)	557	94.58
HfO_2 Flat Tubes	652 ± 14 (2.1%)	565	93.98
Hf Metal 0.09 in. Thick	761 ± 11 (1.4%)	589	94.12
Boral	808 ± 7 (0.9%)	593	94.81
Hf Metal 0.155 in. Thick	812 ± 7 (0.9%)	593	95.08
0.75 HfO_2-0.25 B_4C	834 ± 8 (1.0%)	597	95.06
B_4C Cylinders	841 ± 8 (1.0%)	601	95.03
$Re_2Hf_2O_7$ Tiles	850 ± 7 (0.8%)	601	95.14
B_4C Flat Tubes	881 ± 11 (1.2%)	605	95.58
Boral with Wings	1426 ± 18 (1.3%)	-	-

* *Critical Alpha*

TABLE II. Values of α in Configuration B(593 UO_2-2.35 wt% ^{235}U Fuel Elements, Moderator Level at 94.81 in.) and Critical Loadings for Different Control Blade Materials.

Control Blade Material	Measured Alpha in Configuration B, $sec.^{-1}$	Critical Loading: No. of Elements	Critical Loading: Moderator Level, in.
Boral	135.5 ± 1.2 (0.9%)*	593	94.81
0.75 HfO_2-0.25 B_4C	153.5 ± 2.1 (1.4%)	597	95.06
B_4C Cylinders	159.8 ± 1.7 (1.1%)	601	95.03
$Re_2Hf_2O_7$ Tiles	163.9 ± 1.6 (1.0%)	601	95.14
B_4C Flat Tubes	188.2 ± 1.9 (1.0%)	605	95.58
Boral with Wings	535 ± 10 (1.9%)	-	-

* *Critical Alpha*

TABLE III. Value of α in Configuration C(593 UO_2-2.35 wt% ^{235}U Fuel Elements, Moderator Level at 95.66 in.) and Critical Loadings for Different Control Blade Materials.

Control Blade Materials	Measured Alpha in Configuration C, sec^{-1}	Critical Loading: No. of Elements	Critical Loading: Moderator Level, in.
B_4C Cylinders	135.9 ± 1.5 (1.1%)*	593	95.66
B_4C Flat Tubes	167.6 ± 2.0 (1.2%)	605	95.58
Boral with Wings	500 ± 6 (1.2%)	-	-

* *Critical Alpha*

TABLE IV. Measured and Calculated Values of Critical Alpha in Configuration R (385 UO_2-2.35 wt% ^{235}U Fuel Elements, Regular Loading, Moderator Level at 97.02 in.)

Measured α_c $sec.^{-1}$	4-Group Calculation, $sec.^{-1}$	5-Group Calculation, $sec.^{-1}$
165.7 ± 1.8	163.9	162.8

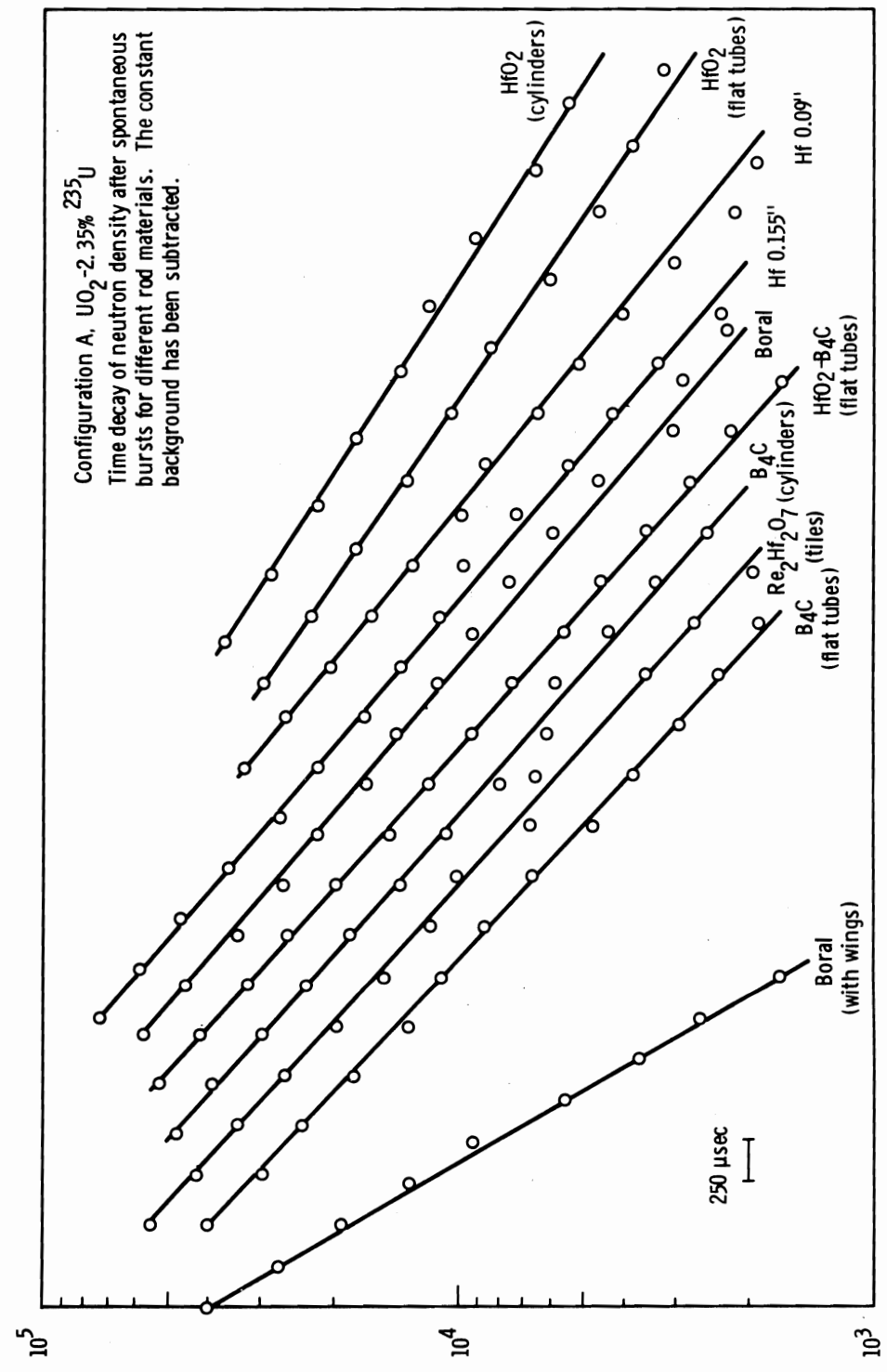

FIGURE 11. COMPARISON OF CONTROL BLADE MEASUREMENTS IN CONFIGURATION A

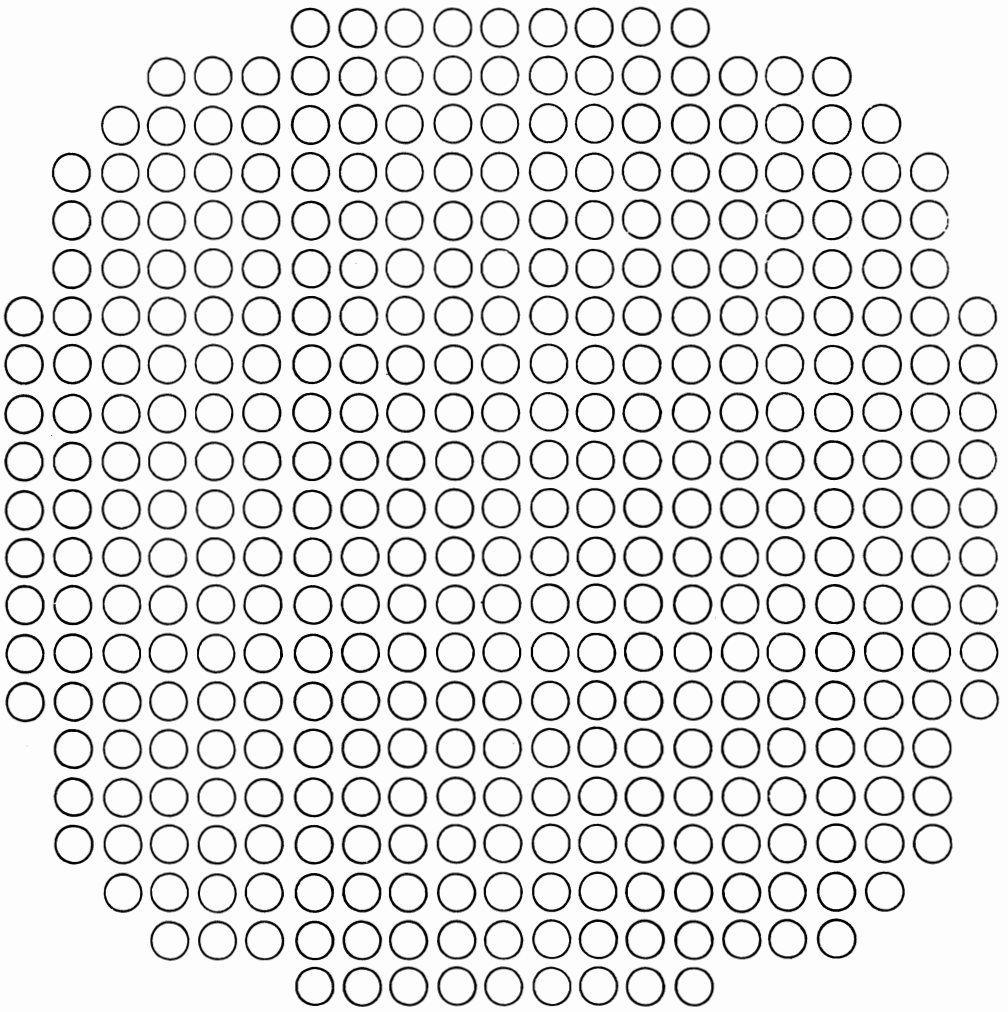

Configuration R

Regular, UO_2 - 2.35% ^{235}U

385 Elements

Moderator Level - 97.02"

FIGURE 12

EXPERIMENTS IN UO_2-2 wt% PuO_2 (8% ^{240}Pu) CORES

The parameter α was measured for the basic 9 x 9 core at slightly subcritical levels and for configurations made subcritical by test cruciform blade loadings identical to those previously investigated in UO_2 cores. The high spontaneous fission background, due to the presence of ^{240}Pu, made measurements at criticality practically impossible because of the large dead time in the BF_3 counting system. It didn't help to place the detector at a greater distance from the fuel because the diminished efficiency (the ratio of the number of effective counts to the total number of fission events in the reactor) made the amplitude and repetition rate of the spontaneous bursts smaller and lower, respectively. Thus, the value of α at critical was obtained by extrapolation of the results from a series of α measurements made in configurations which were slightly subcritical by known amounts. These slightly subcritical configurations were obtained by insertion of a calibrated reflector control sheet. The reactivity scale was calibrated by inverse multiplication measurements. A survey of these results, together with the extrapolated value of critical α, is shown in Table V.

TABLE V. Results of Near-Critical α and Inverse Multiplication Measurements to Extrapolate Critical α in Configuration D (257 UO_2-2 wt% PuO_2 8% ^{240}Pu Fuel Elements, Moderator Level at 95.00 in.)

Reflector Control Sheet, % Withdrawn	Measured Alpha $sec.^{-1}$	Inverse Counting Rate Arbitrary Units	Reactivity $
46	127.8 ± 1.4 (1.1%)	0.130	-0.284
42	140.8 ± 1.7 (1.2%)	0.185	-0.404
39	153.7 ± 1.2 (0.8%)	0.232	-0.506
36	164.9 ± 1.7 (1.0%)	0.294	-0.642
33	176.1 ± 1.2 (0.7%)	0.345	-0.753
30 1/4	184.1 ± 1.1 (0.6%)	0.385	-0.841

Extrapolated Critical Alpha: 100.5 ± 0.4 $sec.^{-1}$ (0.4%)

Reactivity Calibration: Delayed critical to prompt-critical ≡ 1$ ≡ 0.458 inverse counting rate units

The value of α_c was determined only for the clean core in the UO_2-PuO_2 measurements. Configurations E and F, which are the rod-containing critical cores, were assumed to have the same value of α_c. A comparison of the results from α measurements in Configurations D, E, and F and critical loadings with different control blade materials installed in the core are given in Tables VI through VIII. Satisfactory agreement can be seen between the results of the two procedures. A graphical comparison of the data from the cruciform blade measurements in Configuration D can be seen in Figure 13.

TABLE VI. Values of α in Configuration D (257 UO_2-2 wt% PuO_2 8% ^{240}Pu Fuel Elements, Moderator Level at 95.00 in.) and Critical Loadings for Different Control Blade Materials.

Control Blade Material	Measured Alpha in Configuration D, sec^{-1}	No. of Elements	Moderator Level, in.
No Blade in Core	100.5 ± 0.4 (0.4%)*	257	95.00
HfO_2 Cylinders	855 ± 10 (1.2%)	309	94.77
HfO_2 Flat Tubes	941 ± 9 (1.0%)	317	93.63
Hf Metal 0.09 in.	1132 ± 15 (1.3%)	325	95.21
Hf Metal 0.155 in.	1199 ± 15 (1.2%)	333	94.62
Boral	1194 ± 19 (1.6%)	333	94.78
0.75 HfO_2-0.25 B_4C	1268 ± 18 (1.4%)	333	95.11
B_4C Cylinders	1299 ± 17 (1.3%)	333	95.31
$Re_2Hf_2O_7$ Tiles	1292 ± 18 (1.4%)	333	95.41
B_4C Flat Tubes	1322 ± 15 (1.1%)	333	96.47
Boral with Wings	1924 ± 25 (1.3%)	397	94.18

* *Critical Alpha*

TABLE VII. Values of α in Configuration E(333 UO_2-2 wt% PuO_2 8% ^{240}Pu Fuel Elements, Moderator Level at 94.78 in.) and Critical Loadings for Different Control Blade Materials.

Control Blade Material	Measured Alpha in Configuration E, $sec.^{-1}$	Critical Loading: No. of Elements	Critical Loading: Moderator Level, in.
Boral	(100.)*	333	94.78
0.75 HfO_2-0.25 B_4C	140.7 ± 1.6 (1.1%)	333	95.11
B_4C Cylinders	153.7 ± 1.3 (0.3%)	333	95.31
$Re_2Hf_2O_7$ Tiles	160.8 ± 1.4 (0.9%)	333	95.41
B_4C Flat Tubes	216.0 ± 1.7 (0.8%)	333	96.47
Boral with Wings	831 ± 1.4 (1.7%)	397	94.18

* *Estimate of Critical α from Configuration D*

TABLE VIII. Values of α in Configurations F(333 UO_2-2 wt% PuO_2 8% ^{240}Pu Fuel Elements, Moderator Level at 95.31 in.) and Critical Loadings for Different Control Blade Materials.

Control Blade Material	Measured Alpha in Configuration F, $sec.^{-1}$	Critical Loading: No. of Elements	Critical Loading: Moderator Level, in.
B_4C Cylinders	(100.)*	333	95.31
B_4C Flat Tubes	179.6 ± 2.4 (1.3%)	333	96.47
Boral with Wings	736 ± 10 (1.4%)	397	94.18

* *Estimate of α_c from Configuration D*

The measured value of α_c for the basic 9 x 9 core compares favorably with the results from the 4- and 5-energy group calculations shown in Table IX.

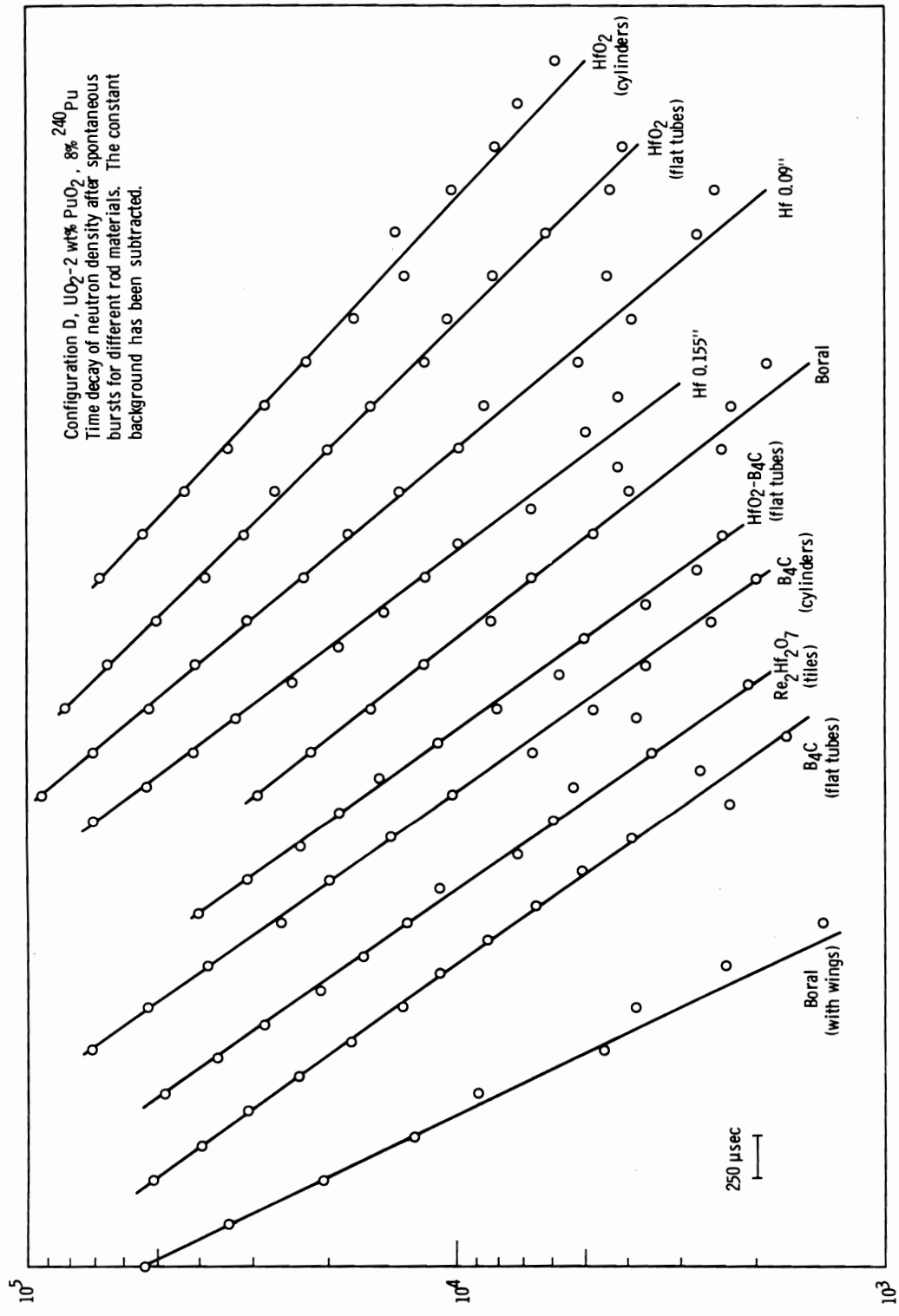

FIGURE 13. COMPARISON OF CONTROL BLADE MEASUREMENTS IN CONFIGURATION D

TABLE IX. Measured and Calculated Values of α_c for Configuration D

Measured α_c sec.$^{-1}$	4-Group Calculation sec.$^{-1}$	5-Group Calculation sec.$^{-1}$
100.5 ± 0.4	104.1	102.5

The effect of loading nonuniformities was also checked for the plutonium loadings. A value of α = 135.1 ± 1.0 sec^{-1} (0.7%) was measured for the 321 fuel element regular core (see Figure 14 for Configuration U) as compared with a value of 100.5 ± 0.4 sec^{-1} (0.4%) for the basic 9 x 9 core. Values of α for two subcritical configurations, containing Boral and Hf metal (0.155 in. thick) rods respectively, have been calculated for different parameters of the rod and compared with measured values of α. The blades were considered as transparent media for fast neutron groups while they were not so for epithermal and thermal groups. In fact, rod characteristics are schematized in terms of boundary conditions for neutron energy Groups 3 and 4, viz. the ratio is given between neutron currents and fluxes, as calculated in Appendix G. A summary of these results is given in Table X. The theory-experiment correlation is not fully complete, and further investigation is considered necessary before making any substantial comment.

TABLE X. Values of α Calculated Via Different Epithermal and Thermal Boundary Conditions Versus Measured α for Selected Rods in Configuration D.

Control Blade Material	J_3/ϕ_3	J_4/ϕ_4	Calculated α, sec.$^{-1}$	Measured α, sec.$^{-1}$
Hf Metal, 0.155 in.	0.1271	0.3507	1208	1199 ± 15
Boral	0.2055	0.4695	1316	1194 ± 19
	0.1500	0.4695	1264	1194 ± 19

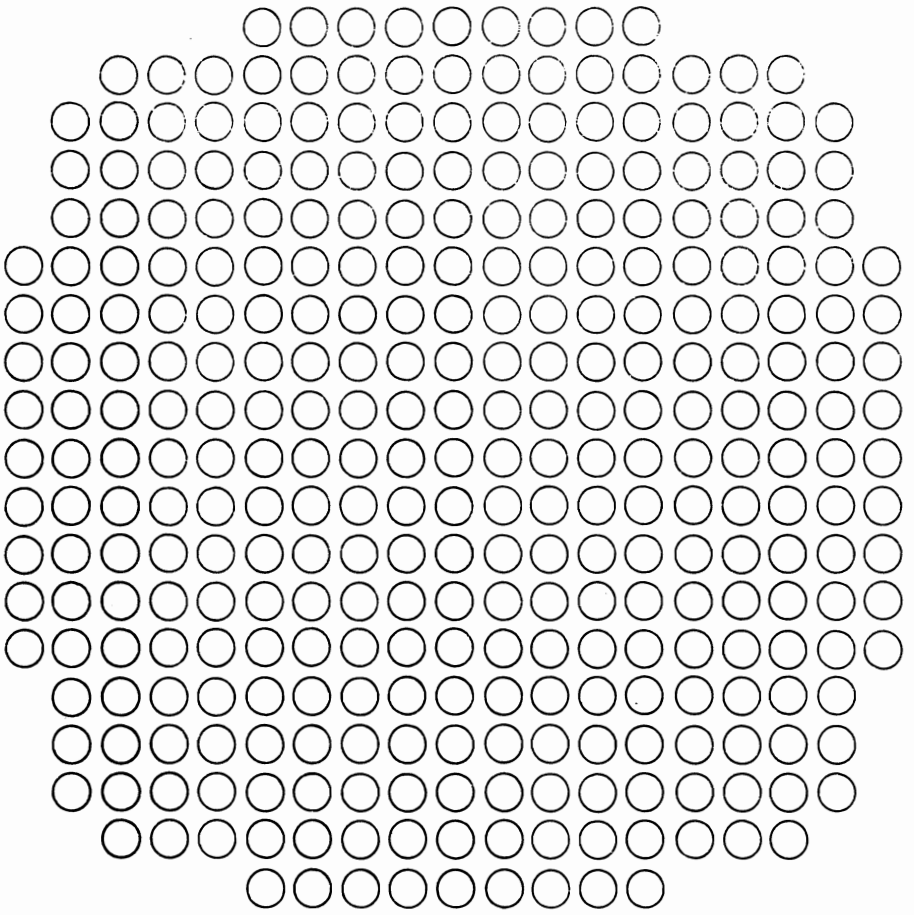

Configuration U

Regular, UO_2 - 2 wt% PuO_2 (8% ^{240}Pu)

321 Elements

Moderator Level - 99.70"

FIGURE 14

DESCRIPTION OF THE CALCULATIONAL MODELS AND RESULTS OF THE CALCULATIONAL STUDIES

In the reactivity and power distribution calculations, a fuel rod was assumed to be sensitive only to its own spectrum. The validity of this concept, especially in nonuniform loadings, is dependent upon whether the nonuniformities can be adequately described by a geometrical model. The microscopic cross sections used were derived under the hypothesis that fuel rod cells were surrounded by similar cells containing fuel rods.

Unless otherwise specified, the calculational method was as follows:

- A set of constants (D, Σ_a, Σ_f, etc.) was generated with an infinite lattice model - RIBOT,[13] HRG[19]-THERMOS/BATTELLE.[20] Suitable constants for the water regions were also generated, assuming that the neutron spectrum was not perturbed by the neighboring fuel region.
- The experimental configuration was simulated with a two-dimensional diffusion theory code in X-Y geometry - EXTERMINATOR - 2.[21] The mesh size in the reflector was the same as in the core, to a point past the reflector flux peak (about 6 cm beyond the core edge), where it was then increased. The thickness of the reflector was always more than 20 cm. When a water zone (water gap, water hole, etc.) was present in the core region, it was described with the same constants as the reflector water.
- An axial buckling of 0.00089 cm^{-2} was used, which corresponds to a full axially reflected core. All experimental k_{eff} values were for fully reflected cores.
- The power generated by a single rod was assumed to be proportional to the number of fissions occurring in the location corresponding to that fuel rod. Corrections were not made for the different energy releases at fission from ^{235}U and ^{239}Pu.

A series of calculations has shown that small deviations from this procedure may result in systematic alterations of the power profile (see case 15 in Table XI). The code RIBOT was used in most of the calculations, although different lattice calculational models were also checked for the most interesting configurations. The reasons for the reliance on RIBOT are:

- The extensive theory-experiment correlations made on past experiments using RIBOT make the code ready to be used and free of preliminary normalization.
- The compact and standard form of the results, which are obtained without intervention of human hands, produces results which are free from uncontrolled mistakes; i.e., the simple physical assumptions used in RIBOT might be wrong, but at least are self-consistent.
- RIBOT is a model in which the most important physical choices have been already made and built-in, so that the user is not obligated to answer the puzzling and sometimes embarrassing questions such as, "How many space points should be used for the calculation of the thermal spectrum?" or, "What model should be used for the calculation of the Dancoff factor?" In other words, RIBOT is a design and survey code and it was checked as such against the experimental results.

UO_2-PuO_2 SINGLE REGION EXPERIMENTS

The reactivity and power distribution theory-experiment correlations are summarized in Tables XI and XII for the UO_2-PuO_2 single region loadings. Detailed comparisons are provided in Appendix B. Due to the different number of rods measured at symmetrical positions, it was neither realistic nor considered correct to compare their average gamma activity with the calculations. It was, therefore, decided to compare gamma activity of each measured fuel rod with the calculations and to perform a final statistical analysis on the differences between theory

TABLE XI. Comparison of the Theoretical Models with Experiments' (Basic 9 x 9, UO_2-2 wt% PuO_2 Configuration, Measured $k_{eff} = 1.0078 \pm 0.0001$

Case	Model (Set No.)	Energy Groups	Meshes/ Cell	K_{eff}	δk[1] milli-k	σ_{RPD}, %[2]	δF, %[3]
1	St. RIBOT (1)	5	9	1.0088	1.0	1.36	1.6 ± 1.1
2	St. ROBOT (1)	5	4	1.0122	4.4	1.35	1.9 ± 1.2
3	St. RIBOT (1)	5	1	1.0281	20.3	2.59	4.0 ± 2.0
4	St. RIBOT (1)	4	9	1.0090	1.2	1.12	0.0 ± 1.2
5	St. RIBOT (1)	4	4	1.0120	4.2	1.19	0.5 ± 1.3
6	St. RIBOT (1)	4	1	1.0273	19.5	2.69	2.5 ± 2.0
7	St. RIBOT (1)	2	9	1.0188	11.0	1.18	0.5 ± 2.0
8	BURNY (BNL-325)	2	9	1.0135	5.7	1.48	2.2 ± 1.2
9	BURNY (KFK-120)	2	9	1.0138	6.0	1.42	1.9 ± 1.2
10	BURNY (BNL-325)	2	4	1.0174	9.5	1.67	3.1 ± 1.3
11	BURNY (BNL-325)	2	1	1.0352	27.4	3.12	5.9 ± 2.1
12	HTH-L.W.* (12)	4	4	0.987	-20.8	1.66	1.4 ± 1.3
13	HTH-S.W.* (13)	4	4	0.999	-8.8	1.61	1.2 ± 1.2
14	TH/B-HRG** (14)	4	4	1.0092	1.4	1.20	-0.5 ± 1.3
15	St.RIBOT (1)	4	4 (4 cm in. Reflector)	1.0200	12.2	(4.72)	1.0 ± 1.4
16	RIBOT, M.H. (15)	4	4	1.0065	-1.3	(2.31)	-4.3 ± 1.6

1. $\delta k = k_{eff}$ *(calculated)* $- k_{eff}$ *(measured)*
2. *Standard deviation of the rod power discrepancies* (σ_{RPD}) *for the entire configuration (Defined in Appendix B).*
3. δF *- A theory-experiment rod power discrepancy indicator (Defined in Appendix B)*

* *See text.*
** *TH/B means THERMOS/BATTELLE*

TABLE XII. Comparison of the Theoretical Models with Experiments (All UO_2-2 wt% PuO_2 Configurations.)

Configuration	Exp. k_{eff}	Case	Model (Set No.)	Energy Groups/Mesh	k_{eff}	δk, Milli-k	σ_{RPD}, %	$\delta(P_{max}/P_{av})$ or $\delta F(*)$, %[1]
Regular	1.0005	17	St. RIBOT (1)	4/4	1.0035	2.9	1.06	----------
		18	HTH-L.W. (12)	4/4	0.975	-25.6	1.13	----------
		19	HTH-S.W. (13)	4/4	0.987	-13.6	1.13	----------
		20	TH/B-HRG (14)	4/4	0.9992	1.4	----	----------
		21	St. RIBOT (1)	5/4	1.0018	1.2	----	----------
Water Hole	1.0020	22	St. RIBOT (1)	4/4	1.0048	2.8	1.29	1.2 ± 1.3
		23	St. RIBOT (1)	5/4	1.0031	1.1	1.32	0.5 ± 1.3
Water Slab	1.0068	24	St. RIBOT (1)	4/4	1.0095	2.7	1.08	0.6 ± 1.3
		25	St. RIBOT (1)	5/4	1.0088	2.0	1.35	1.2 ± 1.5
Water Cross	1.0054	26	St. RIBOT (1)	4/4	1.0104	5.0	1.48	0.6 ± 1.6
		27	St. RIBOT (1)	5/4	1.0109	5.5	1.54	2.0 ± 1.6
		28	St. RIBOT (1)	4/9	1.0092	4.8	1.33	0.8 ± 1.4
		29	Mod. RIBOT (11)	4/9	1.0069	1.5	1.66	2.2 ± 1.7
Basic 7 x 7	1.0038	30	St. RIBOT (1)	4/4	1.0080	4.9	1.58	-1.6 ± 1.2*
		31	St. RIBOT (1)	5/4	1.0086	4.8	1.11	0.0 ± 1.1*
9 x 9 Voids	1.001	32	RIBOT,Unif (16)	4/4	1.0073	7.2	3.54	-6.5 ± 2.9*
		33	RIBOT, (17-19) Nonunif.	4/4	1.0055	5.4	2.04	0.4 ± 1.8*
		34	RIBOT, (17-19) Nonunif.	5/4	1.0061	6.0	2.26	3.0 ± 1.6*

1. *$\delta(P_{max}/P_{av})$ and δF - Theory-experiment rod power discrepancy indicators (Defined in Appendix B)*

and measurement. All results were normalized to the average gamma activity for the most active rod, except in those configurations where the results for the most active rod were somewhat uncertain. Because the basic 9 x 9 loading most closely simulates an actual BWR fuel element, the most extensive set of calculations was performed for that loading. It can be seen, from the analytical results in Appendix B, that the expected experimental deviation of the single region gamma measurements is of the order of 1%. Agreement of the same order was the goal of the theory-experiment correlations.

The initial calculations for the UO_2-PuO_2 configurations were for the basic 9 x 9 loading. Their main purpose was to determine the optimum number of mesh points and energy groups to be utilized in the calculational models (Cases 1 to 11 of Table XI; Cases 1 to 7 use RIBOT + EXTERMINATOR 2, referred to as Standard RIBOT). In each case, individual cells were described by 1 x 1 (1), 2 x 2 (4), and 3 x 3 (9) meshes, which corresponded to mesh sizes of 1.9050, 0.9525, and 0.6350 cm, respectively. The various experimental configurations were simulated in the calculations by meshes ranging from 20 x 20 to 45 x 45. In order to describe the reflector peaking region in detail, core mesh sizes were maintained for three lattice units into the reflector. The remainder of the reflector, to a point at least 20 cm from the fuel boundary, was depicted by 5 meshes (3 cm each).

By comparing the results summarized in Table XI (Cases 1 to 3, 4 to 6, and 7 to 11) it can be seen that the effect of the variation in mesh size is very small between 4 and 9 meshes per cell, but is significant for the 1 mesh per cell description. In fact, the 1 mesh cell description is inadequate with every scheme; an increase in reactivity of 1.5% and an increase in the ratio of the power of the corner rod to the power of the central rods of 2 to 3% are the net results of the coarse

detail of the fuel regions. Calculations using 4 meshes instead of 9 meshes overestimate the reactivity by about 4 milli-k and predict the power distribution with a similar degree of accuracy. For almost all successive calculations, only the 4 meshes per cell description was used.

Case 15 shows results for variations of the mesh size in the reflector. In this case, while using the 4 mesh scheme in the core, the mesh size in the reflector was increased from 0.9525 to 4 cm at the core boundary. As a result, the calculated k_{eff} increased by 8 milli-k and the power from rod position 2 (see Appendix B, Figure B-6) increased by 20% as compared with Case 5. This variation of reflector mesh size also produced an effect in the center of the core, changing δF (defined in Appendix B) from $(0.5 \pm 1.3)\%$ to $(1.0 \pm 1.4)\%$.

Variation in the number of neutron energy groups did not produce major changes in the reactivity and power distribution calculations. In fact, the 4- and 5-group (4G and 5G) calculations produced similar reactivity results, while the 2-group (2G) calculation showed about a 1% overestimate. Comparing the power distribution calculations (Cases 1, 4, and 7 of Table XI), one realizes that the standard deviation of the discrepances between theory and experiment go from 1.36% (5G) to 1.12% (4G) to 1.18% (2G). This slight decrease in precision for the 5-group model is due essentially to a small overestimate of the peaking factor. Using one of the theory-experiment correlation indicators for the power peaking discussed in Appendix B, one finds δF is $(1.6 \pm 1.1)\%$ for Case 1, $(0 \pm 1.2)\%$ for Case 4, and $(0.5 \pm 2.0)\%$ for Case 7. This indicator suggests that the 4-group model best predicts the critical areas where power peaking occurs.

Cases 8 to 11 show results employing the code BURNY[14] instead of Standard RIBOT. A 2-group model and an earlier version of RIBOT are utilized in BURNY. In Standard RIBOT, the thermal group is divided into two zones (break point at 0.2 eV)

each with different spectra and disadvantage factors. The constants for the two thermal groups are eventually collapsed to give the 2- and 4-group models or are utilized as such to give the 5-group model. In BURNY, only one thermal group is considered and one disadvantage factor calculated. Cases 7, 8, and 9 of Table XI show the results of these different schemes. Cases 8 and 9 employing BURNY demonstrate that using different thermal libraries (Schmidt's KFK-120 in Case 9 and BNL-325, an old TEMPEST library, in Case 8) do not significantly change k_{eff} or the power distribution. Using the KFK-120 library, the BURNY model in Case 9 underpredicts k_{eff} by 5 milli-k and overpredicts the power peak relative to Standard RIBOT in Case 7. It is worth noticing, however, that although less precise than Standard RIBOT, BURNY is faster by a factor of 2.5. This decreased computer time is due to the possibility of allowing for diagonal symmetries and to the greater intrinsic speed of the code EQUIPOISE, used in BURNY to calculate the fluxes.

Case 16 shows the results of a different homogenization model in the thermal group. In RIBOT, like all models for H_2O reactors, an "average flux homogenization" is used; namely, the cross section is expressed by:

$$\bar{\Sigma} = (\Sigma_f V_f \phi_f + \Sigma_m V_m \phi_m)/(V_f \phi_f + V_m \phi_m).$$

In other words, the flux in the subsequent diffusion calculations is assumed to be the cell average flux $(V_f \phi_f + V_m \phi_m)/(V_f + V_m)$.

A different homogenization scheme is sometimes used in D_2O systems (SGHWR group at Winfrith). This scheme is sometimes called "moderator edge flux homogenization," which is abbreviated (M.H.). It assumes that the flux of the diffusion calculations represents the maximum flux in the moderator, and the fuel only produces a perturbation to a moderator. The average cross sections for this model were defined in the following manner:

$$\bar{\Sigma}(\text{M.H.}) = (\Sigma_f V_f \phi_f + \Sigma_m V_m \phi_m)/[(V_f + V_m) \times \phi_m].$$

There is no theoretical justification for either of the two definitions. Perhaps a somewhat philosophical justification should favor the M.H. scheme if one assumes that the flux in the moderator must be continuous between cells or between core and reflector. The M.H. model (using Cross Section Set 15 in Appendix F) strongly underpredicts the peaking factor ($\delta F = -4.3 \pm 1.6$)%. This suggests that the diffusion length in the fuel should be calculated with the standard scheme since it is overpredicted using the M.H. method.

The results of calculations made with codes other than RIBOT are shown as Cases 12, 13, and 14. In all three schemes, the codes HRG and THERMOS/BATTELLE were used to calculate the 4-group constants. In the first two cases, a group structure similar to RIBOT was used. The break points of the four groups were at 183 keV, 5.5 keV, and 0.683 eV. With both codes, heterogeneous self-shielding factors were introduced for ^{238}U, ^{239}Pu, ^{240}Pu, and ^{241}Pu. These factors were calculated in the code assuming a black rod model for the Dancoff correction.* In both cases, THERMOS/BATTELLE, contained in the code HTH,[22] was used to calculate the thermal constants. The most significant features of these cases from the physics standpoint are:

- The source of thermal neutrons is calculated from HRG; varies with the energy as well as with the space, and
- The diffusion coefficient is calculated as:

$$D_{th} = \int_E j(E)D(E)dE / \int_E j(E)dE,$$

where $j(E)$ is the net neutron current across the cell.

In Case 12 (Cross-Section Set 12), the Leonard-Westcott Library was used for ^{239}Pu in the thermal region. These values were derived from the values $\sigma_a(E)$ and $\sigma_f(E)$ given by Leonard, normalized to the values at 2200 m/sec given by Westcott ($\eta_{2200} = 2.11$).[23]

---

* *The cross section calculations for Cases 12 and 13 were executed by W.L. Purcell.*

The Schmidt library (KFK-120) was used in Case 13 (Cross-Section Set 13) for ^{239}Pu in the thermal region with the 2200 m/sec values normalized to the Westcott values. For this case, the Schmidt library, which is used in RIBOT, was normalized to Schmidt's values at 2200 m/sec ($\eta_{2200} = 2.079$).[24]

The group structure was quite different in the fast region for Case 14 (Cross-Section Set 14).* The break points were 5.5 keV, 2.38 eV, and 0.683 eV. The library used in the thermal region was the same as in Set 12. Cross Section Sets 12, 13, and 14 are synthetically compared with Set 1 (Standard RIBOT) in Table XIII.

TABLE XIII. Comparison of the Cross-Section Sets for the UO_2-2 wt% PuO_2 Models

Cross-Section Set No.		$(\eta f)_\infty$	k_∞	k_{eff} (B^2=0.00934)	τ, cm^2	L_{th}, cm
1	(Standard RIBOT)	1.679	1.364	0.999	37.4	1.19
12	(HTH-L.W.)	1.660	1.355	0.990	35.0	1.48
13	(HTH-S.W.)	1.685	1.352	1.002	35.0	1.50
14	(TH/B-HRG)	1.666	1.333	1.010	32.5	1.23

A comparison of Set 12 with Set 13 in Table XIII shows, that for H_2O systems, the Schmidt cross sections produce a value of ηf which is 1.5% higher than that obtained using the Leonard cross sections when normalized to the same η value at 2200 m/sec. This means that, if the Schmidt library is normalized at $\eta_{2200} = 2.079$, it will produce the same value of ηf as the Leonard-Westcott library. By comparing ηf of Set 1 with that of Set 13, it can be seen that the calculation of the spectrum as done by RIBOT (TEMPEST model versus THERMOS/BATTELLE) together with the possible difference in the tabulated libraries,

* *The calculations with this model (THERMOS/BATTELLE-HRG Cross-Section Sets 14, 32, 41, 51) were done by Dimitri Gournelos of General Electric Company (San Jose).*

almost compensate for the different normalization value at 2200 m/sec. The difference in the epithermal fissions and absorptions produces differences in k_∞ of the order of 1% between the RIBOT and the HTH models; part of the difference is due to the "greyness" correction on Dancoff factor used in RIBOT. Finally, the smaller value of τ calculated by HRG compensates the lower value of k_∞ in such a way that the four values of k_{eff} (Sets 1, 12, 13, and 14) do not vary a great deal.

Cases 5, 12, 13, and 14 in Table XI show that Set 1 (Standard RIBOT) and Set 14 (THERMOS/BATTELLE-HRG) yield similar reactivity and power distribution results. It is worthwhile to mention that Set 1 required 1/2 hr of preparation and 1 sec of operating time on UNIVAC 1108, while Set 14 required 1 working day and 5 min on UNIVAC 1108. Cases 12 and 13 underestimate k_{eff} by 25 milli-k and 13 milli-k, respectively, relative to Standard RIBOT (Case 5). The power distribution calculations for these two cases are comparable with Standard RIBOT (Case 5) and THERMOS/BATTELLE-HRG (Case 14).

The experimental results from Rod Location 12 in the basic 9 x 9 configuration were discarded in all comparisons because the large theory-experiment discrepancies were inconsistent with the good agreement of the neighboring rods. On the other hand, the discrepancies found for Rod Location 2 were considered a failure of all the calculational models. Rod Location 2 was next to the reflector and the overestimate of the power by 4% (5-group) and 3% (4-group) was not surprising.

Inspection of the calculational results for the other UO_2-PuO_2 single region experiments shown in Table XII reiterates the most important conclusions drawn from the basic 9 x 9 comparisons They are:

- Set 1 (Standard RIBOT) predicted the reactivity effects well, with both 4- and 5-energy group calculations. The

largest trend from the regular case was the voided 9 x 9 element where the reactivity differences were less than 3 milli-k for the 4-group model and about 5 milli-k for the 5-group model.

- The peaking factor was well predicted by the 4-group model and overpredicted by 2 to 3% by the 5-group model. The only possible exception was basic 7 x 7 loading; however, there were insufficient experimental points inside the cluster to draw definite conclusions.
- Sets 12 and 13 underestimated k_{eff} by 26 and 14 milli-k, respectively.
- Set 14 produces results which are similar to Standard RIBOT.
- The power of the rod next to the reflector is generally overestimated by 2 to 3%.

For the "water cross" configuration, by normalizing the calculated rod powers to the corner rod (Rod 2) as shown in Table B-4, it is apparent that all the models underestimate the rod power next to the water slabs. Additionally, consistent with the general trend indicated by the aforementioned second conclusion, the 4-group models better predicted the peaking factor. Use of the 9 mesh point cell description did not reduce this water slab discrepancy.

A new cross-section set (Set 11) was generated in order to test the effect of the epithermal cross sections (Case 29). This set was derived from Set 1 by decreasing the group-3 absorption, removal, and fission cross sections such that there was a 10% increase in the ratio of the source of thermal neutrons in H_2O to the source of neutrons in the fuel. This reduction tended to simulate a departure of the epithermal spectrum from the 1/E law assumed in RIBOT. The only effect of the modification was to increase the peaking factor by 1.4%; hence, producing the same results as the Standard RIBOT 5G model.

A completely new fact became apparent in the basic 9 x 9 element, when a 25% moderator void was introduced. The peaking factor was underestimated by about 6% when the voids in the calculations were uniformly distributed. When allowances were made for the actual void distribution (called nonuniform), the theory-experiemnt agreement became much better (for the details on the density adjustment see Appendix G-1). Cases 33 and 34, 4G and 5G nonuniform density models, both predicted the power distribution within the voided element much better than the 4G uniform density Case 32. The reason for this trend is not due to the spectral effect on σ_f of ^{239}Pu (see the cross-section set in Appendix F), but to the variations of L as a function of the void content.

In conclusion, when voids are present and only k_{eff} is of concern, it is sufficient to conserve, on the average, the proper material balance. If the power distribution is important, it is necessary to allow for the actual void distribution at least in the calculation of the diffusion length. Consequently, when the void distribution in a power reactor is known to be non-uniform, calculation of the local peaking factor requires the coupling of neutronic and thermal hydraulic calculations in a microscopic way; i.e., at the level of the single hydraulic channel. As an alternate method, one could assume a uniform void distribution which corresponds to the center of the cluster, and not to the average cluster, in order to minimize the errors.

UO_2-2.35% ^{235}U SINGLE REGION EXPERIMENTS

In general, there are two basic differences between these experiements and the UO_2-PuO_2 experiments. First, the UO_2 rods have a smaller diameter resulting in a higher moderator to fuel ratio. As a consequence, removal of fuel from the interior of the loadings caused a negative reactivity effect. This was not always the case in the UO_2-PuO_2 loadings. Secondly, the symmetry checks on the power measurements demonstrated that the

UO_2 rods were considerably more uniform in density than the mixed oxide rods. For this reason, better agreement between theory and experiment was expected for the UO_2 configurations.

A 4-mesh cell description was used for all the single region UO_2 calculations, as was the case for the majority of the UO_2-2 wt% PuO_2 single region configurations.

Three main sets of cross sections were used in the calculations:

- Set 3 (analogous to Set 1) was calculated with RIBOT.
- Set 31 (analogous to Set 12) was calculated with HTH. In this case, as in the plutonium case, a black rod was considered for the Dancoff correction; the thermal D was averaged on the neutron currents; and the cross sections were normalized to the Westcott 2200 m/sec values. In addition, an epithermal library was used in which the ^{235}U fission cross section was described as 1/v and the fission resonance integral was 340 barns.
- Set 32 (analogous to Set 14) was calculated with THERMOS/BATTELLE and HRG. The thermal diffusion coefficient was calculated by averaging D over the currents and ^{235}U was treated as a resonance absorber.

The comparison is made in Table XIV of results obtained with three cross-section libraries. The reason that the k_{eff} values are not significantly different is primarily due to compensating factors. In particular, the differences in ηf are due to the value of ν for ^{235}U which is 2.45 in Set 3 and 2.43 in Sets 31 and 32. Different treatment of the ^{235}U and ^{238}U resonances in Sets 31 and 32 accounts for the decrease in the resonance escape probability in such a way that the values of k_∞ are 2.5% lower than the value calculated using Set 3. The differences in τ and L, however, tend to compensate the other differences when k_{eff} is calculated.

TABLE XIV. Comparison of the Cross Section Sets for the UO_2-2.35% ^{235}U Models

Set No. (Model)	$(\eta f)_\infty$	k_∞	k_{eff} (B^2=0.00934)	τ,cm^2	L_{th}cm
3 (Standard RIBOT)	1.493	1.333	0.997	36.4	1.66
31 (HTH)	1.476	1.300	0.992	32.1	1.99
32 (TH/B-HRG)	1.472	1.301	1.005	31.8	1.59

The results of the UO_2 comparisons are summarized in Table XV. Cases 35 to 38 show that k_{eff} is correctly predicted by RIBOT and THERMOS/BATTELLE-HRG, and are underestimated by about 1 to 2% by HTH. The results of the remaining UO_2 cases summarized in Table XV revealed that the models yielded trends similar to those found in the UO_2-PuO_2 calculations.

- The 4-group model predicts the power and peaking factors better than the 5-group model.
- Fuel rods adjacent to the water gap in the water cross configuration (excluding the corner rod) are underestimated by 1 to 2%. As in the UO_2-PuO_2 comparisons, no reason could be found for this discrepancy.
- The HTH cross sections produced a 5.6% underestimate of the power peaking in the 9 x 9 basic element (Case 47). This underestimation is due to the value used for the thermal diffusion length. Here, the calculations made using a correct value for the thermal diffusion coefficient gave the correct power distribution (Case 48).
- The calculation of the basic 9 x 9 voided element under estimated the peaking factor by 8% when a uniform void distribution was assumed. The 4-group model using the nonuniform void distribution calculations produced better reactivity and power distribution results than the 5-group model. The 4-group model underestimated the peaking factor by 2.5% while the 5-group model overestimated it by a similar amount.

TABLE XV. Comparison of the Theoretical Models with Experiments (All UO_2-2.35% ^{235}U Configurations)

Configuration	Exp. k_{eff}	Case	Model (Set No.)	Group	k_{eff}	δk, milli-k	σ_{RPD}, %	$\delta(P_{max}/P_{av})$ or δF(*), %
Regular	1.0032	35	St. RIBOT (3)	4	0.9999	-3.3	0.73	-0.7 ± 0.7
		36	St. RIBOT (3)	5	0.9990	-4.2	1.11	-0.7 ± 1.1
		37	HTH (31)	4	0.9853	-17.9	1.12	-0.8 ± 1.1
		38	TH/B-HRG (32)	4	0.9956	-7.6	1.36	0.3 ± 1.4
Water Hole	1.0025	39	St. RIBOT (3)	4	0.9994	-3.1	0.68	-0.3 ± 0.8
Water Slab	1.0018	40	St. RIBOT (3)	4	0.9993	-2.5	0.83	0.2 ± 1.0
		41	St. RIBOT (3)	5	0.9991	-2.7	1.29	0.7 ± 1.4
Water Cross	1.0010	42	St. RIBOT (3)	4	0.9990	-2.0	0.70	0.5 ± 0.7
		43	St. RIBOT (3)	5	0.9998	-1.2	1.34	2.4 ± 1.3
Basic 7 x 7	1.0010	44	St. RIBOT (3)	4	1.0014	0.4	1.00	-1.5 ± 0.8(*)
Basic 9 x 9	1.0027	45	St. RIBOT (3)	4	1.0038	1.1	0.71	1.2 ± 0.8(*)
		46	St. RIBOT (3)	5	1.0058	3.1	1.32	2.5 ± 0.8(*)
		47	HTH (31)	4	0.9892	-13.5	2.14	-5.6 ± 0.8(*)
		48	TH/B-HRG (32)	4	0.9955	-7.2	1.86	-1.7 ± 0.9(*)
Basic 9 x 9	1.0030	49	RIBOT- Uniform (33)	4	1.0064	3.4	3.61	-8.4 ± 1.9(*)
With Voids		50	RIBOT- Uniform (33)	5	1.0084	5.4	2.68	-3.2 ± 1.8(*)
		51	RIBOT- Non-Unif. (35-37)	4	1.0052	2.2	1.64	-2.5 ± 1.3(*)
		52	RIBOT- Non-Unif. (35-37)	5	1.0071	4.1	1.95	2.3 ± 1.0(*)

A slight trend is noticeable in the reactivity calculations. Since the removal of fuel rods from the interior of the uranium configuration had a negative reactivity effect, the number of fuel rods required for critical in the more heterogeneous configuration was considerably greater than for the uniform core. When a calculation was performed for a water slab in the regular configuration, the effect of removing the fuel (making the water slab) decreased the reactivity by about 16 milli-k. Based on the discrepancies of the reactivity calculations seen in Cases 35 and 40, the relative discrepancy on the calculated 16 milli-k "water slab" worth is about -1 milli-k.

Reactivity differences on the same order of magnitude can be determined from relatively simple calculations; e.g., the RIBOT 4-group model underestimated the negative effect of the water gaps by about 10%. Using the 6.5 cm radial reflector savings calculated for a uniform configuration with 385 fuel rods (see Case 35, Table XV) one obtains a value of k_{eff} = 1.051 for a similar configuration with 441 fuel rods or an increase of 52 milli-k. This value is consistent with the worth of the water gaps in the basic 9 x 9 configuration in Case 45 relative to the regular loading. The calculated relative discrepancy for these two cases is 4.4 milli-k; i.e., less than 10% of the total effect.

MULTIREGION CONFIGURATIONS

These measurements were the last to be performed and there was insufficient time to carry out calculations with all the models as was done in the single region configurations. The majority of the calculations were carried out on two-region configurations (basic 9 x 9 plutonium in uranium and uranium in plutonium, 11 x 11 plutonium in uranium); only a few calculations were made investigating configurations with greater than two fuel zones; i.e., Composite Element 1. The results of the multiregion calculations are shown in Tables XVI and XVII.

TABLE XVI. Comparison of the Theoretical Models with Experiments (Multiregion, UO_2-2.35% ^{235}U Driver Configuration)

Configuration (Element)	Exp. k_{eff}	Case	Model (Set No.)	Group	k_{eff}	δk, milli-k	σ_{RPD}, %	σ_{RPD}, %, After Correction(1)
9 x 9 PuO_2	1.0039	53	St. RIBOT (1&3)	4	1.0074	3.5	2.69	1.79
		54	St. RIBOT (1&3)	5	1.0087	4.8	2.16	1.37
		55	M.H.RIBOT (15&34)	5	1.0045	0.6	2.75	----
		56	TH/B-HRG (14&32)	4	1.0012	-2.7	3.30	3.30
11x11 PuO_2 (no water gap)	1.0033	57	St. RIBOT (1&3)	4	1.0028	-0.5	1.94	1.12
		58	St. RIBOT (1&3)	5	1.0035	0.2	1.57	1.25
		59	M.H.RIBOT (15&34)	4	1.0013	-2.0	2.04	0.85
		60	M.H.RIBOT (15&34)	5	1.0017	-1.6	1.60	0.83
Composite 1	1.0026	61	TH/B-HRG (14,32, 41&51)	4	1.0014	-1.2	----	----
Composite 2	1.0022	62	St. RIBOT (1&3)	4	1.0042	2.0	3.36	2.68
		63	St. RIBOT (1&3)	5	1.0052	3.0	2.00	1.34
		64	TH/B-HRG (14&32)	4	0.9967	-5.5	2.13	2.13

1. *The power from the UO_2-2.35% ^{235}U was increased by 2.5% in RIBOT calculations (see text).*

TABLE XVII. Comparison of the Theoretical Models with Experiments (Multiregion, UO_2-2 wt% PuO_2 Driver Configuration)

Configuration (Element)	Exp. k_{eff}	Case	Model, (Set No.)	Group	k_{eff}	δk, milli-k	σ_{RPD}, %	σ_{RPD}, %, After Correction(1)
7 x 7 24% ^{240}Pu	1.0051	65	St. RIBOT (1&6)	4	1.0158	10.7	1.62	1.62
9 x 9 UO_2	1.0068	66	St. RIBOT (1&3)	4	1.0098	3.0	2.30	1.71
		67	St. RIBOT (1&3)	5	1.0104	3.6	1.72	1.25
		68	TH/B-HRG(14&34)	4	1.0047	-2.1	1.28	1.28
Composite 1	1.0028	69	St. RIBOT (1,4&5)	4	1.0096	6.7	3.80	3.80
		70	TH/B-HRG (14,41&51)	4	1.0077	4.9	2.57	2.57

1. *The power from the UO_2-2.35% ^{235}U was increased by 2.5% in RIBOT calculations (see text).*

Calculations of reactivity for the multiregion loadings were found to agree with experiments as well as the single region loadings (in the range of ±5 milli-k). The only exception was the basic 7 x 7 24% ^{240}Pu element shown in Table XVII where the calculations gave an overestimate of k_{eff} of about 1%. This overestimate is consistent with a slight trend previously noted in the eigenvalue calculated by RIBOT. Comparison with approach-to-critical data from the Critical Approach Facility (CAF) at Battelle-Northwest revealed that k_{eff} is overestimated as a function of increasing ^{240}Pu content.*

The agreement in power distribution between theory and experiments is not as good as in the single zone experiments, irrespective of the theoretical model used. The standard deviation of the discrepancies for the single region configuration range from 0.6 to 2% (Tables XI, XII, and XV), where the multiregion experiment standard deviations are generally larger than 2%

It is not possible from the relatively few calculations to draw definite conclusions for the cause of these increased discrepancies. However, one can obtain some useful indications by analyzing in detail those configurations in which only the UO_2-2 wt% PuO_2(8% ^{240}Pu) and UO_2-2.35% ^{235}U fuels were present (Cases 53 through 60, and 62 through 64 of Table XVI, and Cases 66 through 68 of Table XVII).

Since a source of error in these experiments was in the power normalization between the different fuel types, it was instructive to analyze the behavior of the theory-experiment discrepancies as a function of the power normalization of the plutonium and uranium rods. The region-averaged and relative percent discrepancies for UO_2-2.35% ^{235}U and UO_2-2 wt% PuO_2 two-region loadings are summarized in Table XVIII. It can be seen that the

---

* *Paulo Loizzo, unpublished calculations.*

TABLE XVIII. Region-Averaged and Relative Discrepancies from Theory-Experiment Comparisons for Multi-region Configurations

Case	Average Percent Discrepancy on Power from UO_2-PuO_2 Rods	Average Percent Discrepancy on Power from UO_2 Rods	Relative Percent Discrepancy [δ(%) UO_2-PuO_2 - δ(%) UO_2]
53 (1)	0.32 ± 1.51	-4.72 ± 0.54	5.04 ± 1.60
54 (1)	0.16 ± 1.12	-3.55 ± 1.47	3.71 ± 1.35
56 (1)	1.36 ± 2.35	-3.97 ± 1.58	5.33 ± 2.34
57 (2)	3.40 ± 1.40	0.21 ± 0.56	3.19 ± 1.52
58 (2)	3.93 ± 1.44	0.26 ± 0.61	3.54 ± 1.37
62 (2)	7.31 ± 1.59	1.06 ± 1.02	6.25 ± 1.38
63 (2)	1.86 ± 1.20	-1.27 ± 1.38	3.13 ± 1.86
64 (2)	4.89 ± 1.32	1.28 ± 0.91	3.62 ± 1.59
66 (2)	4.74 ± 2.85	1.22 ± 0.92	3.52 ± 2.99
67 (2)	1.52 ± 2.08	-1.07 ± 0.79	2.59 ± 2.33
68 (2)	0.32 ± 2.16	0.72 ± 0.72	-0.40 ± 2.28
Average relative percent discrepancy			3.67 ± 0.56

1. *The UO_2 rod powers were normalized to UO_2-PuO_2 rod powers using the intercalibration factor.*
2. *The UO_2-PuO_2 rod powers were normalized to UO_2 rod powers using the intercalibration factor.*

power from the UO_2-2.35% ^{235}U fuel is, on the average, underestimated relative to the UO_2-2 wt% PuO_2 fuel by 3.67%. Case 68 is the only one in which the power from the UO_2-2.35% ^{235}U fuel is overestimated with respect to the UO_2-PuO_2 fuel.

The behavior of the standard deviations of the rod power discrepancies is shown in Table XIX for changes in the UO_2-2.35% ^{235}U and UO_2-2 wt% PuO_2 power intercalibration factor. This was prompted by the results of Table XVIII where the UO_2-2.35% ^{235}U rod power was underestimated relative to the UO_2-2 wt% PuO_2 fuel. Standard deviations are shown in the last two columns of Table XIX where the UO_2-2.35% ^{235}U rod powers were increased by 3.67 and 2.00%, respectively. It is evident from the adjustment of the standard deviation that some systematic effect must be present which tends to underestimate the UO_2-2.35% ^{235}U rod power. The adjusted values are consistent with single region comparison shown in Tables XI, XIII, and XV.

It was felt that the effect was not due to the models used in the calculation but to an error either in the power normalization measurements (intercalibration) or in the fissile content of the fuel rods.

A careful check of all calculations and experimental data revealed that the source of the discrepancy was connected with the RIBOT calculated cross sections for the UO_2-2.35% ^{235}U fuel regions. It was determined that in the early stages of the program, all RIBOT calculations were done for a ^{235}U enrichment of 2.30% instead of 2.35% (Fuel Specifications in Appendix A indicate 2.35 + 0.03%).

The low value used for the enrichment has no appreciable consequence in terms of k_{eff} or power distribution in the single region experiments. However, this 2.5% understatement of the number of ^{235}U atoms results in a similar underestimate of the UO_2-2.35% ^{235}U rod power with respect to the other fuel types in the multiregion loadings. This effect is not present

TABLE XIX. Multiregion Configurations - Variations in Theory-Experiment Agreement Produced by Changes in the Power Intercalibration Factor Between UO_2-2.35% ^{235}U and UO_2-2 wt% PuO_2 Fuel.

		UO_2-2.35% ^{235}U Rod Power Increased by 3.67%			Rod Power Increased by 2%
Case	σ_{RPD},(1) % from Tables XVI and XVII	Rod Power Discrepancy, % UO_2-2 wt% PUO_2 Rods Only	Rod Power Discrepancy, % UO_2-2.35% ^{235}U Rods Only	Modified σ_{RPD} %	Modified σ_{RPD} %
53	2.69	0.32 ± 1.51	-1.06 ± 0.54	1.42	1.90
54	2.16	0.16 ± 1.12	0.12 ± 1.47	1.23	1.46
56	3.30	1.36 ± 2.35	-0.30 ± 1.59	2.25	2.62
57	1.94	3.40 ± 1.40	3.88 ± 0.60	1.10	1.23
58	1.57	3.93 ± 1.44	3.93 ± 0.61	1.10	1.39
62	3.36	7.30 ± 1.58	4.73 ± 1.02	1.80	2.47
63	2.00	1.88 ± 1.23	2.40 ± 1.38	1.33	1.42
64	2.13	4.90 ± 1.30	4.95 ± 0.91	1.06	1.35
66	2.30	4.74 ± 2.85	4.90 ± 0.92	1.66	1.79
67	1.72	1.52 ± 2.08	2.60 ± 0.79	1.35	1.28
68	1.28	0.29 ± 2.16	4.39 ± 0.73	2.26	1.68

1. σ_{RPD} = *Standard deviation of rod power discrepancies for all regions of the configuration.*

in THERMOS/BATTLLE-HRG calculations (Cases 56, 64, and 68) where the proper enrichment was used.

The last columns of Tables XVI and XVII show the standard deviations of the modified rods power discrepancy when allowances were made for the 2.5% error in the ^{235}U content.

It is interesting that such a small error, which can only be measured with a careful isotopic analysis, can be detected by a theory-experiment comparison.

A similar consideration holds true for the theory-experiment comparison for Composite Element 1 with the UO_2-2 wt% PuO_2 driver. Here the situation is complicated by the fact that three different types of fuel are present. It can be seen in Table D-3 that the average loading discrepancy is degraded by the 5 to 7% underestimate of the power from the UO_2-0.9 wt% PuO_2 rods. It was felt that the previously observed nonhomogeneity of these fuel rods accounted for the discrepancy either through the power intercalibration correction or the actual gamma scanning. The overall quality of the theory-experiment comparison is comparable to the other experiments when the UO_2-0.9 wt% PuO_2 rods are excluded.

CONFIGURATIONS WITH POISON RODS

Power distribution and critical measurements were made for two basic 9 x 9 single region configurations containing the Boral cruciform blade; i.e., 325 UO_2-2 wt% PuO_2 fuel rods (Figure B-15) and 573 UO_2-2.35% ^{235}U fuel rods (Figure B-16). About 40 fuel rods were gamma scanned in each configuration. The cruciform was off-center from the 9 x 9 element as shown in Figures 2 and 5 because insufficient fuel rods of either type were available to provide critical loadings with the blade in the center of the loading. This nonsymmetrical condition was the source of many troubles in the calculations.

The usual theories adopted for calculations with a cruciform blade in the core are generally extensions and reinterpretations of the Milne problem; i.e., the poison is treated as a boundary condition in a diffusion problem, where an appropriate extrapolation distance is derived using transport theory.

When the net neutron current across the rod is zero; i.e., if the rod is placed in the center of symmetry of the reactor, one can assume that on the boundary of the rod the following relationship holds:

$$\frac{D}{\phi} \text{grad}_n \phi = - C,$$

where, D is the diffusion coefficient in the medium surrounding the rod;

grad_n is the normal component of the gradient;

C is the "absorbance" factor for the blade;

$$C = \frac{D}{d} \geq 0;$$

where, d is the extrapolation distance of the rod.

$$C = C_o(1-P)/(1+P),$$

where, P is the transmission probability of a neutron across the blade. When the rod is black, P = 0; thus $C = C_o$ = 1/(3 x 0.71) = 0.4695.

In PRCF experiments this theory is not valid for two reasons:

- The net current across the rod is not zero;
- The rod has a nonzero scattering cross section.

In spite of these conditions, the theory was applied to the PRCF experiments. The transmission probability and the "absorbance" C of the Boral blade were calculated (see Appendix G). The results are:

$$C_1 = 0$$

$$C_2 = 0.013$$

$C_3 = 0.205$

$C_4 = 0.4695$

These constants were used in the UO_2 core. The calculations were repeated putting $C_2 = 0.25$ (Case 72), and $C_3 = 0.3$ (Case 73).

The geometrical detail used in the blade calculations was somewhat different from the clean core calculations, owing to the fact that only 3025 mesh points were allowed in the version of EXTERMINATOR 2 which was used.

Due to this limitation, a cell description of 4 meshes was used in and around the water gaps, while 1 mesh was used elsewhere. It is difficult to evaluate the effect of the less detailed geometry; however, it was considered adequate since the nonuniformities in the loading were sufficiently described. In the water between the fuel and the poison rod, one or two (Case 74) extra meshes were used.

Some results of the calculations are compared to experimental results in Table XX. The detailed results are shown in Appendix B (Tables B-15 and B-16).

From Table XX, one can see that the agreement in k_{eff} is good, while the agreement in power distribution is bad. The power from the fuel rod next to the cruciform (toward core center) is overestimated by 30% and the power from the fuel rod opposite to it is underestimated by about 25%. The use of an artificially increased C_3 (epithermally "blacker" rod) produces only a slight improvement of the agreement (Cases 72 and 73 of Table XX).

This disagreement is attributed to a "lack of communication" across the poison blade. It is not valid to describe a cruciform as a boundary condition in the fast energy groups, when the cruciform is not in a central position.

TABLE XX. Synopsis of Theory-Experiment Comparisons in Single Region Configurations with Boral Cruciform Blade.

Case	Boundary Group 1	Absorbance Constant C_3	Fuel Type	k_{eff}	Δk on Rod Worth, milli-k	Rod Power Discrepancy, %	
						Rod 17	Rod 18
71	Yes	0.205	UO_2	1.0037	-1.5	+31%	-26%
72	Yes	0.25	UO_2	1.0027	-0.5	+25%	-32%
73	Yes	0.3	UO_2	1.0018	+0.4	+20%	-38%
74	No	0.205	UO_2	0.9994	+2.8	+18%	-10%
75	No	0.205	UO_2-PuO_2	1.0039	-2.1	+22%	-20%(1)

1. *The power measurement from Rod 18 was considered nonreliable; here the result from Rod 19 is shown.*

The poison rod acts as a neutron transmitter (from the central high flux regions to the core boundary), while the null derivative condition produces a "dam effect". This effect acts in two ways:

- It effectively reflects neutrons in the core, thereby increasing the value of k_{eff};
- It produces a source of epithermal and thermal neutrons which is higher than the real one, causing the power in the central regions of the core to be overestimated.

Increasing the value of C_3, shown in Cases 72 and 73, decreases the power around the cruciform in such a way that the rod power discrepancy is decreased for Rod 17 but increased for Rod 18.

In Case 74 of Table XX, the zero derivation condition on the poison was removed for the first group and the cruciform was treated as a diffusive region in the Group 1. One can see that the removal of the boundary derivative for Group 1 decreases k_{eff} and also improves the overall agreement between calculations and experiments. This, of course, is not sufficient because the "dam effect" is still present in Groups 2 and 3. The only UO_2-PuO_2 cruciform blade calculation was Case 75. It was made using the same conditions as Case 74.

The results for the two cruciform configurations were comparable, even though it appeared that the overall quality of the UO_2-PuO_2 experiment was not equal to that of the UO_2 experiment.

REFERENCES

1. B.J. Toppel, P.J. Vogelberger, Jr., and E.A. Wimunc. Safety Analysis Associated with the Plutonium Recycle Experiment in EBWR, ANL-6841, Argonne National Laboratory, Argonne, Illinois. November 1964.

2. B.J. Toppel and R. Avery. Some Physics Aspects of the Plutonium Experiment in EBWR, ANL-7019, Argonne National Laboratory, Argonne, Illinois. April 1965.

3. R.C. Liikala, V.P. Jenquin, and W.A. Reardon. The PuO_2-UO_2 Experiment in EBWR, BNWL-126, Battelle-Northwest, Richland, Washington. June 1965.

4. P.H. Kier. Analysis of the Initial Critical Experiments of the EBWR Plutonium Recycle Program. ANL-7368, Argonne National Laboratory, Argonne, Illinois. August 1967.

5. D.E. Christensen and E.S. Murphy. Determination of Relative Burnup by Gamma Scanning EBWR Fuel Rods, BNWL-653, Battelle-Northwest, Richland, Washington. April 1968.

6. R.P. Matsen. EBWR Burnup Data, BNWL-978, Battelle-Northwest, Richland, Washington. November 1968.

7. E.S. Murphy, G. Manca, and D.E. Christensen. Nondestructive Analysis of Fuel Irradiated in the EBWR by Gamma Scanning, BNWL-1005, Battelle-Northwest, Richland, Washington April 1969.

8. R.E. Grajek and K.E. Freese. In-Core Activation Traverses During the Plutonium Recycle Experiment in the Experimental Boiling Water Reactor at Power Levels of 35 to 70 MW, ANL-7414, Argonne National Laboratory, Argonne, Illinois. July 1968.

9. S. Lopez and M. Michelini. Physical Follow-Up of EBWR Operation by Nuclear Codes Developed by C.N.E.N., 1st Part Analysis of the Initial Critical Experiments, RT/FI (68) 22, Italy, Comitato Nazionale per l'Energia Nucleare, Rome. 1968.

10. N. Pacilio. A Survey of Reactor-Noise Time-Analysis Methods, BNWL-875, Battelle-Northwest, Richland, Washington. August 1968.

11. N. Pacilio. Reactor-Noise Analysis in the Time Domain, TID-24512, Division of Technical Information Extension, U.S. Atomic Energy Commission, P. O. Box 62, Oak Ridge, Tennessee. April 1969.

12. G. Buffoni, and S. Lopez. Il Programma RIBOT, C.N.E.N. Doc. Int. L.F.C.R. (66) 26. 1966.

13. P. Loizzo. RIBOT: A Physical Model for Light-Water Lattices Calculations, BNWL-735, Battelle-Northwest, Richland, Washington. February 1968.

14. G. Buffoni, S. Lopez, and I. Maganzani. BURNY - Un Programma di Burn-up a due Dimensioni, C.N.E.N. RT/FI (67) 8. 1967.

15. G. Buffoni, P. Loizzo, S. Lopez, and M. Petilli. Burn-up of Pressurized or Boiling Water Reactor, C.N.E.N. RT/FI (67) 28. 1967

16. N. Pacilio. "Statistical and Pulsed Experiments in Organic Moderated and Reflected Assemblies," Energia Nucleare. Vol. 15, p. 129. 1968.

17. N. Pacilio. "The Polya Model and the Distribution of Neutrons in a Steady-State Reactor," Nuclear Science and Engineering, Vol 26, p. 565. 1966.

18. G.D. Seybold. "Users Aid: Programs Learn and Likely," BNWL-1057, Battelle-Northwest, Richland, Washington. May 1969.

19. J.L. Carter, Jr. "Effective Cross-Sections for Resonances in HRG," and "Computer Code Abstracts," Reactor Physics Department Technical Activities Quarterly Report, July, August, September, 1966, BNWL-340, Battelle-Northwest, Richland, Washington. October 15, 1966.

20. D.R. Skeen and L.J. Page. THERMOS/BATTELLE: The Battelle Version of the THERMOS Code, BNWL-516, Battelle-Northwest, Richland, Washington. September 1967.

21. T.B. Fowler, M.L. Tobias, and D.R. Vondy. Exterminator-2: A FORTRAN-IV Code for Solving Multigroup Neutron Diffusion Equations in Two Dimensions, ORNL-4078, Oak Ridge National Laboratory. April 1967.

22. D.R. Skeen and W.L. Purcell. "Program HTH," Reactor Physics Department Technical Activities Report, July, August, September 1967, BNWL-634, Battelle-Northwest, Richland, Washington. February 1968.

23. C.H. Westcott, et al. "A Survey of Values of the 2200 m/s Constants for Four Fissile Nuclides," Atomic Energy Rev., Vol. 3, no. 2, p. 3-60. 1965.

24. J.J. Schmidt. Neutron Cross Section for Fast Reactor Material, Part 1: Evaluation, KFK-120 (E-ANDC-E-35U) European-American Nuclear Data Committee. February 1966

25. A. Galati. "The Metastatic Method in Nuclear Reactor Core Kinetics Calculations," Nuclear Science and Engineering, Vol. 37, p.30. 1969.

26. W.H. Arnold, JR. "Two Group Calculation of Prompt Neutron Lifetime," Nuclear Science and Engineering, Vol. 4, p. 598. 1958.

27. B.E. Simmons. "The Dynamic Reactivity Interpretations of Pulsed Neutron Measurements." Nuclear Science and Engineering, Vol. 5, p. 254. 1959.

28. H. Hurwitz, Jr., R. Ehrlick. Progress in Nuclear Energy, Series 1, p. 363. 1956.

APPENDIX A

REACTIVITY MEASUREMENTS

J. B. Edgar and L. D. Williams

APPENDIX A

REACTIVITY MEASUREMENTS

J. B. Edgar and L. D. Williams

The numbers of fuel rods and the critical moderator heights for each of the investigated loadings are summarized in Table A-I. With exception of the loadings with the cruciform control blade installed in the core, quarter core symmetry was maintained to simplify calculations. The excess reactivity shown for each loading in the same table is for a clean, fully reflected core. The experimentially determined moderator worth curve seen in Figure A-1 was valid for both the UO_2-PuO_2 and UO_2 loadings. Diagrams of the single region loadings can be seen in Appendix B and the multiregion loadings in Appendix D.

Since the presence of the followers on the reflector sheets was observed to have an effect on the critical loading, their reactivity worth was measured in different positions in the regular and basic 9 × 9 single region configurations for both UO_2-2.35% ^{235}U and the UO_2-2 wt% PuO_2 fuel. From these results the effects of followers for all other core configurations were inferred. In the regular UO_2-2 wt% PuO_2 core with the followers in the Position 4* - one lattice unit from the fuel perimeter, the reactivity for the loading was increased by 1.33 milli-k by the presence of the followers. In the UO_2-2.35% ^{235}U basis 9 × 9 core, followers in Position 2 - adjacent to the fuel perimeter - were found to increase the core reactivity by 0.72 milli-k.

The uncertainty associated with each loading excess reactivity cannot be rigorously defined because in most cases the reflector sheet effect has been inferred from the four measurements outlined above. For this reason, each clean reactivity measurement, with exception of the loadings where the sheets

---

* *Sheet Position 1 is the farthest from the core center and Position 4 is the closest.*

were actually measured, has had its assigned confidence interval increased by ±0.1 milli-k over that of the excess reactivity measured with the sheets in place.

The control rod, described earlier in the text did not require a reactivity adjustment because the fuel followers were exchanged to match the fuel being used in the loading.

The specifications for each type of fuel used in these experiments are listed in Figures A-2 through A-5.

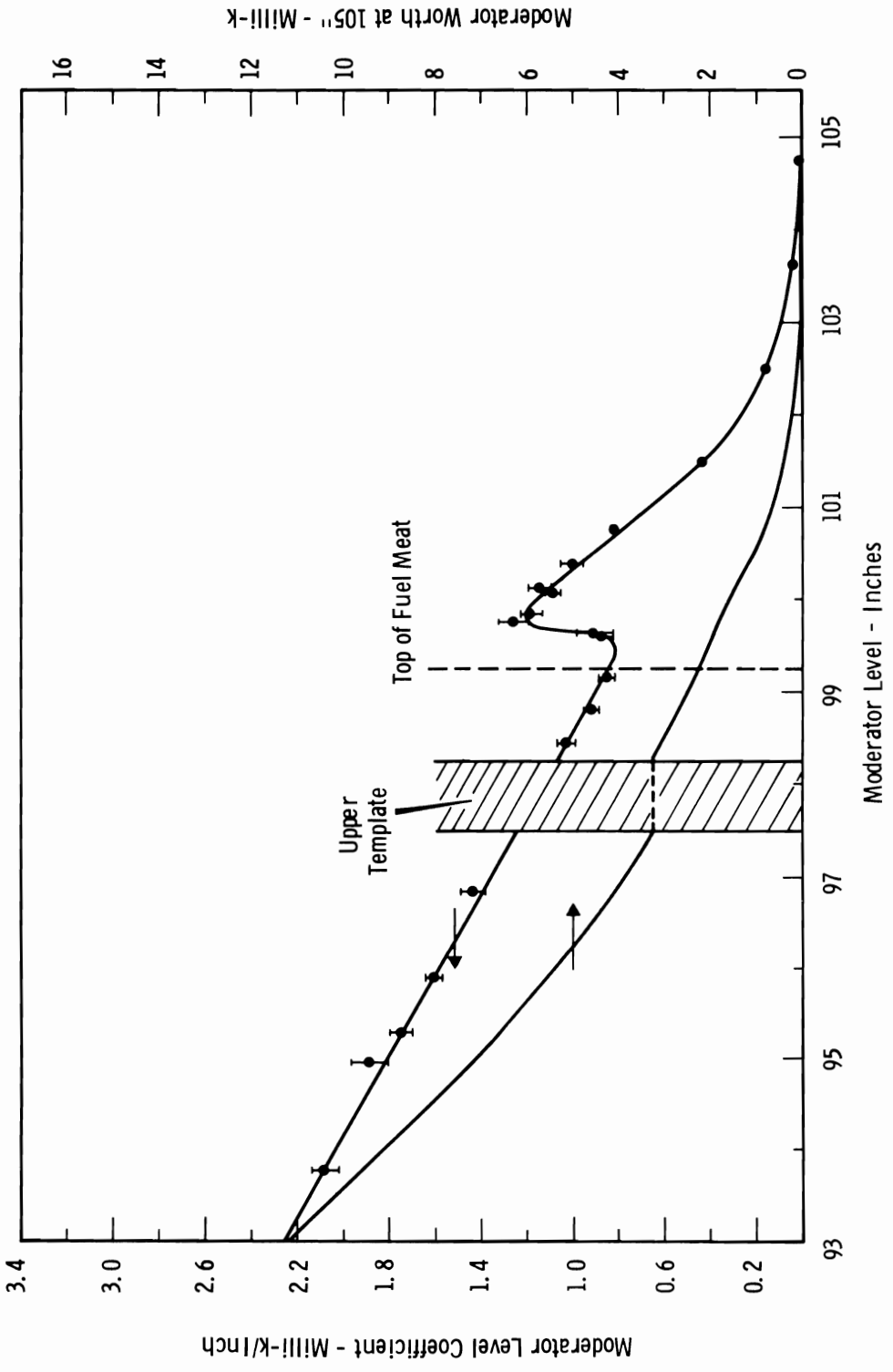

FIGURE A-1. MODERATOR LEVEL SENSITIVITY AND WORTH

TABLE A-1. Experimental Single and Multiregion Loading Summary.

Single Region Loadings	No. of Elements	Critical Moderator Level, in.	Inferred Excess Reactivity, Clean and Fully Reflected, milli-k
UO_2-2 wt% PuO_2 (8 % ^{240}Pu):			
Regular	321	99.70	0.61 ± 0.1
Water Hole	320	98.00	2.00 ± 0.1
Water Slab	302	94.45	6.75 ± 0.4
Water Cross	284	95.31	5.43 ± 0.4
Basic 7 × 7	249	96.50	3.77 ± 0.2
Basic 9 × 9	257	94.27	7.82 ± 0.1
Basic 9 × 9 + Voids	289	100.40	0.14 ± 0.2
Basic 9 × 9 + B_4C Blade	325	98.04	2.24 ± 0.3
UO_2-2.35% ^{235}U:			
Regular	385	97.02	3.19 ± 0.2
Water Hole	384	97.51	2.54 ± 0.2
Water Slab	408	98.81	1.75 ± 0.3
Water Cross	420	99.54	1.04 ± 0.2
Basic 7 × 7	461	99.79	1.04 ± 0.1
Basic 9 × 9	453	97.34	2.72 ± 0.2
Basic 9 × 9 + Voids	477	97.22	2.95 ± 0.3
Basic 9 × 9 + B_4C Blade	573	98.86	1.75 ± 0.3
Multiregion Loadings*			
UO_2-2 wt% PuO_2 (8% ^{240}Pu) Driver:			
Basic 9 × 9, UO_2 Element	301	95.38	6.76 ± 0.3
Basic 7 × 7, UO_2 Element	301	94.43	7.73 ± 0.3
Basic 7 × 7 Pu(24) Element	289	94.88	5.11 ± 0.3
11 × 11, UO_2 Element	329	98.03	2.51 ± 0.2
Basic 9 × 9, Composite Element 1	269	97.53	2.82 ± 0.2
Basic 9 × 9, Composite Element 2	265	99.67	1.44 ± 0.1
UO_2-2.35% ^{235}U Driver:			
Basic 9 × 9, Pu(8) Element	373	96.30	3.85 ± 0.2
11 × 11, Pu(8) Element	373	96.92	3.27 ± 0.2
Basic 7 × 7, Pu(8) Element	389	98.06	2.17 ± 0.2
Basic 9 × 9, Composite Element 1	397	97.18	2.63 ± 0.2
Basic 9 × 9, Composite Element 2	405	97.63	2.21 ± 0.2

* *UO_2 = UO_2-2.35% ^{235}U*
Pu(8) = UO_2-2 wt% PuO_2 (8% ^{240}Pu)
Pu(24) = UO_2-2 wt% PuO_2 (24% ^{240}Pu)
Composite 1 = UO_2-PuO_2 element containing fuel rods with 0.9 wt%, 2 wt%, and 4 wt% PuO_2 enrichments
Composite 2 = Element containing Pu(8) and UO_2 fuel rods

FUEL SPECIFICATIONS: UO_2 - 2.35% ^{235}U

FUEL RODS

1. ROD DIMENSIONS

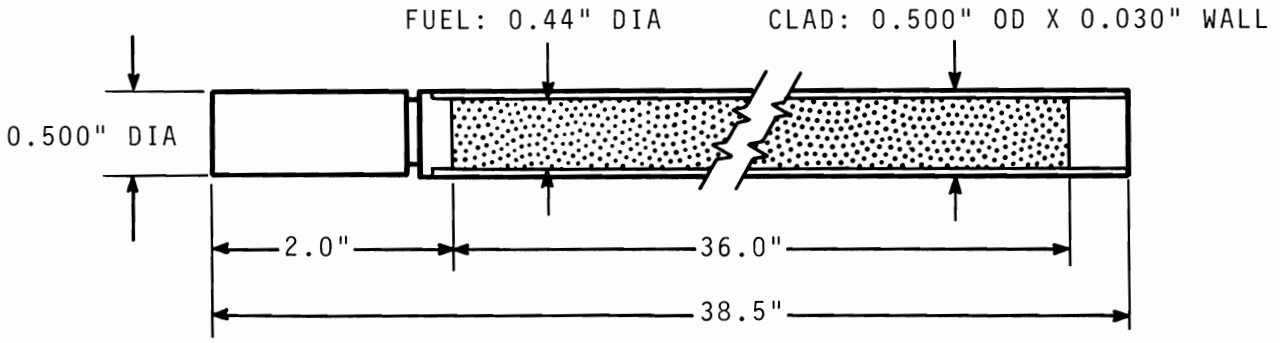

FIGURE A-2

2. CLADDING: 6061 ALUMINUM TUBING SEAL WELDED WITH A LOWER END PLUG OF 5052-H32 ALUMINUM AND A TOP PLUG OF 1100 ALUMINUM.
3. TOTAL WEIGHT OF LOADED FUEL RODS: 917 GM (AVERAGE).

FUEL LOADING

1. FUEL MIXTURE VIBRATIONALLY COMPACTED.
2. 825 GM OF UO_2 POWDER/ROD. 726 GM OF U/ROD, 17.1 GM OF ^{235}U/ROD.
3. ENRICHMENT - 2.35 $\pm$ 0.03% ^{235}U.
4. FUEL DENSITY - 9.20 GM/CM^3 (84% THEORETICAL DENSITY)

FUEL SPECIFICATIONS: UO_2 - 0.9 WT% PuO_2

FUEL RODS

1. ROD DIMENSION

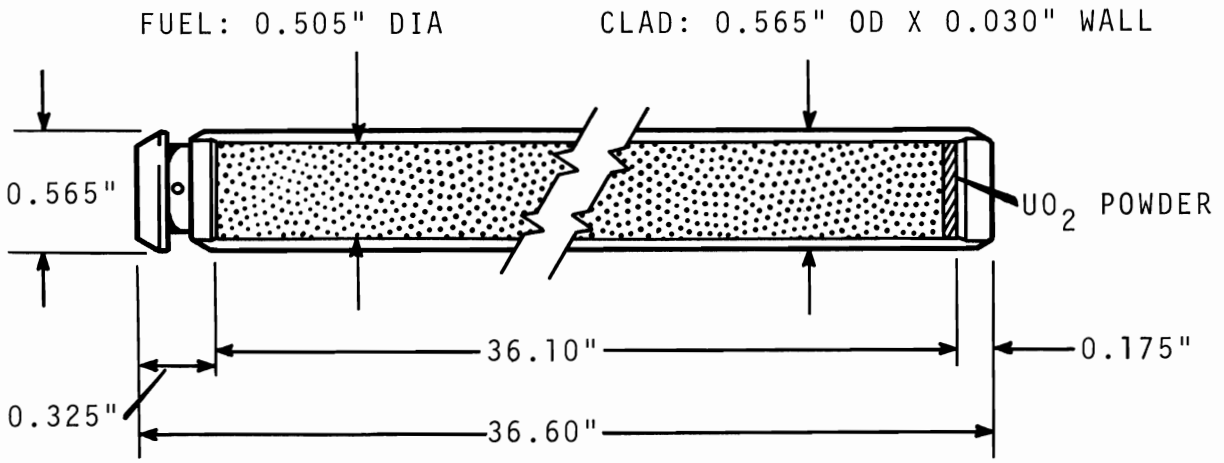

FIGURE A-3

2. CLADDING: ZIRCALOY-2 TUBING WITH PLUGS SEAL WELDED AT BOTH ENDS.
3. TOTAL WEIGHT OF LOADED FUEL RODS - 1316 GMS (AVERAGE).

FUEL LOADINGS

1. PuO_2 MIXED IN DEPLETED UO_2 AND VIBRATIONALLY COMPACTED.
2. 1107 GM OF UO_2-PuO_2 MIX/ROD.
3. CHEMICAL COMPOSITION WT %: Pu/PuO_2 = 88.2 U/UO_2 = 88.0
   Pu/MIX = 0.766
4. PuO_2 IS 0.868 WT% OF TOTAL MIXTURE.
5. FUEL DENSITY - 9.38 GM/CC (~86% THEORETICAL DENSITY)
6. UO_2 POWDER AT THE END OF FUEL COLUMN.
7. ISOTOPIC COMPOSITION.

PLUTONIUM - ATOM %		URANIUM - ATOM %	
92.139 ± 0.050	^{239}Pu	0.005 ± 0.001	^{234}U
7.241 ± 0.055	^{240}Pu	0.234 ± 0.002	^{235}U
0.595 ± 0.005	^{241}Pu	0.006 ± 0.0005	^{236}U
0.025 ± 0.001	^{242}Pu	99.755 ± 0.002	^{238}U

FUEL SPECIFICATIONS: UO_2 - 2 WT% PuO_2

FUEL RODS

1. ROD DIMENSIONS

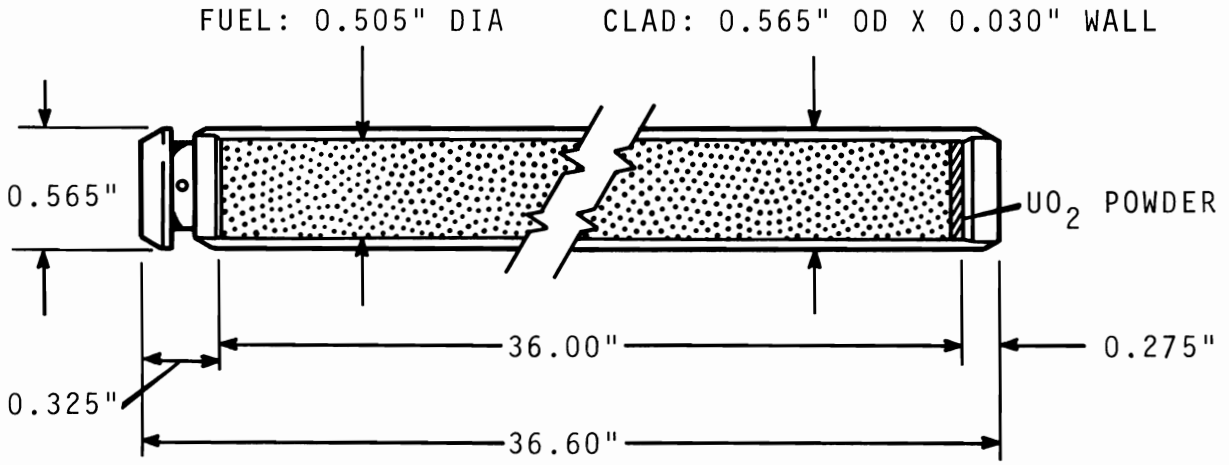

FIGURE A-4

2. CLADDING: ZIRCALOY-2 TUBING WITH PLUGS SEAL WELDED AT BOTH ENDS.
3. TOTAL WEIGHT OF LOADED FUEL RODS: 1340 GMS (AVERAGE)

FUEL LOADINGS

1. PuO_2 MIXED IN NATURAL UO_2 AND VIBRATIONALLY COMPACTED.
2. 1128 GMS OF UO_2-PuO_2 MIX/ROD.
3. PuO_2 IS 2 WT% OF TOTAL MIXTURE.
4. PuO_2 - 22.56 GMS/ROD.
5. Pu - 19.85 GMS/ROD (AVERAGE).
6. NATURAL U.
7. FUEL DENSITY - 9.54 GM/CC (~87% THEORETICAL DENSITY).
8. UO_2 POWDER AT THE END OF FUEL COLUMN.
9. THE ISOTOPIC DISTRIBUTION OF PLUTONIUM IN THE TWO TYPES OF RODS REFERRED TO AS 8% AND 24% IS GIVEN BELOW:

1. 8% (NOMINAL) ^{240}Pu

ATOM PERCENT	
91.615	^{239}Pu
7.654	^{240}Pu
0.701	^{241}Pu
0.031	^{242}Pu

2. 24% (NOMINAL) ^{240}Pu

ATOM PERCENT	
71.762	^{239}Pu
23.503	^{240}Pu
4.08	^{241}Pu
0.656	^{242}Pu

FUEL SPECIFICATIONS: UO_2 - 4 WT% PuO_2

FUEL RODS

1. ROD DIMENSIONS

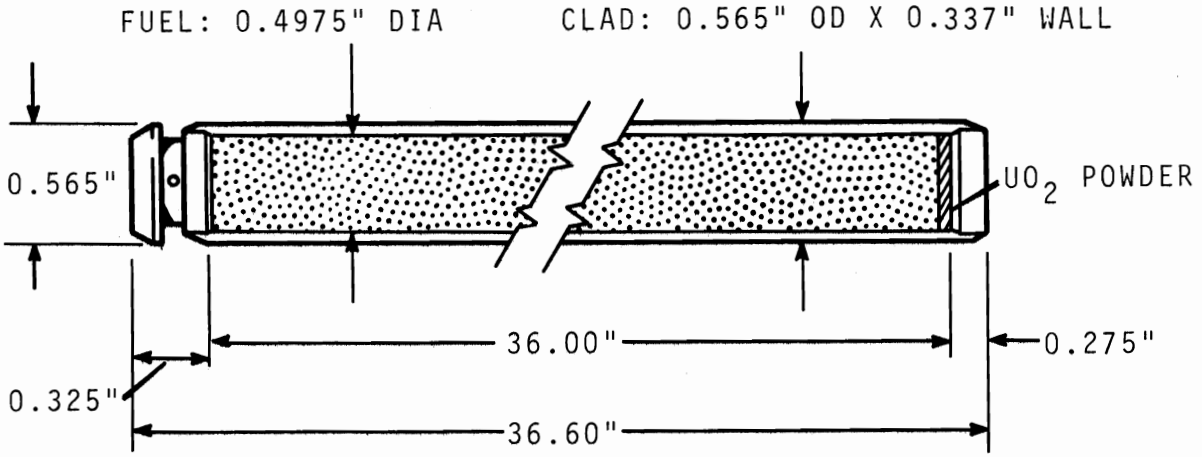

FIGURE A-5

2. CLADDING: ZIRCALOY-2 TUBING WITH PLUGS SEAL WELDED AT BOTH ENDS.
3. TOTAL WEIGHT OF LOADED FUEL RODS - 1327 GMS (AVERAGE).

FUEL LOADINGS

1. PuO_2 MIXED IN NATURAL UO_2 AND VIBRATIONALLY COMPACTED.
2. 1084.5 GM OF MIX/ROD.
3. CHEMICAL COMPOSITION WT %: Pu/PuO_2 = 88.1 U/UO_2 = 88.0
   Pu/MIX = 3.506.
4. PuO_2 IS 3.98 WT% OF TOTAL MIXTURE.
5. FUEL DENSITY = 9.46 GM/CC (~86% THEORETICAL DENSITY).
6. UO_2 POWDER AT THE END OF EACH FUEL COLUMN.
7. ISOTOPIC COMPOSITION

PLUTONIUM - ATOM%

0.28	^{238}Pu
75.38	^{239}Pu
18.10	^{240}Pu
5.08	^{241}Pu
1.15	^{242}Pu

APPENDIX B

SINGLE REGION POWER DISTRIBUTION MEASUREMENTS AND CALCULATIONS

P. Loizzo, R. Martinelli and L. D. Williams

APPENDIX B

SINGLE REGION POWER DISTRIBUTION MEASUREMENTS AND CALCULATIONS

P. Loizzo, R. Martinelli and L. D. Williams

In this section, experimental and theoretical power distributions are presented for eight single region configurations investigated with the UO_2-2.35% ^{235}U and UO_2-2 wt% PuO_2 (8% ^{240}Pu) fuel rods. The techniques employed for the experimental measurements were discussed earlier in the text. Since these loadings contained only one type of fuel, the relative gamma distribution across the various loadings directly reflected the power profiles of the cores. In all cases, the gamma activity measurements were for gammas with energies greater than 0.5 MeV.

Where possible, at least three symmetrical fuel rods were measured for each point of interest. The experimental uncertainty for a given location has been defined as one half the the maximum dispersion of the data from symmetric rods. These uncertainties for locations where symmetry was checked provided a method to determine the relative accuracy of the experimental measurements. The relative accuracy of the experiment (RAE) has been defined as the average of the experimental uncertainties from all locations in a given loading:

$$RAE = \frac{1}{N} \sum_{i=1}^{N} \left(\frac{X_{max} - X_{min}}{X_{ave}} \right)_i$$

where N = number of locations for the loadings where symmetric rods were measured

$$\left(\frac{X_{max} - X_{min}}{X_{ave}} \right)_i = \text{relative (\%) uncertainty of a symmetry measurement.}$$

The loading maps and experimental power distributions for the single region loadings are included in this section. The power distribution results on the loading maps do not include the individual rod power but the average of symmetric rods. The individual rod results can be seen in the tables where experimental and calculational results are compared. The numbers in the fuel position on the loading maps are index numbers used during the calculations and are used as reference numbers for the experimental-theoretical correlation; they have no other significance. The blackened circles in the lattice positions on the loading maps denote the absence of fuel rods and the presence of water.

The tables following each loading map include the individual rod power results and theoretical rod power results from calculational models described in the text. An asterisk shows the normalization point between theory and experiment. Each experimental observation, instead of the average value from symmetrical points, was compared to calculations. This practice placed more importance on the locations where symmetry checks were made. In most measurements, a few of the experimental points had to be discarded because they were out of the range of experimental error (set at 2%) when compared to symmetrical rods. These values are enclosed in parentheses ( ). A few points were also discarded because their theory-experiment discrepancies were significantly different from these of the adjacent rods and the rods were not in unusual spots where a large difference would be expected (i.e., water gaps, poison or any other discontinuities in the lattice.) These values are enclosed by brackets [ ]. Typically, out of 25 to 35 experimentally measured rods, two or three were discarded for the first reason and one or two for the latter. The discards are believed to be primarily due to non-homogeneities of the fuel material in the fuel rods.

Rod power calculations, employing theoretical models described in the text, are compared to experimental measurements in Tables B-1

through B-16 for single region loadings. Tables B-15 and 16 are for UO_2-2 wt% PuO_2 and UO_2-2.35% ^{235}U loadings, respectively, with the Boral cruciform blade in place.

The calculational models are compared against each other for particular loadings by examination of the discrepancy from experimental values. If δ_i* is the relative discrepancy between theory and experiment for the i^{th} position, the average discrepancy and standard deviation for a loading or a group of fuel rods is defined as:

$$\overline{\delta} = \frac{\Sigma_i \delta_i}{N} \pm \sqrt{\Sigma_i (\overline{\delta} - \delta_i)^2/(N - 1)}$$

where N equals the number of rod measurements. The "goodness of fit" of rod powers calculated from a model is also compared for rods with dissimilar environments within the loading. This comparison provides a measure of how well a model describes critical areas such as voids, water gaps, etc., with respect to regions less severe from the calculational standpoint. These comparisons are seen in the tables as "Group Average δ".

There are two other theory-experiment discrepancies examined for the various loadings; both provide a measure of how well the maximum rod power is calculated. One describes the error of the maximum rod power compared to the average error for the loading while the other relates the error on the rod of maximum power to the average power error on the simulated fuel element (9 × 9, 7 × 7). These errors are designated as $\delta(P_{max}/P_{ave})$ and δF, respectively. The definition of these errors and their standard deviation is:

$$\delta(P_{max}/P_{ave}) \text{ or } \delta F = \left(\frac{1 + \delta_{max}}{1 + \overline{\delta}} - 1 \right) \pm \sqrt{\sigma^2_{\delta_{max}} + \sigma^2_{\overline{\delta}}}$$

* $\delta_i = \left(\frac{P_C - P_E}{P_E} \right)$, *where P_E is the experimental rod power and P_C is the calculated rod power normalized to the experimental values as explained in the text.*

where δ_{max} = discrepancy on maximum power rod, $\overline{\delta}$ = average discrepancy in entire loading for $\delta(P_{max}/P_{ave})$ and average discrepancy in the simulated element for δF. In spite of the lack of mathematical rigorousness, the definitions of "errors" and "standard deviations" given above, can be regarded as appropriate indexes of precision, from the point of view of the core designer. An arbitrary criterion was adopted for the normalization of the calculated power distribution, since the choice of different reference rods did not significantly affect the value of the "standard deviation of the fit".

The case numbers listed in the following tables for each calculational model are related to corresponding numbers used in Tables XI, XII, and XV and in the text.

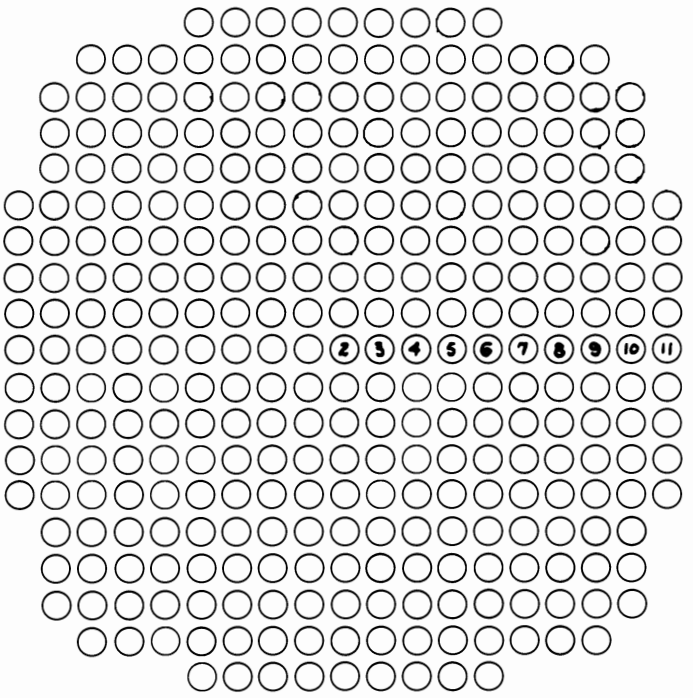

REGULAR, UO_2-2 WT% PuO_2 (8% ^{240}Pu)

Experimental Power Distribution:

Position No.	Relative Power
2	1.000
3	.987
4	.983
5	.926
6	.886
7	.825
8	.753
9	.688
10	.671
11	.860

Relative Accuracy of Experiment = 0.62%

FIGURE B-1

TABLE B-1. Experimental-Calculational Power Distribution Comparisons, Regular UO_2-wt% PuO_2 (8% ^{240}Pu)

Rod Location	Symmetry Points	Experimental Rod Power, Arbitrary Units	Case No. 17 St. RIBOT 4G - 4M** Set No. 1		Case No. 18 HTH, L.W.(1) 4G - 4M Set No. 12		Case No. 19 HTH, S.W.(2) 4G - 4M Set No. 13	
			Power	δ, %	Power	δ, %	Power	δ, %
2	1	1.000	*1.0	0	*1.0	0	*1.0	0
3	1	0.992	0.992	0	0.992	0	0.992	0
	2	0.983		0.9		0.9		0.9
	3	0.985		0.7		0.7		0.7
4	1	0.986	0.970	-1.6	0.970	-1.6	0.970	-1.6
	2	0.980		-1.0		-1.0		-1.0
5	1	0.922	0.933	1.1	0.933	1.1	0.933	1.1
	2	0.930		0.3		0.3		0.3
6	1	0.874	0.882	0.9	0.882	0.9	0.882	0.9
	2	0.900		-2.0		-2.0		-2.0
	3	0.884		-0.3		-0.3		-0.3
7		0.825	0.818	-0.8	0.818	-0.8	0.818	-0.8
8	1	0.759	0.745	-1.9	0.744	-2.0	0.744	-2.0
	2	0.747		-0.3		-0.4		-0.4
9	1	0.688	0.673	-2.2	0.671	-2.5	0.671	-2.5
	2	(0.710)		(-5.3)		(-5.6)		(-5.6)
	3	0.667		0.8		0.5		0.5
10	1	0.675	0.644	[-4.5]	0.642	[-4.8]	0.642	[-4.8]
	2	0.667		[-5.4]		[-5.7]		[-5.7]
11	1	0.859	0.857	-0.3	0.849	-1.2	0.849	-1.2
	2	0.861		-0.5		-1.5		-1.5
Loading Average δ, 18 points			(-0.34 ± 1.06)%		(-0.49 ± 1.13)%		(-0.49 ± 1.13)%	
K_{eff}		1.0006	1.0035		0.975		0.987	

1. *Leonard-Westcott, see text for details*
2. *Schmidt-Westcott, see text for details*

** *4G - 4M means 4-energy groups and 4(2 × 2) meshes per rod*

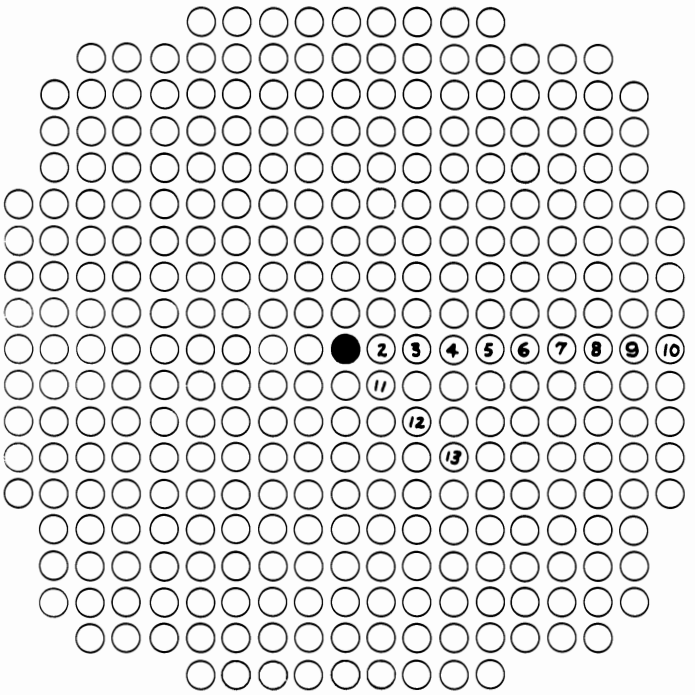

WATER HOLE, UO_2-2 WT% PuO_2 (8% ^{240}Pu)

Experimental Power Distribution:

Position No.	Relative Power
2	1.207
3	1.018
4	.956
5	.923
6	.832
7	.732
8	.678
9	.658
10	.856
11	1.068
12	.959
13	.861

Relative Accuracy of Experiment = 0.80%

FIGURE B-2

TABLE B-2. Experimental-Calculational Power Distribution Comparisons, Water Hole, UO_2-2 wt% PuO_2 (8% ^{240}Pu)

Rod Location	Symmetry Points	Experimental Rod Power, Arbitrary Units	Case No. 22 St. RIBOT 4G - 4M Set No. 1 Power	Case No. 22 St. RIBOT 4G - 4M Set No. 1 δ, %	Case No. 23 St. RIBOT 5G - 4M Set No. 1 Power	Case No. 23 St. RIBOT 5G - 4M Set No. 1 δ, %
2	1	1.206	*1.207	0.1	*1.207	0.1
	2	(1.177)		(2.5)		(2.5)
	3	1.208		-0.1		-0.1
3	1	1.020	1.024	0.4	1.017	-0.3
	2	1.017		0.7		0
	3	1.017		0.7		0
4	1	0.959	0.958	-0.1	0.951	-0.8
	2	0.954		0.4		-0.3
	3	(0.942)		(1.7)		(1.0)
5		0.923	0.901	[-2.4]	0.894	[-3.2]
6		0.832	0.834	0.3	0.828	-0.5
7		0.732	0.759	3.7	0.752	2.7
8		0.678	0.685	0.9	0.677	-0.2
9		0.658	0.656	-0.3	0.645	-2.0
10		0.856	0.872	1.9	0.867	1.3
11	1	1.073	1.096	2.1	1.091	1.7
	2	(1.117)		(-1.9)		(-2.3)
	3	1.064		3.0		2.5
	4	(1.051)		(4.4)		(3.8)
12	1	0.966	0.967	0.1	0.960	-0.6
	2	(0.998)		(-3.1)		(-3.6)
	3	0.952		1.6		0.9
13	1	(0.886)	0.887	(0.1)	0.880	(-0.7)
	2	0.861		3.0		2.2
	3	0.861		3.0		2.2
Loading Average δ, 18 points			(1.19 ± 1.29)%		(0.49 ± 1.32)%	
$\delta(P_{max}/P_{ave})$			(1.2 ± 1.3)%		(0.5 ± 1.3)%	
K_{eff}		1.0020	1.0048		1.0031	

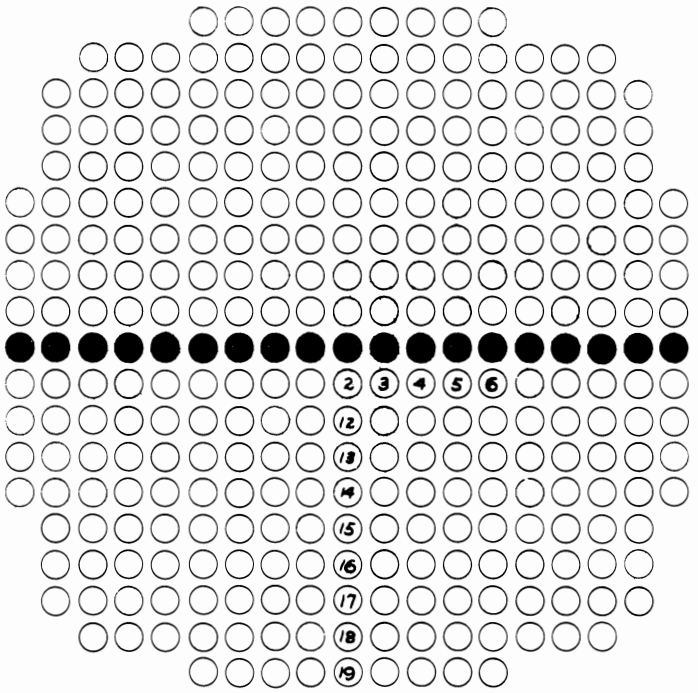

WATER SLAB, UO_2-2 WT% PuO_2 (8% ^{240}Pu)

Experimental Power Distribution:

Position No.	Relative Power
2	1.110
3	1.097
4	1.092
5	1.035
6	.990
12	.788
13	.690
14	.646
15	.603
16	.533
17	.490
18	.465
19	.606

Relative Accuracy of Experiment = 0.75%

FIGURE B-3

TABLE B-3. Experimental Calculational Power Distribution Comparisons, Water Slab, UO_2-2 wt% PuO_2 (8% ^{240}Pu)

Rod Location	Symmetry Points	Experimental Rod Power, Arbitrary Units	Case No. 24 St. RIBOT 4G - 4M Set No. 1 Power	Case No. 24 St. RIBOT 4G - 4M Set No. 1 δ, %	Case No. 25 St. RIBOT 5G - 4M Set No. 1 Power	Case No. 25 St. RIBOT 5G - 4M Set No. 1 δ, %
2	1	1.102	1.127	2.2	1.127	2.2
	2	1.118		0.8		0.8
3	1	(1.13)	1.118	(-1.1)	1.118	(-1.1)
	2	1.104		1.2		1.2
	3	1.090		2.5		2.5
	4	1.098		1.8		1.8
4	1	1.089	1.092	0.3	1.092	0.3
	2	1.091		0.1		0.1
	3	1.097		-0.5		-0.5
	4	1.091		0.1		0.1
5	1	1.040	1.050	0.9	1.049	0.9
	2	1.041		0.8		0.8
	3	1.034		1.5		1.5
	4	1.024		2.5		2.5
6	1	0.979	0.992	1.3	0.991	1.2
	2	1.003		-1.1		-1.2
	3	0.975		1.7		1.6
	4	1.003		-1.1		-1.2
Group Average δ, 17 points			(0.88 ± 1.13)%		(0.86 ± 1.14)%	
12	1	0.794	0.797	0.3	0.785	-1.1
	2	0.782		1.8		0.4
13	1	0.692	0.701	1.3	0.691	-0.2
	2	0.688		1.9		0.4
14	1	0.646	0.648	0.3	0.639	-1.1
	2	0.646		0.3		-1.1
15		0.603	0.598	-0.8	0.589	-2.3
16		0.533	0.543	1.9	0.535	0.3
17		0.490	0.490	0	0.481	-1.9
18		0.465	0.469	0.8	0.457	-1.6
19		0.606	0.623	2.7	0.614	1.4
Group Average δ, 11 points			(0.95 ± 1.05)%		(-0.62 ± 1.15)%	
Loading Average δ, 28 points			(0.91 ± 1.08)%		(0.28 ± 1.35)%	
$\delta(P_{max}/P_{ave})$			(0.6 ± 1.3)%		(1.2 ± 1.5)%	
K_{eff}		1.0068	1.0095		1.0088	

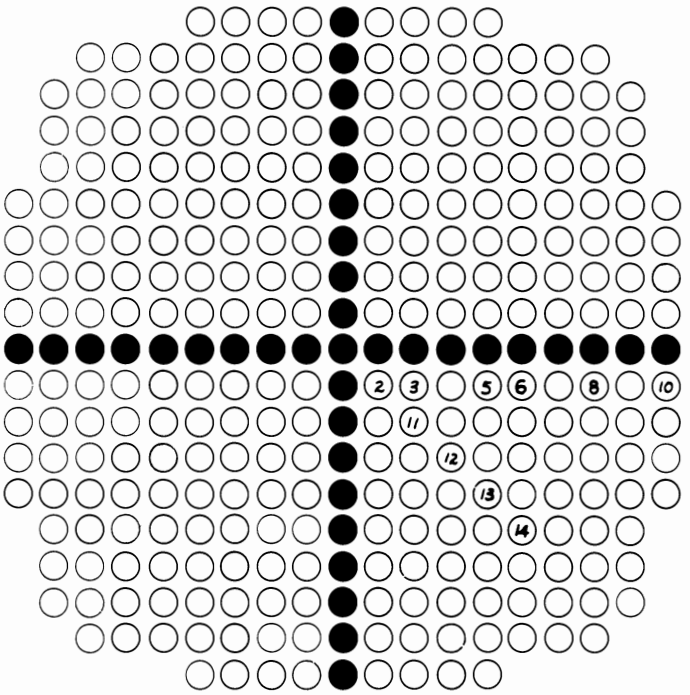

WATER CROSS, UO_2-2 WT% PuO_2 (8% ^{240}Pu)

Experimental Power Distribution:

Position No.	Relative Power
2	1.396
3	1.086
5	.904
6	.848
8	.684
10	.724
11	.771
12	.603
13	.516
14	.439

Relative Accuracy of Experiment = 1.25%

FIGURE B-4

TABLE B-4. Experimental-Calculational Power Comparisons, Water Cross, UO_2-2 wt% PuO_2 (8% ^{240}Pu)

Rod Location	Symmetry Points	Experimental Rod Power, Arbitrary Units	Case No. 26 St. RIBOT 4G - 4M Set No. 1 Power	δ, %	Case No. 27 St. RIBOT 5G - 4M Set No. 1 Power	δ, %	Case No. 28 St. RIBOT 4G - 9M Set No. 1 Power	δ, %	Case No. 29 Mod. RIBOT 4G - 9M Set No. 11 Power	δ, %
2	1	1.398	*1.396	-0.1	*1.396	-0.1	*1.396	-0.1	*1.396	-0.1
	2	1.389		0.5		0.5		0.5		0.5
	3	1.406		-0.7		-0.7		-0.7		-0.7
	4	1.391		0.4		0.4		0.4		0.4
3	1	1.089	1.069	-1.8	1.060	-2.7	1.067	-2.0	1.059	-2.8
	2	1.083		-1.3		-2.1		-1.5		-2.2
	3	1.097		-2.6		-3.4		-2.8		-3.5
	4	1.075		-0.6		-1.4		-0.8		-1.5
5	1	0.894	0.893	[-0.1]	0.887	[-0.8]	0.893	[-0.1]	0.886	[-0.9]
	2	0.892		[0.1]		[-0.6]		[0.1]		[-0.7]
	3	0.925		-3.5		-4.1		-3.5		-4.2
6	1	0.845	0.825	-2.4	0.819	-3.1	0.825	-2.4	0.819	-3.1
	2	0.851		-3.1		-3.8		-3.1		-3.8
	3	(0.829)		(-0.5)		(-1.2)		(-0.5)		(-1.2)
8	1	0.687	0.674	-1.9	0.666	-3.1	0.673	-2.0	0.667	-2.9
	2	(0.700)		(-3.7)		(-4.9)		(-3.8)		(-4.7)
	3	0.680		-0.9		-2.1		-1.0		-1.9
10	1	0.729	0.744	2.1	0.734	0.7	0.738	1.2	0.735	0.8
	2	(0.738)		(0.8)		(-0.5)		(0)		(-0.4)
	3	0.718		3.6		2.2		2.8		2.3
Group Average δ, 15 points			(-0.82 ± 1.93)%		(-1.52 ± 1.92)%		(-1 ± 1.74)%		(-1.51 ± 1.95)%	
11	1	0.769	0.770	0.1	0.753	-2.1	0.767	-0.3	0.750	-2.5
	2	0.775		-0.6		-2.8		-1.0		-3.2
	3	0.771		-0.1		-2.4		-0.5		-2.8
	4	0.770		0		-2.2		-0.4		-2.6
12	1	0.601	0.601	0	0.587	-2.4	0.599	-0.3	0.584	-2.8
	2	0.605		-0.7		-3.0		-1.0		-3.4
13	1	0.515	0.514	-0.2	0.503	-2.3	0.513	-0.4	0.500	-2.9
	2	0.513		0.2		-1.9		0		-2.5
	3	0.519		-1.0		-3.1		-1.2		-3.7
14	1	0.436	0.435	-0.2	0.426	-2.3	0.436	0	0.424	-2.8
	2	0.442		-1.6		-3.7		-1.4		-4.2
	3	0.438		-0.7		-2.7		-0.5		-3.1
Group Average δ, 12 points			(-0.4 ± 0.53)%		(-2.57 ± 0.51)%		(-0.58 ± 0.46)%		(-3.04 ± 0.51)%	
Loading Average δ, 27 points			(-0.63 ± 1.48)%		(-1.99 ± 1.54)%		(-0.81 ± 1.33)%		(-2.19 ± 1.66)%	
$\delta(P_{max}/P_{ave})$			(0.6 ± 1.6)%		(2.0 ± 1.6)%		(0.8 ± 1.4)%		(2.2 ± 1.7)%	
K_{eff}		1.0054	1.0104		1.0109		1.0092		1.0069	

1. Constants for group 3 (Σ_a, Σ_r, $\nu\Sigma_f$) were decreased by 10%

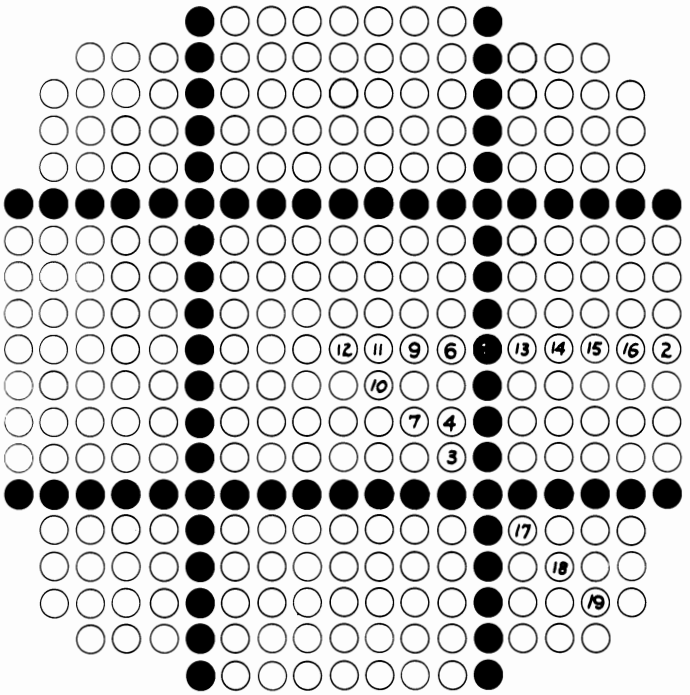

BASIC 7x7, UO_2-2 WT% PuO_2 (8% ^{240}Pu)

Experimental Power Distribution:

Position No.	Relative Power
12	.742
11	.736
9	.773
6	1.030
13	.945
14	.620
15	.482
16	.456
2	.595
10	.748
7	.823
3	1.339
4	1.086
17	1.056
18	.508
19	.421

Relative Accuracy of Experiment = (0.35%)

FIGURE B-5

TABLE B-5. Experimental-Calculational Power Distribution Comparisons, Basic 7 × 7, UO_2 wt% PuO_2 (8% ^{240}Pu)

Rod Location	Symmetry Points	Experimental Rod Power, Arbitrary Units	Case No. 30 St. RIBOT 4G - 4M Set No. 1 Power	Case No. 30 St. RIBOT 4G - 4M Set No. 1 δ, %	Case No. 31 St. RIBOT 5G - 4M Set No. 1 Power	Case No. 31 St. RIBOT 5G - 4M Set No. 1 δ, %
3	1	(1.306)	*1.340	(2.6)	*1.340	(2.6)
	2	1.336		0.3		0.3
	3	1.333		0.4		0.4
	4	1.349		-0.7		-0.7
4	1	(1.103)	1.094	(-0.8)	1.087	(-1.4)
	2	(1.064)		(2.8)		(2.1)
	3	(1.062)		(3.0)		(2.4)
	4	1.085		0.8		0.2
	5	1.089		0.4		-0.2
	6	1.081		1.2		0.5
	7	1.089		0.4		-0.2
	8	1.087		0.6		0
6		1.030	1.049	1.8	1.044	1.3
Group Average δ, 9 points			(0.58 ± 0.68)%		(0.18 ± 0.56)%	
7		0.823	0.842	2.2	0.826	0.3
9		0.773	0.794	2.8	0.780	1.0
10		0.748	0.755	0.9	0.742	-0.8
11		0.736	0.750	1.9	0.738	0.3
12		0.742	0.745	0.4	0.743	-1.1
Group Average δ, 5 points			(1.64 ± 0.98)%		(-0.06 ± 0.87)%	
2		0.595	0.620	4.3	0.612	2.8
13		0.945	0.947	0.2	0.946	0.1
14		0.620	0.620	0	0.609	-1.9
15		0.482	0.507	5.2	0.496	2.9
16		0.456	0.472	3.6	0.460	0.9
17		1.056	1.071	1.4	1.075	0.4
18		0.508	0.518	2.0	0.504	-0.7
19		0.421	0.439	4.2	0.425	0.8
Loading Average δ, 22 points			(1.56 ± 1.58)%		(0.30 ± 1.11)%	
$\delta(P_{max}/P_{ave})$			(-1.5 ± 1.7)%		(-0.3 ± 1.3)%	
δF			(-1.6 ± 1.2)%		(0 ± 1.1)%	
K_{eff}		1.0038	1.0080		1.0086	

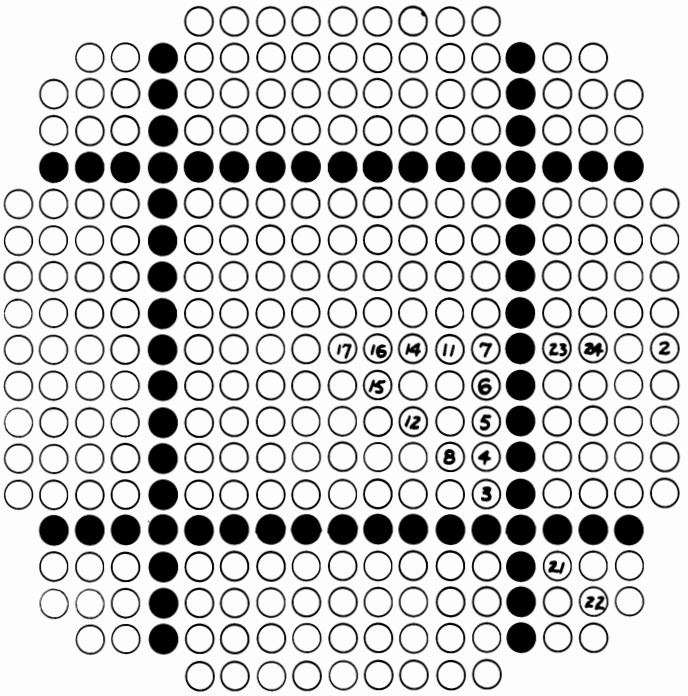

BASIC 9x9, UO_2-2 WT% PuO_2 (8% ^{240}Pu)

Experimental Power Distribution:

Position No.	Relative Power
17	1.000
16	.988
14	.984
11	1.012
7	1.305
23	1.148
24	.753
2	.818
15	.995
12	1.009
8	1.041
3	1.598
4	1.325
5	1.286
6	1.310
21	1.241
22	.686

Relative Accuracy of Experiment = 0.86%

FIGURE B-6

TABLE B-6. Experimental-Calculational Power Distribution Comparisons, Basic 9 × 9, UO_2-wt% PuO_2 (8% ^{240}Pu)

Rod Location	Symmetry Points	Experimental Rod Power Arbitrary Units	Case No. 1 St. RIBOT 5G - 9M Set No. 1		Case No. 2 St. RIBOT 5G - 4M Set No. 1		Case No. 3 St. RIBOT 5G - 1M Set No. 1		Case No. 4 St. RIBOT 4g - 9M Set No. 1		Case No. 5 St. RIBOT 4G - 4M Set No. 1		Case No. 6 St. RIBOT 4G - 1M Set No. 1		Case No. 7 St. RIBOT 2G - 9M Set No. 1		Case No. 8 BURNY 2G - 9M BNL-325		Case No. 9 BURNY(1) 2G - 9M KFK-120		Case No. 10 BURNY 2G - 4M BNL-325		Case No. 11 BURNY 2G - 1M BNL-325		Case No. 12 HTH, L.W.(2) 4G - 4M Set No. 12		Case No. 13 HTH, S.W.(3) G - 4M Set No. 13		Case No. 14 THERMOS - HRG(4) 4G - 4M Set No. 14		Case No. 15 St. RIBOT(5) 4G - 4M Set No. 1		Case No. 16 RIBOT, H.M.(6) 4G - 4M Set No. 15	
			Power	δ, %	Power	δ, %	Power	δ, %	Power	δ, %	Power	δ, %	Power	δ, %	Power	δ, %	Power	δ, %	Power	δ, %	Power	δ, %	Power	δ, %	Power	δ, %	Power	δ, %	Power	δ, %	Power	δ, %	Power	δ, %	Power	δ, %	Power	δ, %
3	1	1.583	*1.598	0.9	*1.598	0.9	*1.598	0.9	*1.598	0.9	*1.598	0.9	*1.598	0.9	*1.598	0.9	*1.598	0.9	*1.598	0.9	*1.598	0.9	*1.598	0.9	*1.598	0.9	*1.598	0.9	*1.598	0.9	*1.598	0.9	*1.598	0.9	*1.598	0.9
	2	1.582		1.0		1.0		1.0		1.0		1.0		1.0		1.0		1.0		1.0		1.0		1.0		1.0		1.0		1.0		1.0		1.0		1.0
	3	1.614		-1.0		-1.0		-1.0		-1.0		-1.0		-1.0		-1.0		-1.0		-1.0		-1.0		-1.0		-1.0		-1.0		-1.0		-1.0		-1.0		-1.0
	4	1.614		-1.0		-1.0		-1.0		-1.0		-1.0		-1.0		-1.0		-1.0		-1.0		-1.0		-1.0		-1.0		-1.0		-1.0		-1.0		-1.0		-1.0		-1.0
4	1	1.329	1.321	-0.6	1.321	-0.6	1.321	-0.6	1.33	0.1	1.329	0	1.328	-0.1	1.34	0.8	1.321	-0.6	1.322	-0.5	1.319	-0.8	1.314	-1.1	1.330	0.1	1.331	0.2	1.334	0.4	1.327	-0.1	1.359	2.2
	2	1.330		-0.7		-0.7		-0.7		-0.1		-0.1		-0.2		0.7		-0.7		-0.6		-0.8		-1.2		0.0		0.0		0.3		-0.2		2.1		3.3
	3	1.328		-0.5		-0.5		-0.5		0.1		0.1		0		0.9		-0.6		-0.5		-0.7		-1.0		0.1		0.2		0.4		0		2.3		3.5
	4	1.326		-0.4		-0.4		-0.4		0.3		0.2		0.1		1.0		-0.4		-0.3		-0.5		-0.9		0.3		0.4		0.6		0.1		2.5		3.5
	5	1.312		0.7		0.7		0.7		1.4		1.3		1.2		2.1		0.7		0.8		0.5		0.2		1.4		1.3		1.7		1.2		3.5		3.3
5		1.286	1.299	1.0	1.295	0.7	1.284	-0.2	1.305	1.5	1.312	1.2	1.293	0.5	1.309	1.8	1.300	1.1	1.303	1.3	1.297	0.8	1.280	-0.5	1.304	1.4	1.305	1.5	1.310	1.9	1.300	1.1	1.328	3.3
6		1.310	1.313	0.2	1.311	0.1	1.293	-1.3	1.320	0.8	1.319	0.7	1.299	-0.9	1.324	1.1	1.317	0.5	1.319	0.7	1.311	0.1	1.289	-1.6	1.319	0.7	1.320	0.8	1.326	1.2	1.313	0.2	1.339	2.2
7		1.305	1.321	1.2	1.319	0.7	1.299	-0.4	1.328	1.8	1.327	1.7	1.305	0	1.332	2.1	1.324	1.5	1.327	1.7	1.319	1.1	1.295	-0.8	1.328	1.8	1.328	1.8	1.334	2.2	1.321	1.2	1.346	3.2
Group Average δ, 12 points			(0.07 ± 0.85)%		(-0.01 ± 0.77)%		(-0.29 ± 0.76)%		(0.48 ± 0.92)%		(0.37 ± 0.83)%		(0.04 ± 0.76)%		(0.87 ± 1.00)%		(0.11 ± 0.92)%		(0.21 ± 0.95)%		(-0.03 ± 0.85)%		(-0.58 ± 0.84)%		(0.48 ± 0.90)%		(0.51 ± 0.86)%		(0.68 ± 1.03)%		(0.28 ± 0.80)%		(1.77 ± 1.52)%	
8		1.041	1.022	-1.8	1.023	-1.7	1.025	-1.6	1.042	0.1	1.042	0.1	1.042	0.1	1.035	-0.6	1.014	-2.6	1.018	-2.2	1.013	-2.7	1.007	-3.3	1.034	-0.6	1.037	-0.4	1.050	0.8	1.039	-0.2	1.102	5.8
11		1.012	1.004	-0.8	1.003	-0.9	0.990	-2.2	1.022	1.0	1.019	0.7	1.005	-0.7	1.017	0.5	0.999	-1.3	1.002	-1.0	0.993	-1.9	0.970	-4.2	1.011	-0.1	1.013	0.1	1.029	1.7	1.015	0.3	1.071	5.8
12		1.009	0.954	[-5.5]	0.951	[-5.7]	0.935	[-7.3]	0.971	[-3.8]	0.967	[-4.1]	0.950	[-5.8]	0.967	[-4.2]	0.950	[-5.8]	0.953	[-5.6]	0.943	[-6.5]	0.917	[-9.2]	0.956	[-5.3]	0.958	[-5.1]	0.976	[-3.3]	0.962	[-4.6]	1.018	0.9
14		0.984	0.968	-1.6	0.964	-2.0	0.941	-4.4	0.983	-0.1	0.978	-0.6	0.955	-2.9	0.979	-0.5	0.962	-2.1	0.967	-1.8	0.956	-2.9	0.921	-6.4	0.968	-1.6	0.970	-1.4	0.988	0.4	0.973	-1.1	1.025	4.2
15		0.995	0.971	-2.4	0.966	-2.9	0.939	-5.6	0.985	-1.0	0.979	-1.6	0.953	-4.2	0.981	-1.4	0.967	-2.8	0.968	-2.7	0.957	-3.8	0.920	-7.6	0.969	-2.6	0.971	-2.4	0.989	-0.6	0.973	-2.2	1.023	2.9
16		0.988	0.976	-1.2	0.971	-1.7	0.943	-4.7	0.990	0.2	0.984	-0.4	0.956	-3.2	0.986	-0.2	0.971	-1.8	0.973	-1.5	0.962	-3.8	0.922	-6.6	0.974	-1.4	0.976	-1.2	0.995	0.7	0.978	-1.0	1.028	4.0
17		1.000	0.982	-1.8	0.976	-2.4	0.946	-5.4	0.995	-0.5	0.989	-1.1	0.959	-4.1	0.991	-0.9	0.975	-2.5	0.978	-2.2	0.966	-3.4	0.925	-7.5	0.979	-2.1	0.981	-1.9	1.000	0	0.982	-1.8	1.032	3.2
Group Average δ, 6 points			(-1.6 ± 0.55)%		(-1.93 ± 0.68)%		(-3.97 ± 1.68)%		(-0.05 ± 0.68)%		(-0.48 ± 0.82)%		(-2.5 ± 1.79)%		(-0.52 ± 0.64)%		(-2.18 ± 0.56)%		(-1.90 ± 0.60)%		(-3.08 ± 0.74)%		(-5.93 ± 1.78)%		(-1.40 ± 0.93)%		(-1.20 ± 0.93)%		(0.5 ± 0.78)%		(-1 ± 0.94)%		(4.32 ± 1.25)%	
21		1.241	1.219	-1.8	1.220	-1.7	1.224	-1.3	1.216	-2.0	1.217	-2.0	1.221	-1.6	1.231	-0.8	1.233	-0.7	1.233	-0.7	1.234	-0.6	1.240	-0.1	1.216	-2.0	1.217	-1.9	1.202	-3.1	1.225	-1.3	1.253	1.0
22		0.686	0.666	-2.9	0.676	-1.7	0.721	5.1	0.687	0.1	0.694	1.2	0.739	7.8	0.685	-0.1	0.669	-2.5	0.671	-2.2	0.675	-1.6	0.720	5.0	0.688	0.3	0.690	0.6	0.678	-1.2	0.706	2.9	0.742	8.2
23		1.148	1.169	1.8	1.164	1.4	1.142	-0.6	1.169	1.8	1.164	1.4	1.142	-0.5	1.183	3.2	1.180	2.8	1.182	2.9	1.175	2.3	1.150	0.2	1.172	2.1	1.172	2.1	1.170	1.9	1.169	1.8	1.179	2.7
24		0.753	0.741	-1.6	0.741	-1.6	0.744	-1.3	0.756	0.4	0.755	0.3	0.756	0.5	0.761	1.1	0.746	-0.9	0.750	-0.5	0.745	-1.1	0.739	-1.8	0.750	-0.4	0.752	-0.1	0.758	0.7	0.768	2.0	0.801	6.3
25		0.652	0.637	-2.3	0.639	-2.0	0.649	-0.4	0.653	0.2	0.655	0.4	0.664	1.9	0.656	0.6	0.642	-1.5	0.644	-1.2	0.642	-1.6	0.645	-1.1	0.646	-1.0	0.644	-1.2	0.650	-0.2	0.694	6.4	0.697	6.9
2		0.818	0.832	1.7	0.838	2.4	0.860	5.1	0.845	3.3	0.848	3.6	0.868	6.2	0.831	1.6	0.826	0.9	0.826	0.9	0.828	1.2	0.847	3.5	0.832	1.7	0.833	1.8	0.818	0	0.996	21.8	0.861	5.3
Loading Average δ, 24 points			(-0.58 ± 1.36)%		(-0.62 ± 1.35)%		(-0.86 ± 2.59)%		(-0.39 ± 1.12)%		(0.26 ± 1.19)%		(0 ± 2.69)%		(0.54 ± 1.18)%		(-0.56 ± 1.48)%		(-0.40 ± 1.42)%		(-0.85 ± 1.67)%		(-1.53 ± 3.12)%		(0.34 ± 1.66)%		(0.5 ± 1.61)%		(0.39 ± 1.20)%		(1.29 ± 4.72)%		(3.23 ± 2.31)%	
$\delta(P_{max}/P_{ave})$			(0.6 ± 1.8)%		(0.6 ± 1.8)%		(0.9 ± 2.8)%		(-0.4 ± 1.6)%		(0.3 ± 1.6)%		(0 ± 2.9)%		(-0.5 ± 1.6)%		(0.6 ± 1.9)%		(0.4 ± 1.9)%		(0.9 ± 2.0)%		(1.53 ± 3.3)%		(-0.3 ± 1.9)%		(-0.5 ± 1.9)%		(-0.4 ± 1.6)%		(-1.3 ± 4.9)%		(-3.2 ± 2.6)%	
δF			(1.6 ± 1.1)%		(1.9 ± 1.2)%		(4.0 ± 2.0)%		(0 ± 1.2)%		(0.5 ± 1.3)%		(2.5 ± 2.0)%		(0.5 ± 1.2)%		(2.2 ± 1.2)%		(1.9 ± 1.2)%		(3.1 ± 1.3)%		(5.9 ± 2.1)%		(1.4 ± 1.33)%		(1.2 ± 1.24)%		(-0.5 ± 1.3)%		(1 ± 1.4)%		(-4.3 ± 1.6)%	
K_{eff}		1.0078	1.0088		1.0122		1.0281		1.0090		1.0120		1.0273		1.0188		1.0135		1.0138		1.0174		1.0352		0.987		0.999		1.0092		1.0200		1.0065	

1. *This case was made using for ^{233}Pu the Schmidt (KFK 120) Library; in all other Burny cases an old library (BNL 325 - 1958) was used.*
2. *Cross sections calculated with HTH. In the thermal zone, for ^{239}Pu, the Leonard-Westcott library was used.*
3. *Cross sections calculated with HTH. In the thermal zone, for ^{239}Pu, the Schmidt library (normalized to Westcott values at 2200 m/sec) was used.*
4. *HRG + THERMOS (Leonard, Westcott). Small group for ^{240}Pu and different scheme for Dancoff.*
5. *4 cm meshes in the reflector.*
6. *Homogenized moderator cross section, see text.*

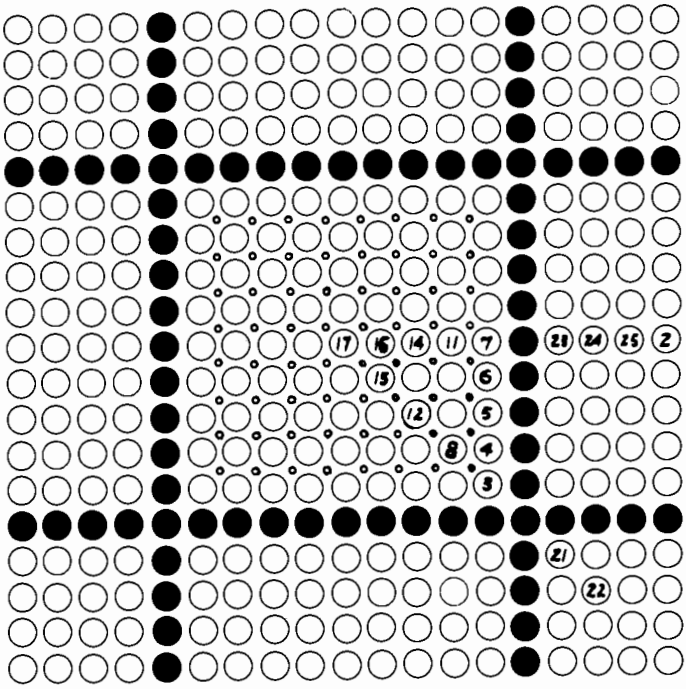

BASIC 9x9 WITH VOIDS, UO_2-2 WT% PuO_2 (8% ^{240}Pu)

Experimental Power Distribution:

Position No.	Relative Power
17	1.000
16	.990
14	1.035
11	1.170
7	1.646
23	1.674
24	1.121
25	.968
2	1.244
15	1.031
12	1.084
8	1.277
3	2.182
4	1.790
5	1.674
6	1.631
21	1.893
22	.881

Relative Accuracy of Experiment = 1.30%

FIGURE B-7

TABLE B-7. Experimental-Calculational Power Distribution Comparisons - Basic 9 × 9, with Voids, UO_2-2 wt% PuO_2 (8% ^{240}Pu)

Rod Location	Symmetry Points	Experimental Rod Power, Arbitrary Units	Case No. 32 RIBOT, Unif[1] 4G - 4M Set No. 16 Power	δ, %	Case No. 33 RIBOT, Non-Unif[2] 4G - 4M Sets No. 17-19 Power	δ, %	Case No. 34 RIBOT, Non-Unif[2] 5G - 4M Sets No. 17-19 Power	δ, %
3	1	2.181	*2.182	0.1	*2.182	0.1	*2.182	0.1
	2	2.219		-1.7		-1.7		-1.7
	3	2.157		1.2		1.2		1.2
	4	2.172		0.5		0.5		0.5
4	1	1.818	1.758	-3.3	1.741	-4.2	1.729	-4.9
	2	1.799		-2.3		-3.2		-3.9
	3	1.782		-1.4		-2.3		-3.0
	4	1.757		0.1		-0.9		-1.6
	5	1.786		-1.6		-2.5		-3.2
	6	1.795		-2.1		-3.0		-3.7
	7	(1.736)		(1.3)		(-0.3)		(-0.4)
5		1.674	1.680	0.3	1.658	-0.9	1.650	-1.4
6		1.631	1.678	2.9	1.655	1.5	1.649	1.1
7		1.646	1.682	2.2	1.659	0.8	1.653	0.4
Group Average δ, 13 points			(-0.39 ± 1.85)%		(-1.12 ± 1.85)%		(-1.54 ± 2.07)%	
8		1.277	1.324	3.7	1.273	-0.3	1.243	-2.6
11		1.170	1.229	5.0	1.160	-0.8	1.136	-2.9
12		1.084	1.144	5.6	1.066	-1.6	1.042	-3.8
14		1.035	1.133	9.5	1.047	1.1	1.000	-3.3
15		1.031	1.120	8.6	1.028	-0.3	1.008	-2.3
16		0.990	1.120	[13.2]	1.026	[3.6]	1.006	[1.7]
17		1.000	1.120	[12.0]	1.023	[2.3]	1.005	[0.5]
Group Average δ, 5 points			(6.48 ± 2.47)%		(-0.38 ± 0.98)%		(-2.98 ± 0.59)%	
21		1.893	1.819	-3.9	1.776	-6.2	1.779	-6.0
22		0.881	0.865	-1.8	0.844	-4.2	0.821	-6.9
23		1.674	1.658	-0.9	1.621	-3.2	1.616	-3.5
24		1.121	1.104	-1.5	1.077	-3.9	1.053	-6.1
25		0.968	0.976	0.8	0.951	-1.7	0.925	-4.4
2		1.244	1.284	3.3	1.253	0.7	1.235	-0.7
Loading Average δ, 24 points			(0.97 ± 3.54)%		(-1.46 ± 2.04)%		(-2.61 ± 2.26)%	
$\delta(P_{max}/P_{ave})$			(-1 ± 3.9)%		(1.5 ± 2.4)%		(2.6 ± 2.6)%	
δF			(-6.5 ± 2.9)%		(0.4 ± 1.8)		(3 ± 1.6)%	
K_{eff}		1.0001	1.0073		1.0055		1.0061	

1. *The water density uniformly decreased by the total void volume.*
2. *The water density adjusted non-uniformly similar to actual case (See Appendix G)*

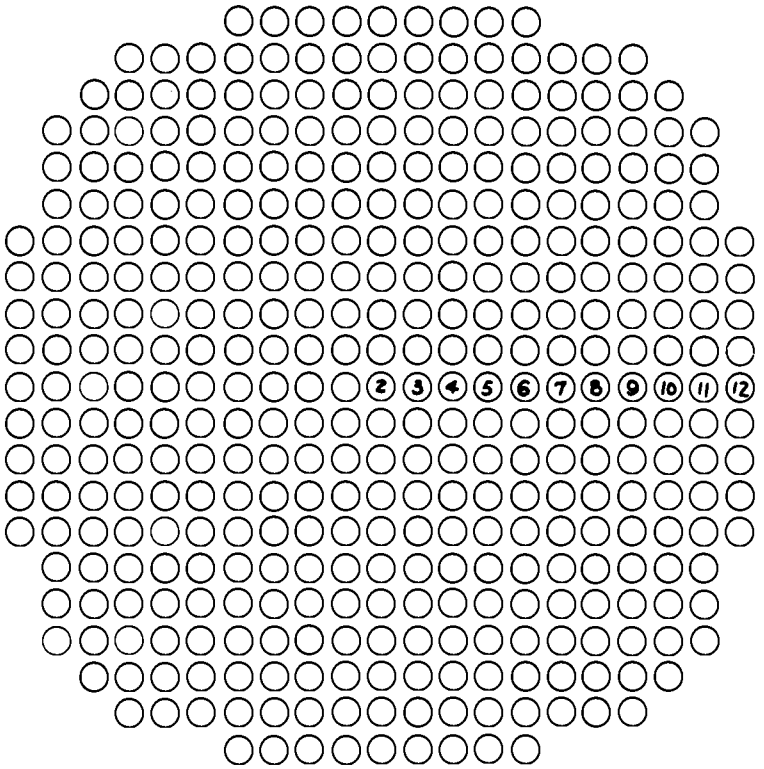

REGULAR, UO_2-2.35% ^{235}U

Experimental Power Distribution:

Position No.	Relative Power
2	.912
3	.906
4	.884
5	.853
6	.804
7	.752
8	.693
9	.633
10	.558
11	.524
12	.567

Relative Accuracy of Experiment = 0.53%

FIGURE B-8

TABLE B-8. Experimental-Calculational Power Distribution Comparisons, Regular, UO_2-2.35% ^{235}U

Rod Location	Symmetry Points	Experimental Rod Power, Arbitrary Units	Case No. 35 St. RIBOT 4G - 4M Set No. 3		Case No. 36 St. RIBOT 5G - 4M Set No. 3		Case No. 37 HTH 4G - 4M Set No. 31		Case No. 38 THERMOS - HRG 4G - 4M Set No. 32	
			Power	δ, %	Power	δ, %	Power	δ, %	Power	δ, %
2		0.912	0.909	-0.4	0.909	-0.4	0.909	-0.4	0.909	-0.4
3	1	0.899	0.902	0.4	0.902	0.4	0.902	0.4	0.903	0.4
	2	0.914		-1.3		-1.3		-1.3		-1.2
	3	0.904		-0.2		-0.2		-0.2		-0.1
4	1	0.883	*0.884	-0.1	*0.884	-0.1	*0.884	-0.1	*0.884	-0.1
	2	0.884		0		0		0		0
	3	0.885		0.1		0.1		0.1		0.1
5	1	0.851	0.853	0.3	0.853	0.3	0.854	0.3	0.853	0.3
	2	0.856		-0.3		-0.3		-0.3		-0.3
	3	(0.828)		(3.0)		(3.0)		(3.1)		(3.0)
6	1	0.805	0.811	0.8	0.811	0.8	0.812	0.9	0.811	0.8
	2	0.799		1.5		1.5		1.7		1.5
	3	0.808		0.4		0.4		0.5		0.4
7	1	0.750	0.759	1.1	0.758	1.1	0.760	1.4	0.757	1.0
	2	(0.768)		(-1.2)		(-1.2)		(-1.0)		-1.4
	3	0.755		0.5		0.5		0.7		0.3
8	1	0.692	0.697	0.7	0.696	0.6	0.700	1.1	0.695	0.4
	2	0.697		0		-0.1		0.4		-0.3
	3	0.689		1.2		1.0		1.6		-0.5
9	1	0.634	0.630	-0.7	0.628	-1.0	0.634	0	0.626	-1.3
	2	0.632		-0.3		-0.6		0.3		-1.0
10	1	0.560	0.565	0.8	0.561	0.2	0.571	2.0	0.557	-0.5
	2	0.556		1.6		0.9		2.7		0.2
	3	0.560		0.9		0.2		2.0		-0.5
11	1	0.527	0.524	-0.5	0.519	-1.4	0.530	0.6	0.510	-3.2
	2	0.520		0.7		-0.2		2.0		-1.9
	3	0.526		-0.4		-1.3		0.8		-3.0
12	1	0.563	0.573	1.7	0.582	3.5	0.561	-0.4	0.55	-2.3
	2	0.570		0.5		2.2		-1.6		-3.5
	3	0.569		0.6		2.3		-1.5		-3.3
Loading Average δ, 28 points			(0.34 ± 0.73)%		(0.32 ± 1.11)%		(0.45 ± 1.12)%		(-0.69 ± 1.36)%	
$\delta(P_{max}/P_{ave})$			(-0.7 ± 0.7)%		(-0.7 ± 1.1)%		(-0.8 ± 1.1)%		(0.3 ± 1.4)%	
K_{eff}		1.0032	0.9999		0.9990		0.9853		0.9956	

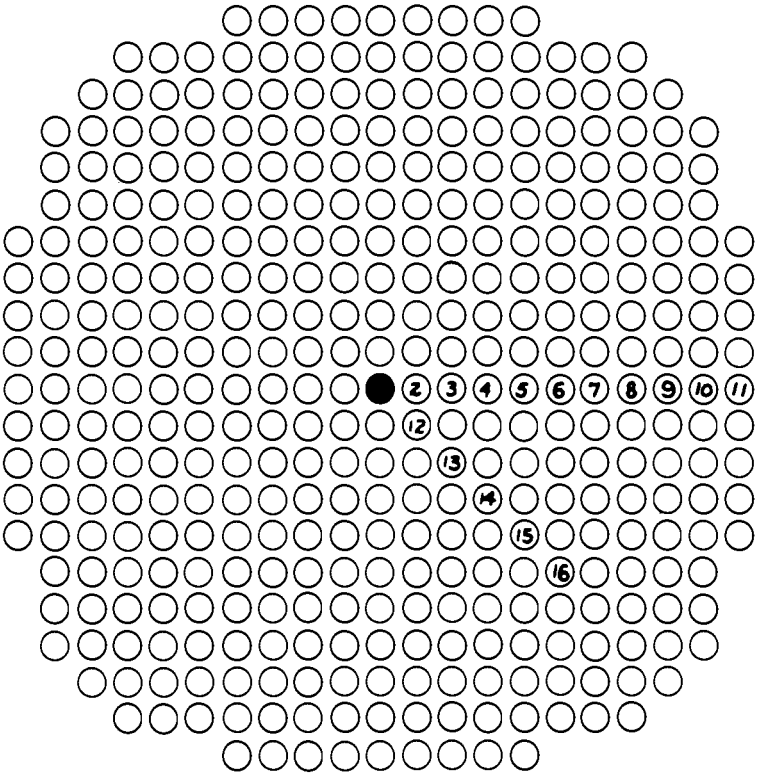

WATER HOLE, UO_2-2.35% ^{235}U

Experimental Power Distribution:

Position No.	Relative Power
2	.876
3	.792
4	.748
5	.709
6	.663
7	.608
8	.552
9	.490
10	.466
11	.501
12	.823
13	.757
14	.700
15	.628
16	.552

Relative Accuracy of Experiment = 0.58%

FIGURE B-9

TABLE B-9. Experimental-Calculation Power Distribution Comparisons, Water Hole, UO_2-2.35% ^{235}U

Rod Location	Symmetry Points	Experimental Rod Power, Arbitrary Units	Case No. 39 St. RIBOT 4G - 4M Set No. 3 Power	δ, %
2	1	(0.899)	0.875	(-2.7)
	2	0.873		0.2
	3	0.874		-0.5
	4	0.880		-0.6
3	1	0.793	*0.792	(-0.2)
	2	0.786		0.7
	3	0.796		-0.5
4	1	0.746	0.749	-0.7
	2	0.749		-0.6
	3	0.750		0.5
5	1	0.714	0.709	-0.7
	2	0.714		-0.6
	3	0.706		0.5
6	1	0.668	0.663	-0.9
	2	0.658		0.7
	3	0.663		0
7		0.608	0.609	0.1
8		0.552	0.550	-0.2
9		0.490	0.494	0.7
10		0.466	0.458	-1.6
11		0.501	0.501	0
12	1	0.820	0.829	1.1
	2	0.817		1.4
	3	0.827		0.2
	4	0.828		0
13	1	0.753	0.756	0.4
	2	0.761		-0.7
	3	0.756		0
14	1	0.703	0.699	-0.6
	2	0.697		0.4
	3	0.699		0
15	1	0.634	0.630	-0.7
	2	0.627		0.4
	3	0.624		0.9
16	1	0.547	0.548	0.2
	2	0.557		-1.6
Loading Average δ, 35 points			(-0.03 ± 0.68)%	
$\delta(P_{max}/P_{ave})$			(-0.3 ± 0.8)%	
K_{eff}		1.0025	0.9994	

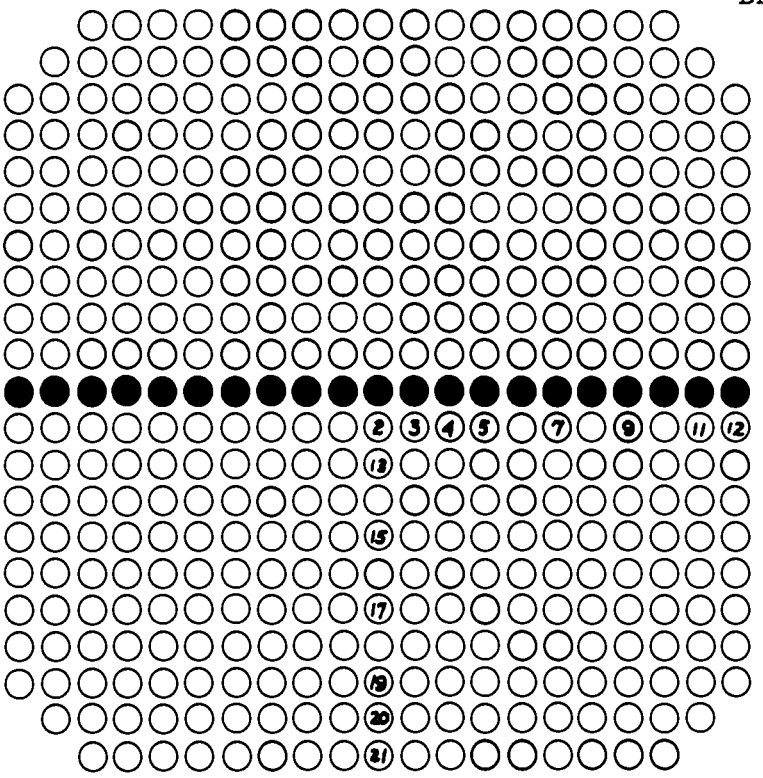

WATER SLAB, UO_2-2.35% ^{235}U

Experimental Power Distribution:

Position No.	Relative Power
2	.949
3	.941
4	.930
5	.903
7	.812
9	.662
11	.549
12	.565
13	.771
15	.656
17	.570
19	.487
20	.449
21	.495

Relative Accuracy of Experiment = 0.37%

FIGURE B-10

TABLE B-10. Experimental-Calculation Power Distribution Comparisons, Water Slab, UO_2-2.35% ^{235}U

Rod Location	Symmetry Points	Experimental Rod Power, Arbitrary Units	Case No. 40 St. RIBOT 4G - 4M Set No. 3 Power	Case No. 40 St. RIBOT 4G - 4M Set No. 3 δ, %	Case No. 41 St. RIBOT 5G - 4M Set No. 3 Power	Case No. 41 St. RIBOT 5G - 4M Set No. 3 δ, %
2	1	0.944	0.949	0.5	*0.949	0.5
	2	0.953		-0.5		-0.5
3	1	0.945	0.942	-0.3	0.942	-0.3
	2	0.938		0.4		0.4
	3	0.942		0		0
	4	0.939		0.3		0.3
4	1	0.931	0.924	-0.7	0.924	-0.7
	2	0.929		-0.5		-0.5
5	1	(0.879)	0.894	(1.7)	0.894	(1.7)
	2	0.899		-0.6		-0.6
	3	0.903		-1.0		-1.0
	4	0.906		-1.3		-1.3
7	1	(0.783)	0.800	(2.1)	0.799	(2.0)
	2	0.816		-2.0		-2.1
	3	0.810		-1.2		-1.3
	4	0.811		-1.5		-1.6
9	1	0.666	0.669	0.5	0.666	0.1
	2	0.659		1.4		1.1
11	1	0.547	0.549	0.3	0.545	-0.5
	2	0.550		-0.3		-1.1
12	1	0.561	0.567	1.1	0.572	1.9
	2	0.568		-0.1		0.7
Group Average δ, 20 points			(-0.27 ± 0.87)%		(-0.32 ± 0.97)%	
13		0.771	0.772	0.1	0.753	-2.3
15		0.656	0.659	0.4	0.642	-2.0
17		0.570	0.573	0.6	0.559	-1.9
19		0.487	0.474	[-2.6]	0.459	[-5.4]
20		0.449	0.445	-1.0	0.430	-4.3
21		0.495	0.492	-0.6	0.488	-1.4
Group Average δ, 5 points			(-0.10 ± 0.68)%		(-2.38 ± 1.12)%	
Loading Average δ, 25 points			(-0.24 ± 0.83)%		(-0.74 ± 1.29)%	
$\delta(P_{max}/P_{ave})$			(0.2 ± 1.0)%		(0.7 ± 1.4)%	
K_{eff}		1.0018	0.9993		0.9991	

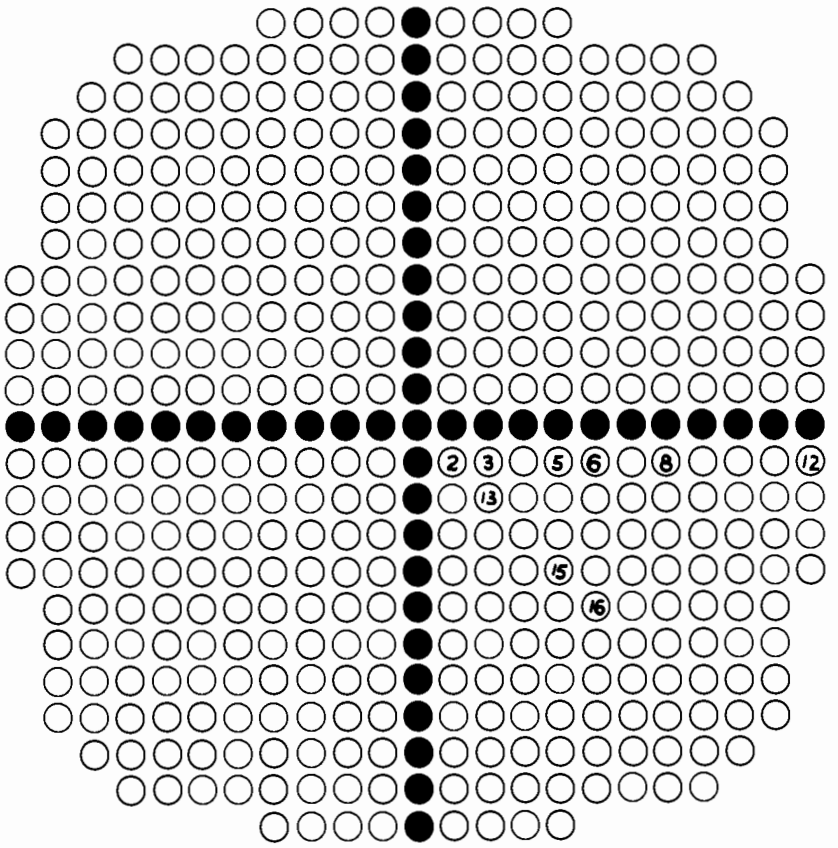

WATER CROSS, UO_2-2.35% ^{235}U

Experimental Power Distribution:

Position No.	Relative Power
2	1.860
3	1.592
5	1.401
6	1.334
8	1.140
12	.856
13	1.305
15	.971
16	.876

Relative Accuracy of Experiment = 0.40%

FIGURE B-11

TABLE B-11. Experimental-Calculational Power Distribution Comparisons, Water Cross, UO_2-2.35% ^{235}U

Rod Location	Symmetry Points	Experimental Rod Power, Arbitrary Units	Case No. 42 St. RIBOT 4G - 4M Set No. 3 Power	δ, %	Case No. 43 St. RIBOT 5G - 4M Set No. 3 Power	δ, %
2	1	1.862	*1.86	-0.1	*1.86	-0.1
	2	1.865		-0.3		-0.3
	3	1.855		0.3		0.3
	4	1.858		0.1		0.1
3	1	(1.575)	1.583	(0.5)	1.557	(-1.2)
	2	1.589		-0.3		-2.0
	3	1.586		-0.2		-1.9
	4	1.589		-0.3		-2.0
	5	1.600		-1.0		-2.7
	6	1.595		-0.7		-2.4
	7	1.592		-0.5		-2.2
	8	(1.614)		(-1.9)		(-3.6)
5	1	1.404	1.39	-1.0	1.366	-2.7
	2	1.393		-0.2		-1.9
	3	1.406		-1.2		-2.9
	4	(1.362)		(2.1)		(0.3)
6	1	1.339	1.315	-1.8	1.292	-3.5
	2	1.335		-1.5		-3.2
	3	1.328		-1.0		-2.7
	4	(1.304)		(0.8)		(-0.9)
8	1	1.148	1.128	-1.7	1.107	-3.6
	2	1.145		-1.5		-3.3
	3	1.134		-0.5		-2.4
	4	1.134		-0.5		-2.4
12	1	0.854	0.847	-0.8	0.839	-1.8
	2	0.855		-0.9		-1.9
	3	0.858		-1.3		-2.3
	4	(0.869)		(-2.5)		(-3.5)
Group Average δ, 23 points			(-0.63 ± 0.66)%		(-1.99 ± 1.16)%	
13	1	1.299	1.309	0.8	1.256	-3.3
	2	1.309		0		-4.1
	3	1.305		0.3		-3.8
	4	1.308		0.1		-4.0
15	1	0.973	0.974	0.1	0.933	-4.1
	2	0.969		0.5		-3.7
16	1	0.882	0.864	[-2.0]	0.829	[-6.0]
	2	0.871		-0.8		-4.8
Loading Average δ, 30 points			(-0.46 ± 0.70)%		(-2.44 ± 1.34)%	
$\delta(P_{max}/P_{ave})$			(0.5 ± 0.7)%		(2.4 ± 1.3)%	
K_{eff}		1.0010	0.9990		0.9998	

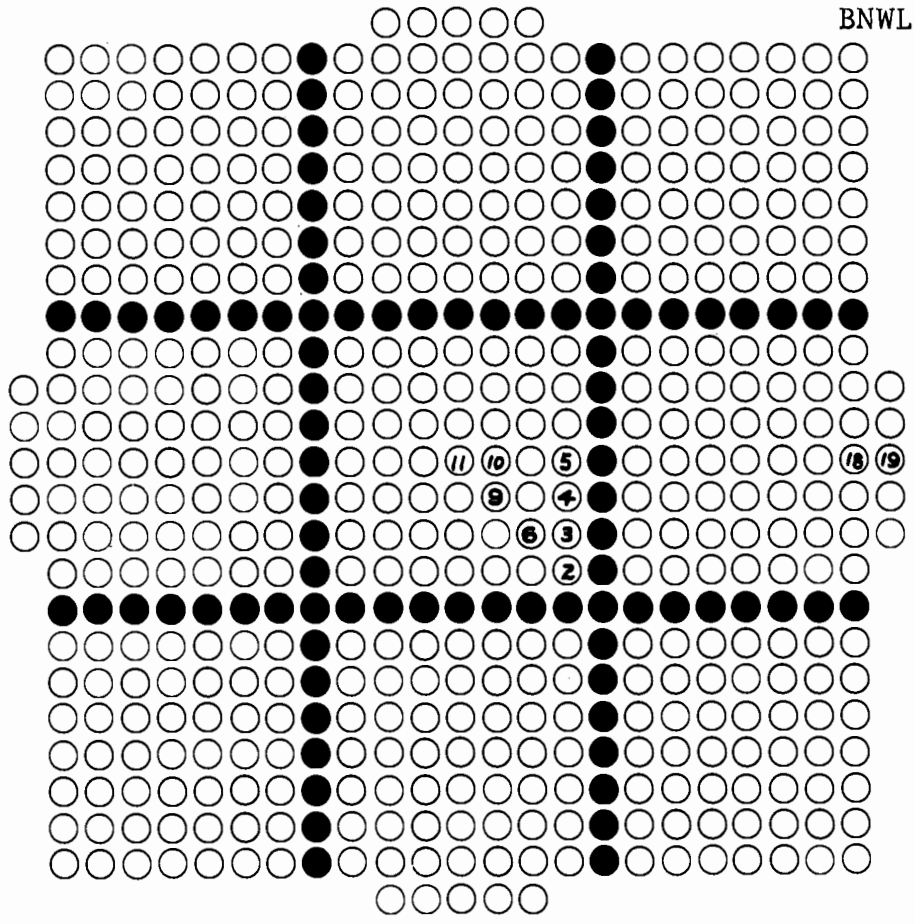

BASIC 7x7, UO_2-2.35% ^{235}U

Experimental Power Distribution:

Position No.	Relative Power
11	.701
10	.712
5	.875
18	.365
19	.390
9	.721
6	.780
2	1.039
3	.919
4	.875

Relative Accuracy of Experiment = 0.47%

FIGURE B-12

TABLE B-12. Experimental-Calculational Power Distribution Comparisons, Basic 7 × 7 UO_2-2.39% ^{235}U

Rod Location	Symmetry Points	Experimental Rod Power, Arbitrary Units	Case No. 44 St. RIBOT 4G - 4M Set No. 3 Power	δ, %
2	1	1.031	*1.039	0.8
	2	1.043		-0.4
	3	1.036		0.3
	4	1.046		-0.7
3	1	0.921	0.922	0.1
	2	0.920		0.3
	3	(0.895)		(2.9)
	4	0.916		0.6
4	1	0.876	0.892	1.9
	2	0.878		1.7
	3	0.870		2.6
5	1	0.873	0.888	1.7
	2	0.873		2.2
	3	0.879		1.5
Group Average δ, 13 points			(0.97 ± 1.07)%	
6	1	0.776	0.794	2.4
	2	0.777		2.3
	3	0.786		1.1
9	1	0.719	0.728	1.2
	2	0.720		1.0
	3	0.724		0.6
10	1	0.711	0.722	1.5
	2	(0.699)		(3.3)
	3	0.715		0.9
	4	0.711		1.5
11		0.701	0.716	2.1
Group Average δ, 10 points			(1.46 ± 0.62)%	
18	1	0.363	0.366	0.8
	2	0.368		-0.4
	3	0.364		0.7
19	1	0.390	0.400	2.6
	2	0.389		3.1
	3	0.391		2.5
Loading Average δ, 29 points			(1.26 ± 1.00)%	
$\delta(P_{max}/P_{ave})$			(-1.3 ± 1.2)%	
δF			(-1.5 ± 0.8)%	
K_{eff}		1.0010	1.0014	

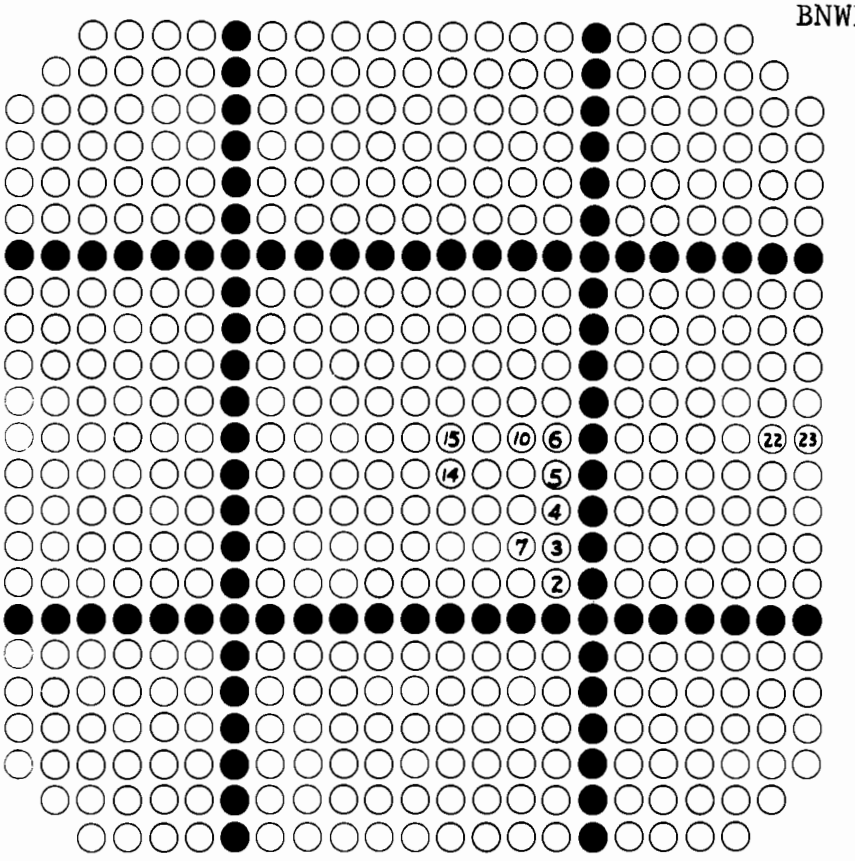

BASIC 9x9, UO_2-2.35% ^{235}U

Experimental Power Distribution:

Position No.	Relative Power
15	.678
10	.693
6	.817
22	.350
23	.387
14	.674
7	.715
2	.918
3	.818
4	.811
5	.816

Relative Accuracy of Experiment = 0.46%

FIGURE B-13

TABLE B-13. Experimental Calculational Power Distribution Comparisons, Basic 9 × 9, UO_2-2,35% ^{235}U

Rod Location	Symmetry Points	Experimental Rod Power, Arbitrary Units	Case No. 45 St. RIBOT 4G - 4M Set No. 3		Case No. 46 St. RIBOT 5G - 4M Set No. 3		Case No. 47 HTH 4G - 4M Set No. 31		Case No. 48 THERMOS-HRG 4G - 4M Set No. 32	
			Power	δ, %	Power	δ, %	Power	δ, %	Power	δ, %
2	1	0.911	*0.918	0.7	*0.918	0.7	*0.918	0.7	*0.918	0.7
	2	0.917		0		0		0		0
	3	0.924		-0.7		-0.7		-0.7		-0.7
	4	0.918		0		0		0		0
3	1	0.815	0.826	1.4	0.813	-0.3	0.841	3.2	0.826	1.4
	2	0.819		1.0		-0.6		2.7		1.0
	3	0.821		0.7		-0.9		2.4		0.7
	4	0.819		0.9		-0.7		2.7		0.9
4	1	0.817	0.811	-0.8	0.798	-2.3	0.826	1.2	0.814	-0.3
	2	0.811		0		-1.6		1.9		0.4
	3	0.805		0.7		-0.9		2.7		1.1
5	1	0.819	0.815	-0.6	0.802	-2.1	0.829	1.2	0.820	0.1
	2	0.811		0.5		-1.0		2.2		1.1
	3	0.818		-0.5		-2.0		1.3		0.3
6	1	0.814	0.818	0.4	0.806	-1.1	0.831	2.1	0.824	1.2
	2	0.815		0.3		-1.2		2.0		1.1
	3	0.820		-0.3		-1.8		1.4		0.5
Group Average δ, 17 points			(0.25 ± 0.63)%		(-0.97 ± 0.82)%		(1.59 ± 1.10)%		(0.56 ± 0.59)%	
7	1	(0.701)	0.723	(3.0)	0.695	(-0.9)	0.755	(7.6)	0.719	(2.6)
	2	0.715		1.1		-2.7		5.5		0.6
	3	0.715		1.1		-2.8		5.5		0.6
10	1	0.695	0.706	1.6	0.680	-2.2	0.737	6.0	-0.708	1.9
	2	0.694		1.8		-2.0		6.2		2.1
	3	0.691		2.1		-1.6		6.6		2.5
14	1	(0.688)	0.681	(-1.0)	0.656	(-4.6)	0.712	(3.4)	0.688	(0)
	2	0.671		1.6		-2.2		6.1		2.6
	3	0.677		0.6		-3.1		5.1		1.7
15	1	0.675	0.683	1.1	0.658	-2.5	0.713	5.6	0.691	2.3
	2	(0.704)		(-3.0)		(-6.5)		(1.3)		(-1.9)
	3	0.678		0.7		-2.9		5.2		1.9
	4	0.682		0.2		-3.4		4.5		1.4
Group Average δ, 10 points			(1.19 ± 0.59)%		(-2.54 ± 0.55)%		(5.63 ± 0.61)%		(1.75 ± 0.72)%	
24	1	0.349	0.350	0.2	0.334	-4.5	0.369	5.8	0.341	2.2
	2	0.350		0.1		-4.7		5.5		-2.5
	3	0.350		0		-4.7		5.5		-2.5
25	1	0.387	0.389	0.4	0.381	-1.6	0.395	2.1	0.371	-4.2
	2	0.384		1.2		-0.8		2.9		-3.4
	3	0.388		0.1		-1.9		1.8		-4.4
Loading Average δ, 33 points			(0.55 ± 0.71)%		(1.82 ± 1.32)%		(3.24 ± 2.14)%		(0.24 ± 1.86)%	
$\delta(P_{max}/P_{ave})$			(-0.5 ± 0.9)%		(1.9 ± 1.4)%		(-3.3 ± 2.1)%		(-0.2 ± 2.0)%	
δF			(-1.2 ± 0.8)%		(2.5 ± 0.8)%		(-5.6 ± 0.8)%		(-1.7 ± 0.9)%	
K_{eff}		1.0027	1.0038		1.0058		0.9892		0.9955	

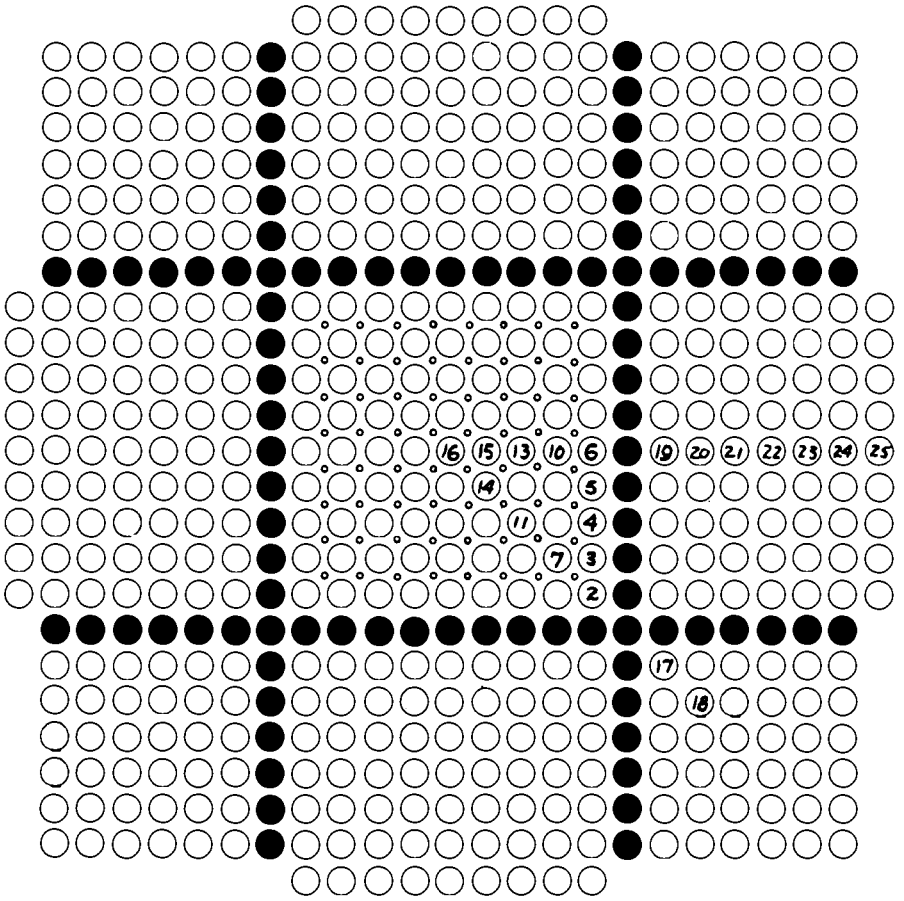

BASIC 9x9 WITH VOIDS, UO_2-2.35% ^{235}U

Experimental Power Distribution:

Position No.	Relative Power
16	.921
15	.917
13	.925
10	1.007
6	1.262
19	1.248
20	.974
21	.822
22	.739
23	.659
24	.607
25	.651
14	.913
11	.935
7	1.093
2	1.507
3	1.311
4	1.270
5	1.258
17	1.296
18	.809

Relative Accuracy of Experiment = 0.40%

FIGURE B-14

TABLE B-14. Experimental-Calculational Power Distribution Comparisons, Basic 9 × 9 with Voids

Rod Location	Symmetry Points	Experimental Rod Power, Arbitrary Units	Case No. 49 RIBOT, unif[1] 4G - 4M Set No. 33 Power	δ, %	Case No. 50 RIBOT, unif[1] 5G - 4M Set No. 33 Power	δ, %	Case No. 51 RIBOT, non-unif[2] 4G - 4M Sets No. 35 - 37 Power	δ, %	Case No. 52 RIBOT, non-unif[2] 5G - 4M Sets No. 35 - 37 Power	δ, %
2	1	1.510	*1.507	-0.2	*1.507	-0.2	*1.507	-0.2	*1.507	-0.2
	2	1.497		0.7		0.7		0.7		0.7
	3	1.517		-0.7		-0.7		-0.7		-0.7
	4	1.504		0.2		0.2		0.2		0.2
3	1	1.309	1.334	1.9	1.309	0	1.319	0.8	1.297	-0.9
	2	1.307		2.0		0.1		0.9		-0.8
	3	1.310		1.8		-0.1		0.7		-1.0
	4	1.316		1.3		-0.6		0.3		-1.4
4	1	1.270	1.289	1.5	1.263	-0.5	1.272	0.2	1.247	-1.8
5	1	1.256	1.283	2.2	1.259	0.3	1.266	0.8	1.242	-1.1
	2	1.261		1.8		-0.1		0.4		1.5
6	1	1.265	1.284	1.5	1.261	-0.3	1.266	0.1	1.243	-1.7
	2	1.259		2.0		0.2		0.6		-1.2
Group Average δ, 13 points			(1.23 ± 0.93)%		(-0.08 ± 0.39)%		(0.08 ± 0.55)%		(-0.88 ± 0.74)%	
7		1.093	1.142	4.5	1.090	-0.3	1.102	0.8	1.058	-3.2
10	1	1.003	1.076	7.3	1.026	2.3	1.028	2.5	0.983	-2.0
	2	1.010		6.6		1.6		1.8		-2.7
11		0.935	1.029	10.0	0.976	4.4	0.977	4.5	0.928	-0.8
13		0.925	1.014	9.6	0.965	4.3	0.957	3.4	0.910	-1.6
14	1	0.916	1.002	9.4	0.954	4.1	0.941	2.7	0.896	-2.2
	2	0.910		10.1		4.8		3.4		1.6
15	1	0.913	1.000	9.5	0.953	4.3	0.937	2.7	0.893	-2.2
	2	0.920		8.7		3.6		1.9		-2.9
16		0.921	0.998	8.3	0.952	3.3	0.934	1.4	0.890	-3.3
Group Average δ, 10 points			(8.4 ± 1.79)%		(3.24 ± 1.60)%		(2.51 ± 1.09)%		(-2.25 ± 0.79)%	
17		1.296	1.301	0.4	1.300	0.3	1.274	-1.7	1.274	-1.7
18		0.809	0.809	0	0.772	-4.6	0.792	-2.1	0.756	-6.5
19		1.248	1.265	1.4	1.241	-0.5	1.240	-0.7	1.219	-2.3
20		0.974	0.983	0.9	0.940	-3.5	0.962	-1.2	0.921	-5.4
21		0.822	0.842	2.4	0.802	-2.4	0.823	0.1	0.786	-4.3
22		0.739	0.743	0.5	0.708	-4.3	0.727	-1.7	0.694	-6.1
23		0.659	0.662	0.4	0.629	-4.6	0.648	-1.7	0.617	-6.4
24		0.607	0.616	1.4	0.584	-3.8	0.603	-0.7	0.573	-5.7
25		0.651	0.681	4.6	0.664	2.0	0.667	2.4	0.651	0
Loading Average δ, 32 points			(3.5 ± 3.61)%		(0.37 ± 2.68)%		(0.71 ± 1.64)%		(-2.26 ± 1.95)%	
δF			(-8.4 ± 1.9)%		(-3.2 ± 1.8)%		(-2.5 ± 1.3)%		(2.3 ± 1.0)%	
$\delta(P_{max}/P_{ave})$			(-3.5 ± 3.7)%		(-0.4 ± 2.7)%		(-0.7 ± 1.7)%		(-2.3 ± 2.1)%	
K_{eff}		1.0030	1.0064		1.0084		1.0052		1.0071	

1. *The water density uniformly decreased by the total void volume.*
2. *The water density adjusted non-uniformly similar to actual case (see Appendix G).*

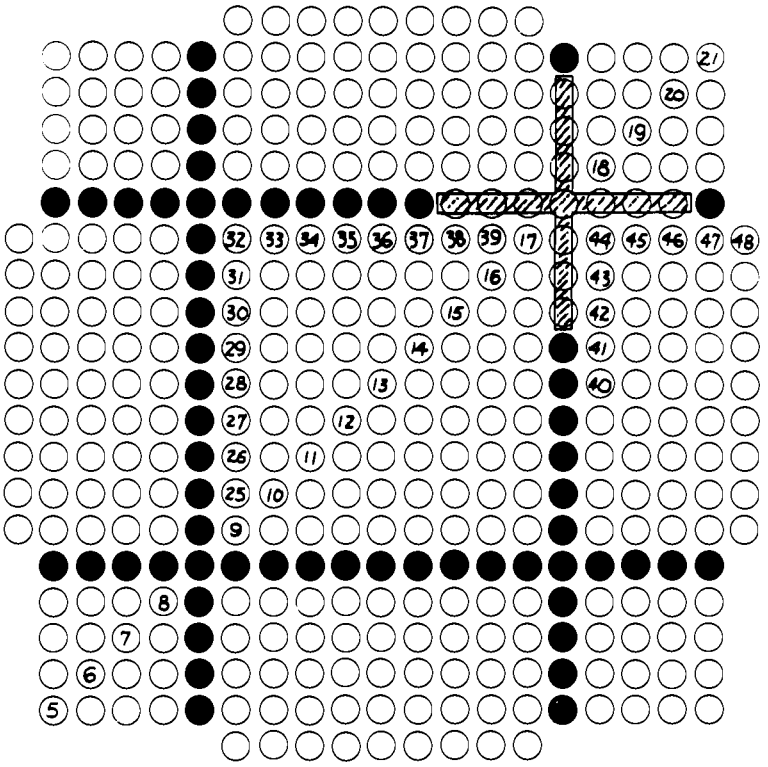

BASIC 9x9 WITH BORAL BLADE, UO_2-2 WT% PuO_2 (8% ^{240}Pu)

Experimental Power Distribution:

Position No.	Relative Power	Position No.	Relative Power
5	1.078	29	1.839
6	.734	30	1.832
7	.957	31	1.881
8	1.974	32	2.030
9	2.451	33	1.737
10	1.560	34	1.621
11	1.344	35	1.533
12	1.327	36	1.395
13	1.251	37	1.121
14	--	38	1.026
15	1.005	39	.619
16	.879	40	1.222
17	.476	41	.957
18	.350	42	.640
19	.277	43	.455
20	.295	44	.333
21	.446	45	.384
25	2.042	46	.403
26	1.908	47	.500
27	1.928	48	.697
28	1.880		

FIGURE B-15

TABLE-B-15. Experimental-Calculational Power Distribution Comparison, Basic 9 × 9 with Boral Blade, UO_2-2 wt% PuO_2 (8% ^{240}Pu)

Rod Location	Experimental Rod Power, Arbitrary Units	Case No. 75 St. RIBOT 4G - 1M(1,2) C_3 = 0.205 Power	δ, %
5	1.078	1.136	5.4
6	0.734	0.778	6.0
7	0.457	0.992	3.7
8	1.974	2.046	3.6
9	2.451	2.500	2.0
10	1.56	1.583	1.4
11	1.344	1.390	3.4
12	1.327	*1.327	---
13	1.251	1.257	0.5
15	1.005	0.942	-1.2
16	[0.879]	0.796	[-9.4]
17	0.476	0.579	21.6
18	[0.35]	0.201	[-42.7]
19	0.277	0.222	-20.0
20	0.295	0.247	-16.2
21	0.446	0.393	-11.9
25	2.042	2.047	0.2
26	1.908	1.958	2.6
27	1.928	1.937	0.4
28	1.880	1.911	1.6
29	1.839	1.87	1.7
30	1.832	1.823	-0.5
31	1.881	1.832	-2.6
32	2.030	2.176	7.2
33	1.737	1.737	0
34	1.621	1.607	-0.9
35	1.533	1.514	-1.3
36	1.395	1.369	-1.8
37	1.121	1.107	-1.3
38	[1.027]	0.846	[-17.6]
39	0.619	0.693	11.9
40	(1.193)	1.153	-3.3
	1.246		-7.4
41	0.957	0.887	-7.3
42	0.660	0.614	-7.0
	0.621		-1.1
43	0.455	0.455	0
44	0.313	0.361	15.3
	0.352		2.5
45	0.384	0.372	-3.1
46	0.403	0.380	-5.8
47	0.500	0.448	-10.3
48	0.686	0.657	-4.1
--	0.708		-7.1
K_{eff}	1.0022	1.0039	

1. 4 meshes were used near water gaps.

2. Zero derivative condition removed, blade treated as diffusive region for energy Group 1.

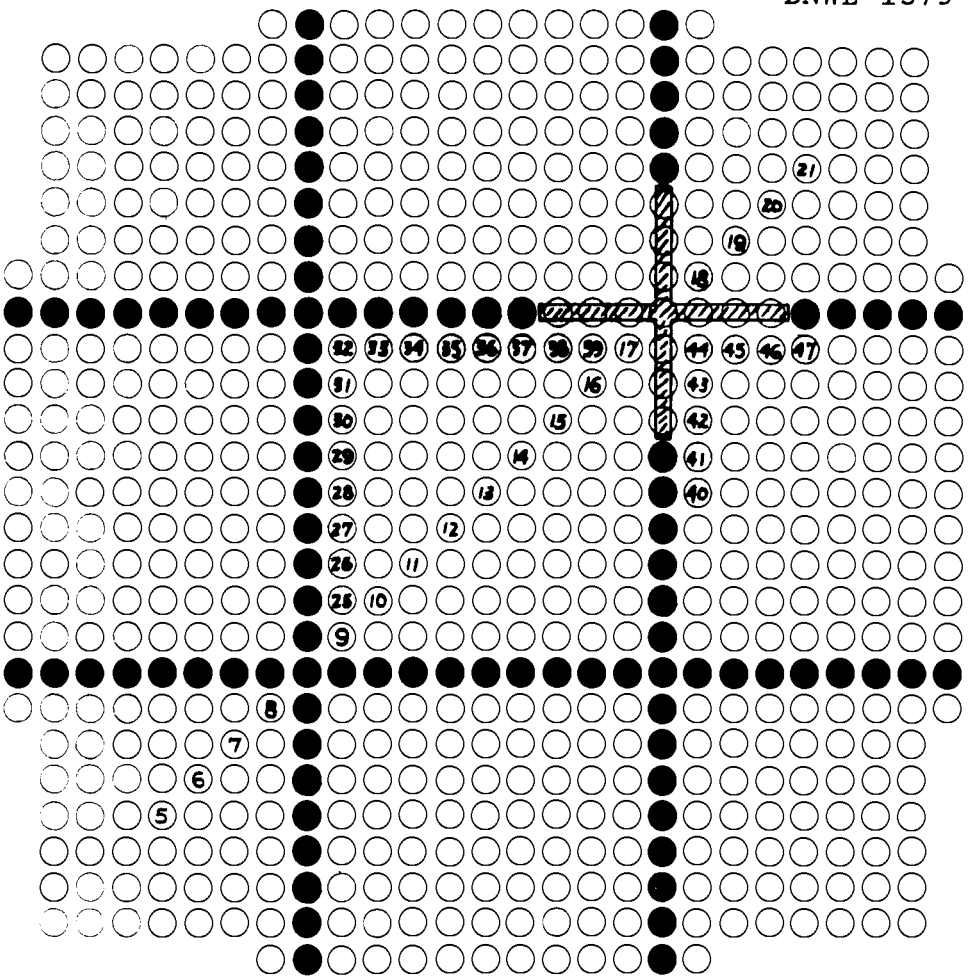

BASIC 9x9 WITH BORAL BLADE, UO_2-2.35% ^{235}U

Experimental Power Distribution:

Position No.	Relative Power	Position No.	Relative Power
5	.667	28	1.581
6	.832	29	1.547
7	1.080	30	1.144
8	1.720	31	1.527
9	1.989	32	1.698
10	1.414	33	1.471
11	1.287	34	1.377
12	1.226	35	1.236
13	1.141	36	1.146
14	1.049	37	.891
15	.886	38	.637
16	.666	39	.478
17	.346	40	.997
18	.200	41	.788
19	.295	42	.515
20	.316	43	.369
21	.287	44	.260
25	1.716	45	.315
26	1.614	46	.370
27	1.633	47	.460

FIGURE B-16

TABLE B-16. Experimental-Calculational Power Distribution Comparison, Basic 9 × 9 with Boral Blade, UO_2-2.35% ^{235}U

Rod Location	Experimental Rod Power, Arbitrary Units	Case No. 71 St. RIBOT 4G - 1M[1] C_3 = 0.205 Power	δ, %	Case No. 72 St. RIBOT 4G - 1M[1] C_3 = 0.25 Power	δ, %	Case No. 73 St. RIBOT 4G - 1M[1] C_3 = 0.3 Power	δ, %	Case No. 74 St. RIBOT 4G - 1M[1] C_3 = 0.205 Power	δ, %
5	6.67	6.49	-2.6	6.59	-1.2	6.67	0	6.82	2.2
6	8.32	8.11	-2.5	8.22	-1.1	8.32	0	8.50	2.3
7	10.80	10.70	-0.4	10.84	0.4	10.96	1.5	11.21	3.8
8	17.18	16.34	-4.9	16.55	-3.6	16.73	-2.6	17.09	-0.5
9	19.89	18.73	-5.8	18.95	-4.8	19.12	-3.9	19.49	-2.0
10	14.14	14.27	0.9	14.41	1.9	14.53	1.8	14.78	4.5
11	12.87	12.78	-0.7	12.89	0.2	12.98	0.9	13.17	2.3
12	12.26	12.10	-1.3	12.18	-0.7	12.24	-0.1	12.38	1.0
13	11.41	11.43	0.1	11.48	0.5	11.52	0.9	11.59	1.5
14	10.49	*10.49	---	*10.49	---	*10.49	---	*10.49	---
15	8.86	9.12	2.9	9.06	2.2	9.00	1.6	8.95	1.0
16	6.67	7.15	7.4	7.01	5.3	6.88	3.4	6.82	2.5
17	3.46	4.53	30.8	4.34	25.4	4.17	20.4	4.10	18.4
18	2.00	1.48	-26.1	1.30	-33.7	1.23	-38.5	1.79	-10.1
19	2.45	2.19	-25.7	1.97	-33.1	1.90	-35.5	2.48	-15.8
20	3.16	2.46	-22.2	2.22	-29.8	2.17	-31.4	2.66	-16.1
21	2.87	2.35	-18.0	2.11	-26.4	2.07	-27.8	2.45	-14.6
25	17.16	16.58	-3.3	16.77	-2.3	16.91	-1.4	17.22	0.4
26	16.14	15.93	-1.3	16.09	-0.3	16.22	0.5	16.50	2.2
27	16.33	15.67	-4.1	15.82	-3.1	15.94	-2.4	16.20	-0.1
28	15.81	15.44	-2.4	15.58	-1.5	15.68	-0.8	15.92	0.7
29	15.46	15.14	-2.1	15.26	-1.3	15.35	-0.7	15.57	0.7
30	[11.44]	14.85	---	14.96	---	15.05	---	15.23	---
31	15.27	14.93	-2.2	15.02	-1.6	15.10	-1.1	15.25	-0.1
32	16.98	16.30	-4.0	16.39	-3.0	16.47	-3.1	16.71	-1.6
33	14.71	14.10	-4.1	14.16	-3.7	14.20	-3.4	14.39	-2.2
34	13.77	13.12	-4.7	13.14	-4.5	13.16	-4.4	13.31	-3.3
35	12.36	12.29	-0.5	12.28	-0.7	12.27	-0.7	12.39	0.2
36	11.44	11.09	-3.0	11.03	-3.6	10.98	-4.0	11.36	-3.2
	11.49		-3.5		-4.0		-4.4		-3.7
37	8.98	9.02	0.4	8.91	-0.7	8.82	-1.8	8.88	-1.1
	8.84		2.0		0.8		-0.2		0.5
38	6.35	6.99	10.1	6.85	7.8	6.72	5.8	6.74	6.1
	6.39		9.5		7.3		5.2		5.5
39	4.78	5.76	20.4	5.59	16.8	5.43	13.5	5.37	12.3
	4.77		20.7		17.0		13.8		12.6
40	10.05	9.48	-5.7	9.39	-6.6	9.34	-7.0	9.55	-5.0
	9.90		-4.2		-5.1		-5.6		-3.5
41	7.92	7.32	-7.6	7.18	-9.2	7.10	-10.3	7.35	-7.1
	7.84		-6.7		-8.3		-9.4		-6.2
42	5.17	5.13	-1.0	4.97	-4.0	4.86	-6.1	5.17	0
	5.13		-0.1		-3.1		-5.2		0.7
43	3.65	3.82	4.5	3.65	0	3.53	-3.3	3.83	4.9
	3.72		2.7		-1.8		-5.0		3.1
44	2.59	2.82	8.7	2.65	2.3	2.53	-2.3	2.82	8.9
	2.60		8.5		2.0		-2.5		8.7
45	3.09	3.31	7.2	3.14	1.7	3.03	-1.8	3.32	7.6
	3.22		(2.7)		-2.6		-5.9		(3.1)
46	3.67	3.57	-2.6	3.40	-7.4	3.31	-9.8	3.61	-1.5
	3.72		-4.0		-8.7		-11.1		-2.9
47	4.65	4.02	-13.6	3.82	-17.9	3.75	-19.4	4.09	-12.0
	4.55		-11.6		-15.9		-17.6		-10.0
K_{eff}	1.0018	1.0037		1.0027		1.0018		0.9994	

1. *4 meshes were used near water gaps.*

APPENDIX C

POWER CALIBRATION OF THE FUEL RODS

R. Martinelli and L. D. Williams

APPENDIX C

POWER CALIBRATION OF THE FUEL RODS

R. Martinelli and L. D. Williams

EXPERIMENTAL TECHNIQUES

In multiregion loadings, gamma activity originating from different types of fuel is insufficient by itself to determine rod power. In order to relate fission product gamma activities from different types of fuel to relative rod power, absolute intercalibration factors must be determined. In actual practice, the problem reduces to normalization of gamma activity ratios for different fuel types such that only relative power intercalibration factors are needed. Relative rod powers were determined from gamma activities by utilizing the factor, $F(t)_{\frac{\text{fuel \#1}}{\text{fuel \#2}}}$, in the following manner:

$$\frac{\text{Power (fuel \#1)}}{\text{Power (fuel \#2)}} = F(t)_{\frac{\text{fuel \#1}}{\text{fuel \#2}}} \times \frac{\gamma_1\ (t)}{\gamma_2\ (t)} : \qquad (1)$$

where γ_1, $_2$ are the fission product gamma activities (>0.5 MeV) measured from any rod of the specified fuel in a multiregion core experiment at a time t following shutdown. Two methods were used to determine the gamma to power factors to be applied to the five different fuel types used in these tests; the former was based on the measurement of cladding heatup rates (calorimetric technique), the latter on the measurement of lanthanum activities (^{140}La technique). The fuels were compared two at a time, using UO_2-2 wt% PuO_2 (8% ^{240}Pu) as the normalizing fuel. The conversion factor F(t) used in Equation (1) is expressed by the following relationships:

CALORIMETRIC TECHNIQUE

$$F(t)_{\frac{\text{fuel \#1}}{\text{fuel \#2}}} = \begin{cases} \dfrac{(dT_c/dt)_1}{(dT_c/dt)_2} \times \dfrac{K_1}{K_2} \times \dfrac{\Gamma_2}{\Gamma_1}\,(t) & (2) \\ \text{or} \\ \dfrac{(^{140}La)_1}{(^{140}La)_2} \times \dfrac{Y_1}{Y_2} \times \dfrac{(1-S_2)}{(1-S_1)} \times \dfrac{\Gamma_2}{\Gamma_1}\,(t): & (3) \end{cases}$$

^{140}La TECHNIQUE

where the symbols denote:

$(dT_c/dt)_{1,2}$ = measured cladding heatup rates at constant power (the time dependence of T_c is linear if the process is adiabatic)

$K_{1,2}$ = calculated factors, allowing for geometry, density and heat capacitance of fuel and cladding materials(*)

$(^{140}La)_{1,2}$ = measured 1.6 MeV gamma activity of ^{140}La from each fuel rod (at the same time following shutdown)

$Y_{1,2}$ = (weighted) ^{140}Ba (^{140}La precursor) fission yield for each fuel type(**)

(*) *The following relationship was derived for relative rod powers from a thermal model of a fuel rod with cladding, where the cladding temperature raises adiabatically:*

$$\frac{K_1}{K_2} = \frac{P_1/(dT_c/dt)_1}{P_2/(dT_c/dt)_2} = \frac{(A_f C_f \rho_f + A_c C_c \rho_c)_1}{(A_f C_f \rho_f + A_c C_c \rho_c)_2}$$

where: P = rod power; A = cross sectional area (all the fuels are of the same length); C = specific heat; ρ = density. Subscripts f and c denote fuel and cladding.

(**) *When more than one fissile isotope is present in the fuel, the fission yields must be weighted by the (calculated) effective macroscopic fission cross sections of the different isotopes. Additionally, the variation in the energy release per fission for the different fissile isotopes must be accounted for in the correction factor.*

$S_{1,2}$ = calculated self absorption factors of rods of each fuel type for the 1.6 MeV gamma of ^{140}La.

$\Gamma_{1,2}(t)$ = measured fission product gross gamma activity (>0.5 MeV) from each fuel rod, at the same time t following shutdown of the "heatup" irradiation.

The fuel rods to be compared were placed in thermally insulated thimbles which were installed at core positions of equal flux in a single region UO_2-2 wt% PuO_2 (8% ^{240}Pu) loading. The cladding heatup rates were measured using 30 gage iron-constantan thermocouples attached to the cladding of the fuel rods at their vertical centers. The reactor power was raised to a nominal 7 kW on about a 20 sec period and maintained at a steady power level during data collection. The voltage output from the two thermocouples was read by means of a digital voltmeter alternately sampling each thermocouple every 6 sec. The experimental setup is shown in line form in Figure C-1. Data collection was terminated when the cladding heatup was no longer linear. This breakthrough was normally observed 60 to 70 sec following reactor stabilization at 7 kW. A linear least squares fit was applied to 10 data points obtained from each fuel rod heatup. A typical calorimetric measurement is shown in Figure C-2. Figure C-3 illustrates the relative cladding heatup of the five compared fuels. Each fuel combination measurement was repeated three times using different rods.

Following the calorimetric measurements, the two fuel rods were removed from the thimbles and their gamma activity (>0.5 MeV) counted as a function of time following shutdown, using the same gamma scanning equipment and energy discrimination employed during power distribution measurements. The relative gamma activities were measured for the fuel rods during the period 4 to 8 1/2 hr following shutdown.

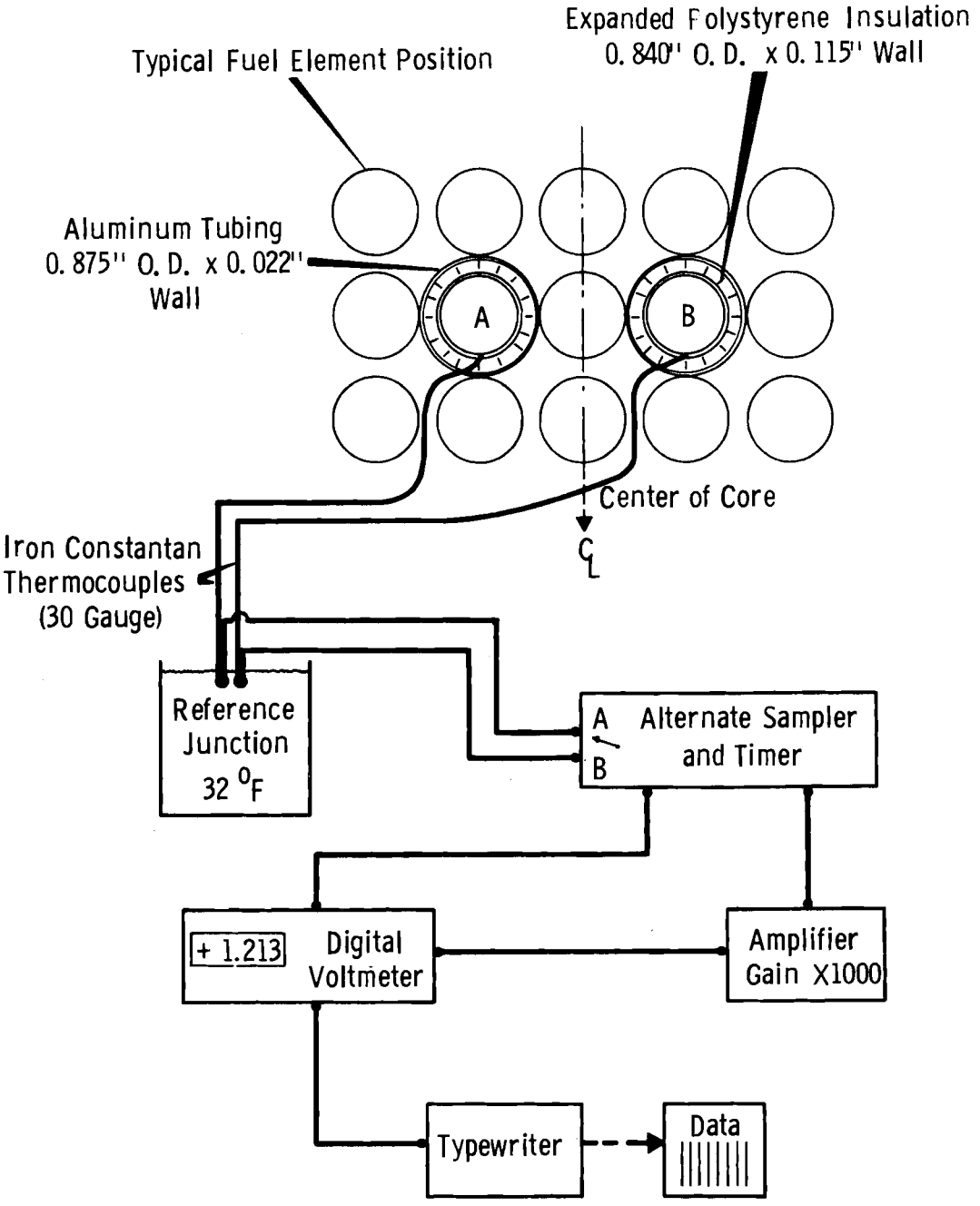

FIGURE C-1. EXPERIMENTAL ARRANGEMENT FOR CALORIMETRIC MEASUREMENTS
(A&B ARE FUEL ELEMENTS BEING COMPARED)

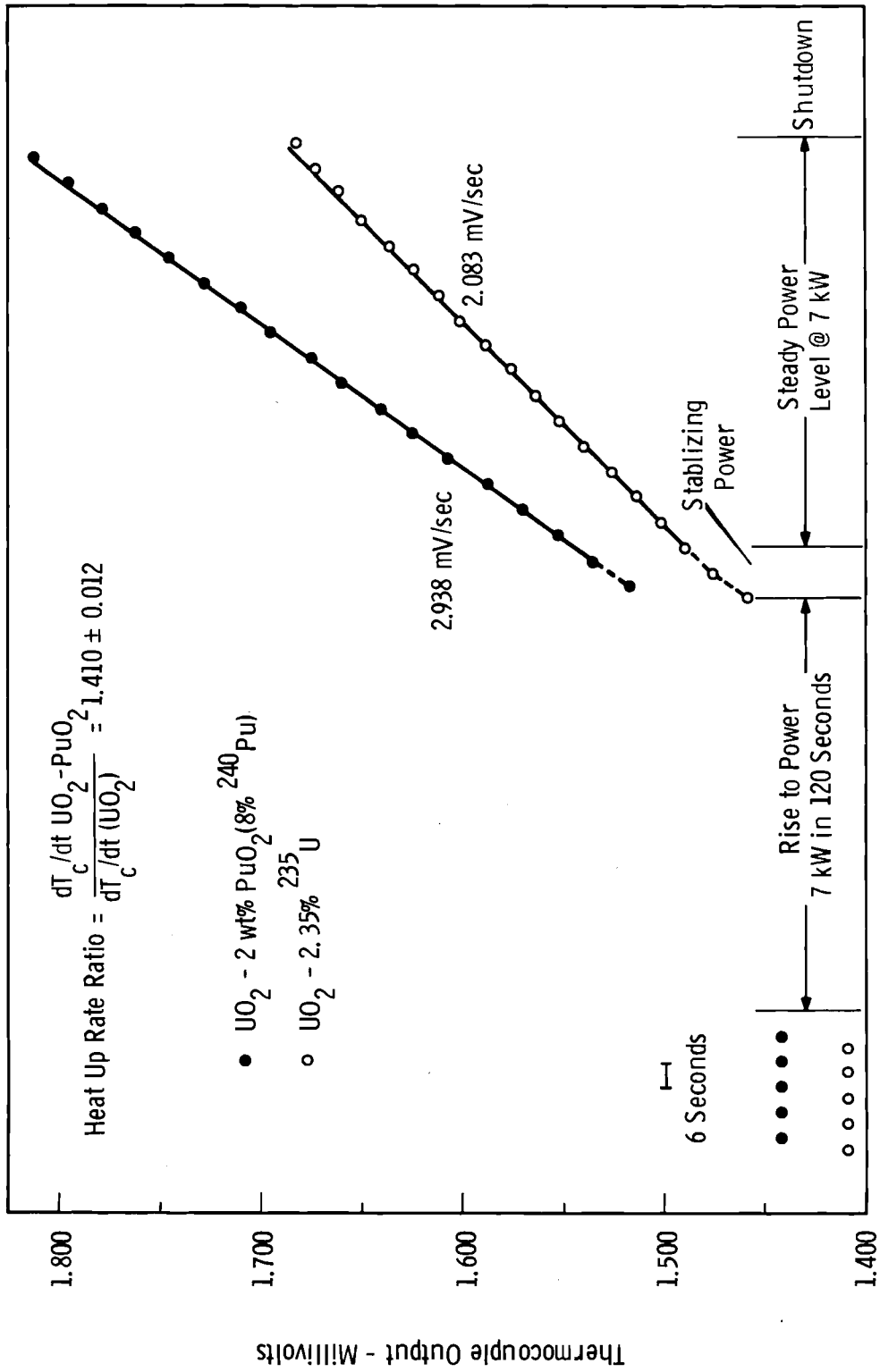

FIGURE C-2. TYPICAL CLADDING HEATUP RATE MEASUREMENT

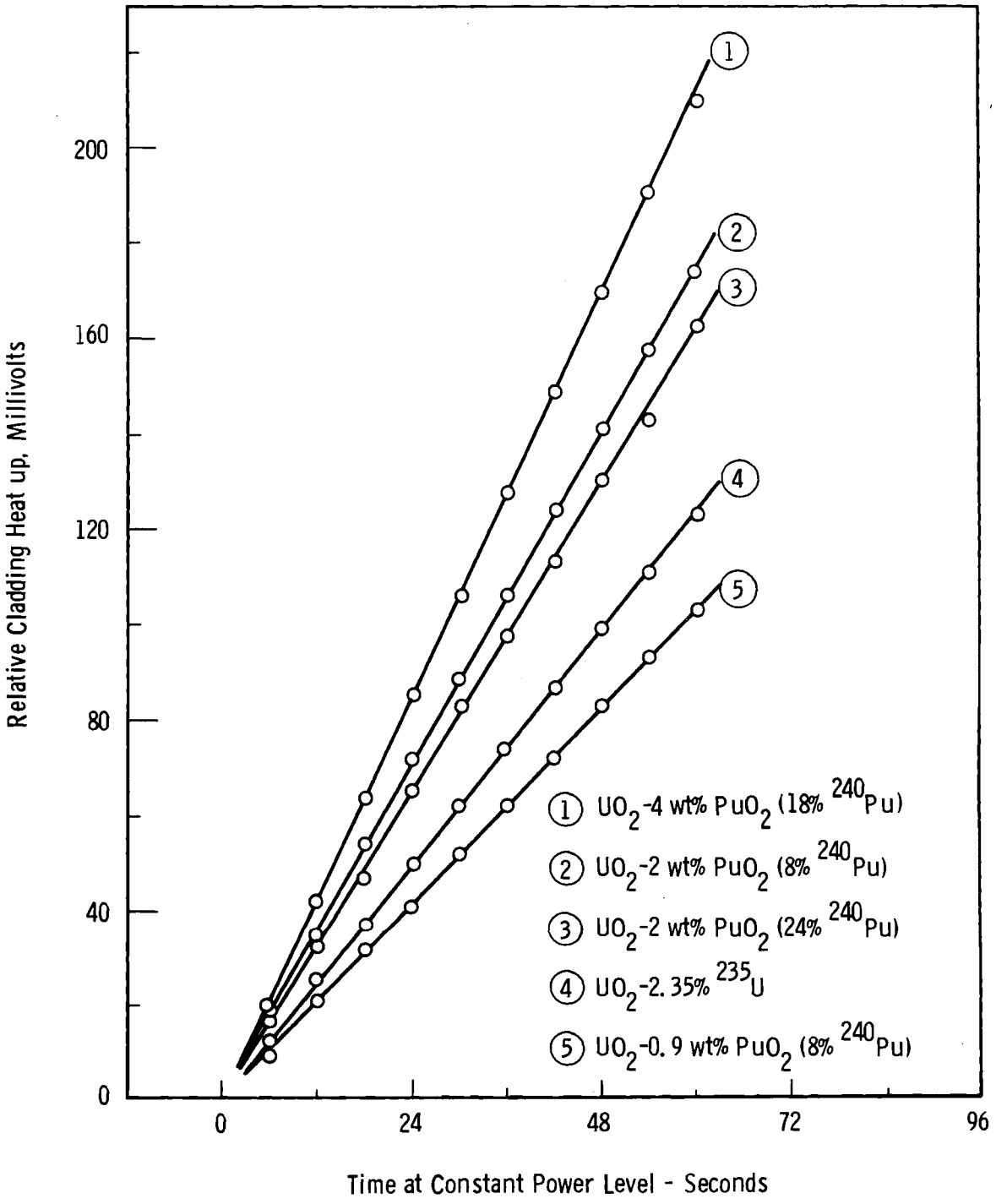

FIGURE C-3. RELATIVE CLADDING HEATUP OF THE COMPARED FUELS (ACTUAL NORMALIZED DATA)

After 12 and up to 30 days following irradiation, the fuel rods used for calorimetric measurements were gamma analyzed for their ^{140}La activities using a multichannel analyzer. The integral counts under the ^{140}La (1.60 MeV) photopeak at half-maximum were compared for each fuel combination. The rods used for these measurements were counted prior to irradiation and found to have no detectable history of ^{140}La activity. The measurement of cladding heatup rates and ^{140}La activities, coupled with the correction factors and the gamma activity ratios, gave two independent determinations of the conversion factor F(t) for each fuel pair, as indicated in Equations (2) and (3).

ACCURACY OF EXPERIMENTAL RESULTS

The results of the intercalibration measurements obtained by the calorimetric method are listed in Table C-I. The uncertainty associated with each heatup rate ratio is practically one-half of the maximum dispersion of the results obtained for different couples of rods of the same fuel pair (the standard deviations of the linear fits were used as weighting factors). The same criterion was adopted to define the confidence interval of the gamma ratios. The gamma ratios for UO_2-PuO_2 fuels were assumed to be constant with time, since the ratio varied less than 0.5% over the times interval of interest.* The UO_2-PuO_2/UO_2 gamma ratios were found to be time dependent and was well represented by a straight line; the slopes were practically identical for both fuel pairs involving UO_2 (see Table C-I). The accuracy of this set of measurements looks quite satisfactory; a cross-check was possible for Cases 1, 4 and 5 of Table C-I, and an agreement was found which was much better than expected on the basis of the uncertainties of the single measurements. On the other hand, the results of the

* *Gamma ratios were sampled about 40 times for each pair of fuel rods in the time range of measurement.*

TABLE C-I. Results of Intercalibration Measurements (calorimetric method)

Case	Compared Fuels	$\frac{(dT_c/dt)_1}{(dT_c/dt)_2}$	$\frac{K_1}{K_2}$ [a]	$\frac{\Gamma_1}{\Gamma_2}$	$F(t)_{\frac{\text{fuel 1}}{\text{fuel 2}}}$
1	$\frac{UO_2\text{-}2\ wt\%\ PuO_2(8)}{UO_2\text{-}2.35\%\ 235_U}$	1.410 ± 0.020	1.26	1.443 ± 0.005 [b]	1.231 ± 0.021 [c]
2	$\frac{UO_2\text{-}2\ wt\%\ PuO_2(8)}{UO_2\text{-}2\ PuO_2(24)}$ [d]	1.085 ± 0.002	1.00	1.096 ± 0.005	0.990 ± 0.007
3	$\frac{UO_2\text{-}2\ wt\%\ PuO_2(8)}{UO_2\text{-}0.9\ wt\%\ PuO_2}$	1.679 ± 0.012 [e]	1.01_6	1.795 ±0.005	[0.950 ± 0.010]
4	$\frac{UO_2\text{-}2\ wt\%\ PuO_2(8)}{UO_2\text{-}4\ wt\%\ PuO_2}$	0.815 ± 0.002	1.01_5	0.827 ± 0.003	1.000 ± 0.006
5 [f]	$\frac{UO_2\text{-}4\ wt\%\ PuO_2}{UO_2\text{-}2.35\%\ 235_U}$	1.728 ± 0.021	1.24	1.755 ± 0.005 [b]	1.221 ± 0.018 [c]

a. Corrections considered to be absolute. The specific heat values used are: Zircaloy-2, 0.071 Btu/lb °F; Aluminum 6061, 0.22 Btu/lb °F; UO_2 and UO_2-PuO_2 fuels, 0.067 Btu/lb °F.

b. Normalized to 306 min following shutdown. The time dependence of these gamma ratios between 4 and 8 1/2 hours following shutdown can be represented by a straight line. The rate of increase of both ratios is (0.73 ± 0.02)%/hr. No appreciable time dependence was observed for the other gamma ratios.

c. Normalized to 306 min following shutdown.

d. (8) and (24) are the isotopic concentrations (%) of ^{240}Pu in the two UO_2-2 wt% PuO_2 fuels

e. Only two heatup rate measurements were accepted for this pair.

f. This additional set of measurements was made to provide a cross check with Cases 1 and 4.

^{140}La measurements were not very satisfactory. Due to instrumentation problems, the useful ^{140}La activity measurements were made late where the counting rate or "signal to background" ratio was not high enough to yield the desired statistical accuracy. The accuracy of these measurements was hardly better than 3%. Therefore, the intercalibration factors derived from these measurements were not applied for rod power normalization.

RELIABILITY OF INTERCALIBRATION FACTORS

The uncertainties associated with the F(t)'s in Table C-I were obtained by propagating the experimental errors defined for heatup rate and gamma activity ratios, since heat capacitance corrections were assumed to be absolute. The presence of systematic errors in the K_1/K_2 correction factors cannot be excluded in principle, but, in practice, it is very unlikely that such errors exceed some tenths of percent. The overall confidence intervals relative to the intercalibration factors were settled around ±2%; this value compares favorably with the confidence on the homogeneity of fuel within the rods which was determined by axially gamma scanning irradiated fuel rods.

The measured F(t) for the UO_2-0.9 wt% PuO_2 fuel is about 5% lower than expected, however, there was evidence to suggest that this value is incorrect.* The reason for this anomaly was identified with nonhomogeneity of the UO_2-0.9 wt% PuO_2 fuel was found to be high relative to the other fuel types during the γ-scanning measurements. The normalized powers of UO_2-0.9 wt% PuO_2 rods, obtained by using the measured intercalibration factor (0.950) should be looked at with suspicion in the analysis of theory-experiment comparison on multiregion loadings.

---

* *The lack of an appreciable time dependence of the Γ_1/Γ_2 ratio in the 4 to 8 1/2 hour decay range is inconsistent with a gamma to power conversion ratio not equal or very close to unity. The calculated fission cross sections, which are considered accurate, indicate that the power sharing between ^{235}U and ^{239}Pu should be similar to other UO_2-PuO_2 fuel types.*

APPENDIX D

MULTIREGION POWER DISTRIBUTION MEASUREMENTS AND CALCULATIONS

P. Loizzo, R. Martinelli and L. D. Williams

APPENDIX D

MULTIREGION POWER DISTRIBUTION MEASUREMENTS AND CALCULATIONS

P. Loizzo, R. Martinelli and L. D. Williams

The gamma activity counting procedure for the mutiregion loadings was slightly different than that for the single region loadings. Using only one type of fuel, as in the single region experiments, a single monitor could be placed in the decay system and utilized for decay correction over the entire counting time. In the multiregion loadings, this method was not practical due to the different time dependent decay characteristics of the various types of fuel. The different types of fuel rods were counted initially by themselves using a decay monitor of their own type of fuel. Following the gamma counting of the individual fuel types, selected rods of each type were counted relative to each other using, in most cases, a UO_2-2 wt% PuO_2 (8% ^{240}Pu) rod as a normalizing fuel. The relative gamma scanning results for all the fuels were then corrected to the same time following shutdown using the normalizing results. At this point, gamma activity to rod power conversion factors, as determined by the methods outlined in Appendix C, were applied to the results. The power normalization factors determined by the calorimetric method were used for the gamma activity to rod power conversion.

The experimental uncertainties of the measurements in the multiregion loadings are not provided for each case as was done in the single region loadings. It was determined that the relative accuracy of the experiment (RAE) for these loadings was generally the same as for single region cores. The uncertainty associated with the power normalization factors is not included in the RAE. The RAE is, in fact, experimental confidence for the rod gamma activities and not the rod power.

Uncertainties associated with rod powers following the application of the power normalization factors cannot be generally related to the entire loading. The confidence intervals for each type of fuel can only be individually applied using the uncertainty for the power conversions listed in Table C-I and the uncertainty derived from the dispersion of the gamma activities observed in rod symmetry checks.

The loading maps and relative rod power for all the multi-region loadings are presented in this section in Figures D-1 through D-11. The types of fuel in the various regions are labeled on the loading maps. The abbreviated designations should be obvious for all fuel except the UO_2-2 wt% PuO_2. Where not specifically denoted as 24% ^{240}Pu, the 2 wt% designates the 8% ^{240}Pu fuel. As for the single region loading, the rod powers shown on the loading maps are the average power of symmetric rods. The individual rod powers for six of the eleven measured configurations are given in Tables D-I through D-VI, where they are compared with rod powers calculated using various theoretical models. Again, the numbers seen on the loading maps and in the tables are only location index numbers used during the calculations and have no other significance. The case numbers listed in the tables for each model are related to corresponding numbers used in Table XVI through XIX and in the text.

The discrepancies between experimental and theoretical rod powers are defined in the same manner in this section as for the single region configurations.

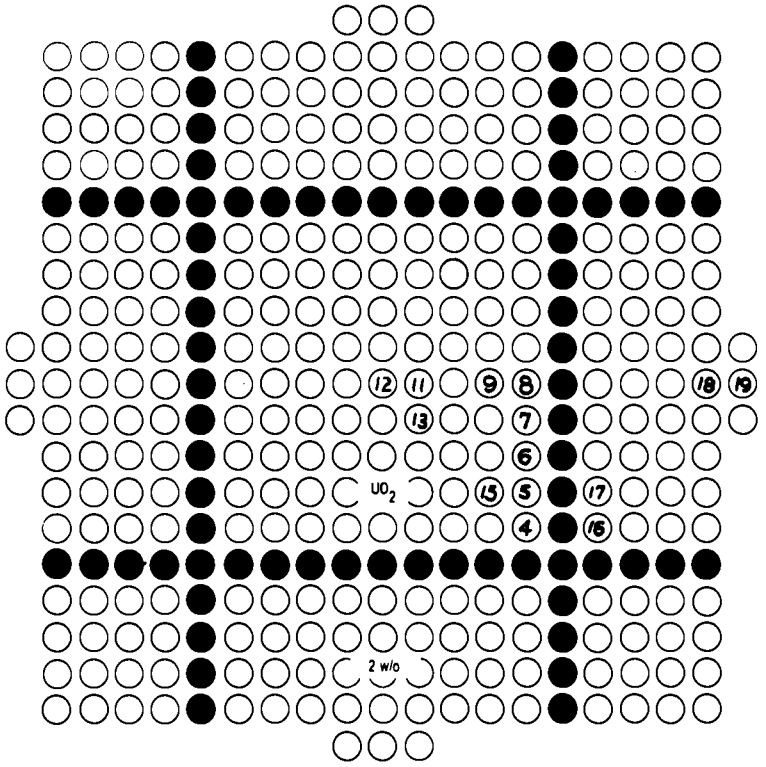

BASIC 9x9, UO_2-2.35% ^{235}U ELEMENT IN UO_2-2 WT% PuO_2 (8% ^{240}Pu)

Experimental Power Distribution:

Position No.	Relative Power
UO_2-2.35% ^{235}U Rods	
12	1.301
11	1.303
9	1.323
8	1.473
13	1.310
15	1.331
4	1.597
5	1.472
6	1.476
7	1.473
UO_2-2 WT% PuO_2 Rods	
16	1.801
17	1.562
18	.702
19	.934

FIGURE D-1

TABLE D-I. Experimental - Calculational Power Distribution Comparisons, Basic 9 × 9 - UO_2-2.35% ^{235}U Element in UO_2-2 wt% PuO_2 (8% ^{240}Pu)

Rod Location	Symmetry Points	Experimental Rod Power, Arbitrary Units	Case No. 66 St. RIBOT 4G - 4M Sets No. 1 and 3		Case No. 67 St. RIBOT 5G - 4M Sets No. 1 and 3		Case No. 68 THERMOS - HRG 4G - 4M Sets No. 14 and 34	
			Power	δ, %	Power	δ, %	Power	δ, %
4	1	1.605	*1.597	-0.5	*1.597	-0.5	*1.597	-0.5
	2	1.600		-0.2		-0.2		-0.2
	3	1.586		+0.7		+0.7		+0.7
5	1	1.483	1.483	0	1.461	-1.5	1.477	-0.4
	2	1.474		+0.6		-0.9		+0.2
	3	1.458		+0.17		+0.2		+1.3
6	1	1.473	1.473	0	1.450	-0.16	1.470	-0.2
	2	1.479		-0.4		-2.0		-0.6
	3	(1.444)		(+2.0)		(+0.4)		(+1.8)
7	1	1.474	1.485	+0.7	1.463	-0.8	1.485	+0.7
	2	1.476		+0.6		-0.9		+0.6
	3	1.471		+1.0		-0.6		+1.0
8	1	1.471	1.492	+1.4	1.469	-0.1	1.492	+1.4
	2	1.472		+1.3		-0.2		+1.3
	3	1.475		+1.1		-0.4		+1.1
9	1	1.324	1.349	+1.9	1.304	-1.5	1.335	+0.8
	2	1.318		+2.3		-1.1		+1.3
	3	1.327		+1.6		-1.8		+0.6
11	1	1.312	1.333	+1.6	1.289	-1.7	1.323	+0.8
	2	1.295		+2.9		-0 5		+2.2
	3	1.302		+2.4		-1.0		+1.6
12	1	1.301	1.337	+2.8	1.294	-0.5	1.328	+2.1
13	1	1.313	1.328	+1.2	1.284	-2.1	1.318	+0.4
	2	1.302		+2.0		-1.4		+1.2
	3	1.318		+0.8		-2.6		0
	4	1.305		+1.8		-1.6		+1.0
15	1	1.332	1.353	+1.5	1.307	-1.9	1.335	+1.0
	2	1.327		+1.9		-1.5		+0.6
	3	1.333		+1.6		-2.0		+0.1
Group Average δ, 28 points			(1.22 ± 0.92)%		(-1.07 ± 0.79)%		(0.72 ± 0.72)%	
16	1	1.798	1.861	+3.5	1.830	+1.8	1.794	-0.2
	2	1.799		+3.4		+1.7		-0.3
	3	(1.839)		(+1.2)		(-0.5)		(-2.4)
17	1	1.557	1.576	+1.2	1.542	-1.0	1.519	-2.4
	2	1.555		+1.3		-0.8		-2.3
	3	1.566		+0.6		-1.5		-3.0
18	1	0.705	0.744	+5.6	0.710	+0.7	0.720	+2.1
	2	0.698		+6.6		+1.7		+3.1
	3	0.699		+6.4		+1.6		+3.0
19	1	0.936	1.005	+7.4	0.971	+3.7	0.943	+0.7
	2	0.933		+7.7		+4.1		+1.1
	3	0.927		+8.4		+4.7		+1.7
Group Average δ, 11 points			(4.74 ± 2.85)%		(1.52 ± 2.08)%		(0.32 ± 2.16)%	
Loading Average δ, 39 points			(2.22 ± 230)%		(-0.34 ± 1.72)%		(0.61 ± 1.28)%	
K_{eff}		1.0068	1.0098		1.0104		1.0047	

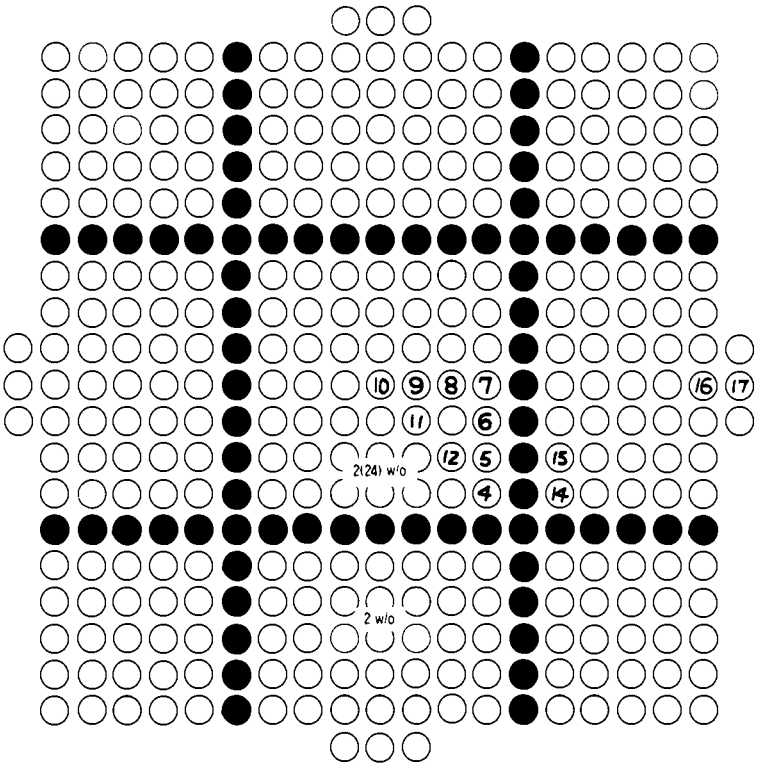

BASIC 7x7, UO_2-2 WT% PuO_2 (24% ^{240}Pu) ELEMENT IN UO_2-2 WT% PuO_2 (8% ^{240}Pu)

Experimental Power Distribution:

Position No.	Relative Power
24% ^{240}Pu Rods	
10	.631
9	.635
8	.691
7	.988
11	.644
12	.751
4	1.188
5	.967
6	.917
8% ^{240}Pu Rods	
14	1.218
15	.946
16	.433
17	.590

FIGURE D-2

TABLE D-II. Experimental - Calculational Power Distribution Comparisons, Basic 7 × 7, UO_2-2 wt% PuO_2 (24% ^{240}Pu) Element in UO_2-2 wt% PuO_2 (8% ^{240}Pu)

Rod Location	Symmetry Points	Experimental Rod Power, Arbitrary Units	Case No. 65 St. RIBOT 4G - 4M Sets No. 1 and 6 Power	δ, %
4	1	1.184	*1.188	+0.3
	2	1.188		0
	3	1.192		-0.3
5	1	0.976	0.971	-0.5
	2	0.965		+0.6
	3	0.960		+1.2
6	1	0.916	0.928	+1.3
	2	0.923		+0.6
	3	0.911		+1.9
7	1	0.905	0.922	+1.9
	2	0.912		+1.1
	3	(0.379)		(+4.9)
Group Average δ, 11 points			(+0.74 ± 0.82)%	
8	1	0.687	0.702	+2.1
	2	0.695		+1.0
	3	(0.670)		(+4.7)
9	1	0.637	0.657	+3.1
	2	0.632		+3.9
	3	0.631		+4.1
	4	0.640		+2.6
10		0.631	0.650	+3.1
11	1	0.646	0.663	+2.7
	2	0.638		+4.0
	3	0.648		+2.4
12	1	0.754	0.751	-0.6
	2	0.749		+0.3
	3	(0.735)		(+2.2)
Group Average δ, 12 points			(2.39 ± 1.49)%	
14	1	(1.193)	1.185	(-0.7)
	2	1.220		-2.9
	3	1.215		-2.5
15	1	0.945	0.964	+2.0
	2	0.945		+2.0
	3	0.947		+1.8
	4	(0.976)		(-1.2)
16	1	0.439	0.440	+0.2
	2	0.433		+1.6
	3	0.430		+2.3
17	1	0.591	0.595	+0.7
	2	(0.571)		(+4.2)
	3	0.588		+1.2
Group Average δ, 10 points			(0.61 ± 1.85)%	
Loading Average δ, 33 points			(1.3 ± 1.62)%	
δF			(-2.4 ± 1.5)%	
K_{eff}		1.0051	1.0158	

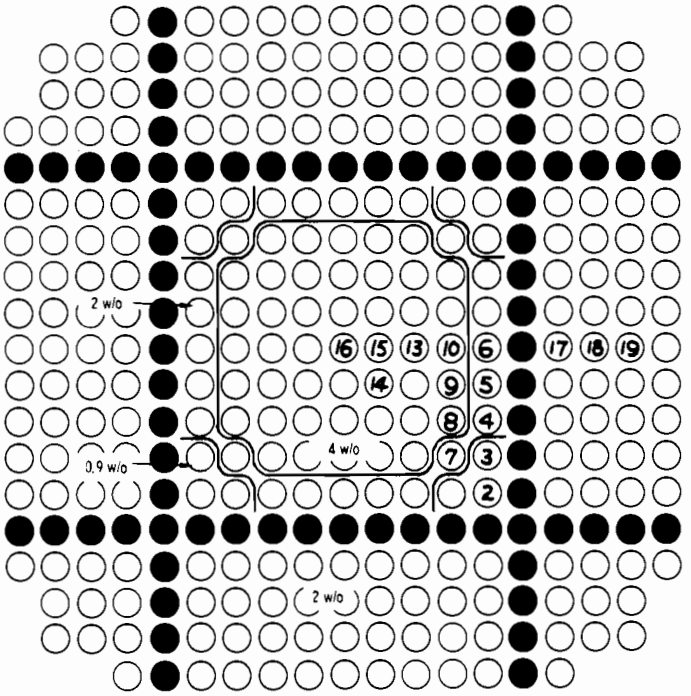

BASIC 9x9, COMPOSITE ELEMENT #1 IN
UO_2-2 WT% PuO_2 (8% ^{240}Pu)

Experimental Power Distribution:

Position No.	Relative Power
0.9 WT% PuO_2 Rods	
2	1.075
3	.881
4 WT% PuO_2 Rods	
16	.997
15	.985
13	.995
10	1.125
14	.979
8	1.176
9	1.106
2 WT% PuO_2 Rods	
4	1.364
5	1.306
6	1.288
7	1.163
17	1.200
18	.785
19	.683

FIGURE D-3

TABLE D-III. Experimental - Calculational Power Distribution Comparisons, Basic 9 × 9, Composite Element No. 1 in UO_2-2 wt% PuO_2 (8% ^{240}Pu)

Rod Location	Symmetry Points	Experimental Rod Power, Arbitrary Units	Case No. 69 St, RIBOT 4G - 4M Sets No. 1, 4, and 5 Power	Case No. 69 St, RIBOT 4G - 4M Sets No. 1, 4, and 5 δ, %	Case No. 70 THERMOS - HRG 4G - 4M Sets No. 14, 41, and 51 Power	Case No. 70 THERMOS - HRG 4G - 4M Sets No. 14, 41, and 51 δ, %
2	1	1.077	1.018	-6.0	1.037	-4.8
	2	1.071		-5.4		-3.7
	3	1.068		-5.1		-3.4
	4	1.085		-6.6		-4.9
3	1	0.882	0.815	-8.2	0.835	-5.9
	2	0.873		-7.1		-4.9
	3	0.892		-9.1		-6.9
	4	(0.951)		(-14.7)		(-12.9)
	5	0.893		-9.2		-7.0
	6	(0.858)		(-5.7)		(-3.3)
	7	0.863		-6.0		-3.7
Group Average δ, 9 points			(-6.97 ± 1.54)%		(-4.97 ± 1.36)%	
4	1	1.360	*1.368	+0.6	*1.368	+0.6
	2	1.372		-0.3		-0.3
	3	1.365		+0.3		+0.3
	4	1.376		-0.6		-0.6
5	1	1.308	1.283	-1.9	1.293	-1.2
	2	1.312		-2.2		-1.5
	3	(1.285)		(-0.1)		(+0.6)
	4	1.297		-1.1		-0.3
6	1	1.292	1.275	-1.3	1.287	-0.4
	2	1.285		-0.7		-0.1
	3	(0.1268)		(+0.6)		(+1.5)
7	1	1.172	1.145	-2.3	1.146	-2.2
	2	1.157		-1.0		-0.9
	3	1.160		-1.1		-1.2
Group Average δ, 12 points			(-0.99 ± 0.90)%		(-0.66 ± 0.78)%	
8	1	1.196	1.232	+3.0	1.205	+0.8
	2	1.199		+2.7		+0.5
	3	1.191		+3.4		+1.2
9	1	1.127	1.153	+2.3		
	2	1.119		+3.1		
	3	1.124		+2.6		
10	1	(1.118)	1.147	(+2.6)	1.134	(+1.4)
	2	1.143		+0.3		-0.8
	3	1.144		+0.4		-0.9
13	1	1.007	1.026	+1.9	1.026	+1.8
	2	1.015		+1.1		+1.0
	3	1.010		+1.6		+1.5
14	1	(0.967)	1.017	(+5.2)	1.019	(+5.4)
	2	0.988		+2.9		+3.1
	3	1.001		+1.6		+1.8
15	1	(1.021)	1.019	(-0.2)	1.022	(+0.1)
	2	0.990		+3.0		+3.3
	3	1.006		+1.3		+1.6
	4	0.987		+3.3		+3.6
16	1	1.013	1.022	+0.9	1.026	+1.3
Group Average δ, 17 points			(2.08 ± 1.02)%		(1.41 ± 1.34)%, (14 points)	
17	1	1.181	1.195	1.1	1.190	+0.8
	2	1.186		0.7		+0.4
	3	1.176		1.6		+1.2
18	1	0.770	0.781	1.4	0.776	+0.8
	2	0.775		0.8		+0.2
	3	0.774		0.9		+0.3
19	1	0.673	0.682	1.3	0.670	-0.5
	2	0.682		0		-0.8
	3	0.671		1.6		-0.2
Group Average δ, points			(1.04 ± 0.51)%		(0.22 ± 0.65)%	
Loading Average δ, 47 points			(-0.63 ± 3.49)%		(-0.84 ± 2.57)%, (44 points)	
Loading Average δ, (excluding 0.9% PuO_2 rods), 38 points			(0.87 ± 1.59)%		(-0.39 ± 1.40)%, (35 points)	
K_{eff}		1.0022	1.0096		1.0077	

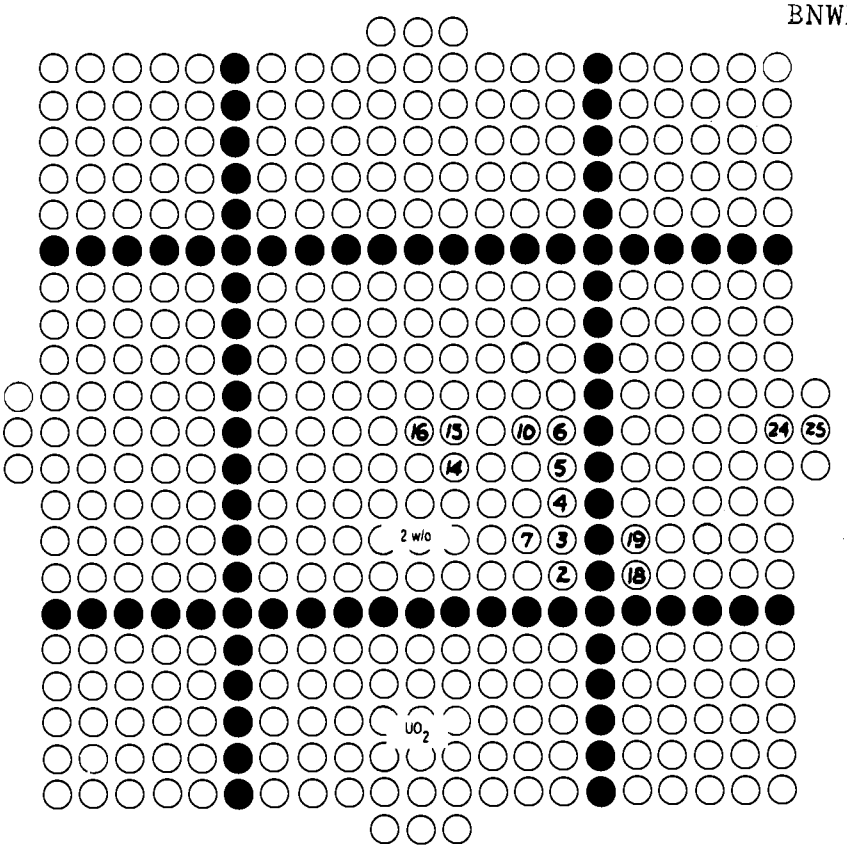

BASIC 9x9, UO_2-2 WT% PuO_2 (8% ^{240}Pu) ELEMENT IN UO_2-2.35% ^{235}U

Experimental Power Distribution:

Position No.	Relative Power
UO_2-2 WT% PuO_2 Rods	
16	.604
15	.603
10	.643
6	.890
14	.600
7	.685
2	1.129
3	.902
4	.891
5	.890
UO_2-2.35% ^{235}U Rods	
18	.783
19	.702
24	.380
25	.416

FIGURE D-4

TABLE D-IV. Experimental - Calculational Power Distribution Comparisons, Basic 9 × 9, UO_2-2 wt% PuO_2 Element in UO_2-2.35% ^{235}U

Rod Location	Symmetry Points	Experimental Rod Power, Arbitrary Units	Case No. 53 St. RIBOT 4G - 4M Sets No. 1 and 3		Case No. 54 St. RIBOT 5G - 4M Sets No. 1 and 3		Case No. 55 RIBOT, M.H.[1] 5G - 4M Sets No. 15 and 34		Case No. 56 THERMOS - HRG 4G - 4M Sets No. 14 and 32	
			Power	δ, %	Power	δ, %	Power	δ, %	Power	δ, %
2	1	1.131	1.124	-0.6	1.130	-0.1	1.104	-2.4	1.114	-1.5
	2	1.127		-0.3		+0.3		-2.0		-1.1
	3	(1.068)		(+5.2)		(+5.8)		(+3.4)		(+4.3)
3	1	0.906	*0.905	-0.1	*0.905	-0.1	*0.905	-0.1	*0.905	-0.1
	2	0.904		+0.1		+0.1		+0.1		+0.1
	3	0.905		0		0		0		0
	4	(0.893)		(+1.3)		(+1,3)		(1.3)		(+1.3)
4	1	0.897	0.877	-2.2	0.879	-2.0	0.877	-2.2	0.881	-1.8
	2	0.894		-1.8		-1.7		-1.8		-1.5
	3	0.884		-0.8		-0.6		-0.8		-0.4
5	1	0.894	0.884	-1.2	0.887	-0.8	0.883	-1.2	0.889	-0.6
	2	0.898		-1.6		-1.2		-1.7		-1.0
	3	0.882		+0.2		+0.6		+0.1		+0.8
6	1	0.892	0.889	-0.4	0.892	0	0.887	-0.6	0.895	+0.3
	2	0.897		-0.9		-0.6		-1.1		-0.2
	3	0.882		+0.8		+1.1		+0.6		+1.5
Group Average δ, 14 points			(-0.63 ± 0.85)%		(-0,36 ± 0.86)%		(-0.94 ± 0.98)%		(-0.39 ± 0.83)%	
10	1	0.641	0.647	+0.9	0.641	0	0.661	+3.1	0.659	+2.8
	2	0.641		+0.9		0		+3.1		+2.8
	3	0.647		0		-0.9		+2.2		+1.9
14	1	0.594	0.610	+2.8	0.606	+2.0	0.621	+4.5	0.624	+5.0
	2	0.602		+1.4		+0.7		+3.2		+3.7
	3	0.589		+3.6		+2.9		+5.4		+5.9
	4	(0.616)		(-1.0)		(-1.7)		(+0.8)		(+1.4)
15	1	0.603	0.613	1.7	0.609	+1.0	0.623	+3.3	0.627	+4.0
	2	0.603		+1.7		+1.0		+3.3		+4.0
	3	0.604		+1.6		+0.8		+3.2		+3.8
	4	(0.591)		(+3.8)		(+3.0)		(+5.4)		(+6.1)
16	1	0.604	0.616	+2.0	0.612	+1.3	0.626	+3.7	0.630	+4.3
Group Average δ, 10 points			(1.66 ± 1.01)%		(0.88 ± 1.07)%		(3.50 ± 0.88)%		(3.82 ± 1.14)%	
18	1	0.784	0.743	-5.2	0.765	-2.4	0.762	-2.8	0.758	-3.3
	2	0.779		-4.6		-1.8		-2.2		-2.7
	3	0.784		-5.2		-2.4		-2.8		-3.3
	4	0.785		-5.3		-2.5		-3.0		-3.4
19	1	0.699	0.667	-4.6	0.677	-3.1	0.681	-2.6	0.683	-2.3
	2	0.701		-4.8		-3.4		-2.9		-2.6
	3	0.706		-5.5		-4.1		-3.5		-3.3
	4	0.702		-4.9		-3.6		-3.0		-2.7
24	1	0.382	0.364	-4.7	0.357	-6.5	0.365	-4.4	0.360	-5.8
	2	0.379		-4.0		-6.3		-3.7		-5.0
	3	(0.370)		(-1.6)		(-3.5)		(-1.4)		(-2.7)
25	1	0.417	0.400	-4.1	0.403	-3.4	0.405	-2.9	0.389	-6.7
	2	0.416		-3.8		-3.1		-2.6		-6.5
	3	(0.408)		(-2.0)		(-1.2)		(-0.7)		(-4.7)
Group Average δ, 12 points			(-4.72 ± 0.54)%		(-3.55 ± 1.47)%		(-3.03 ± 0.58)%		(-3.97 ± 1.5)%	
Loading Average δ, 36 points			(-1.39 ± 2.69)%		(-1.03 ± 2.16)%		(-0.40 ± 2.74)%		(-0.41 ± 3.30)%	
K_{eff}		1.0039	1.0074		1.0087		1.0045		1.0012	

1. *Homogenized moderator cross sections, see text.*

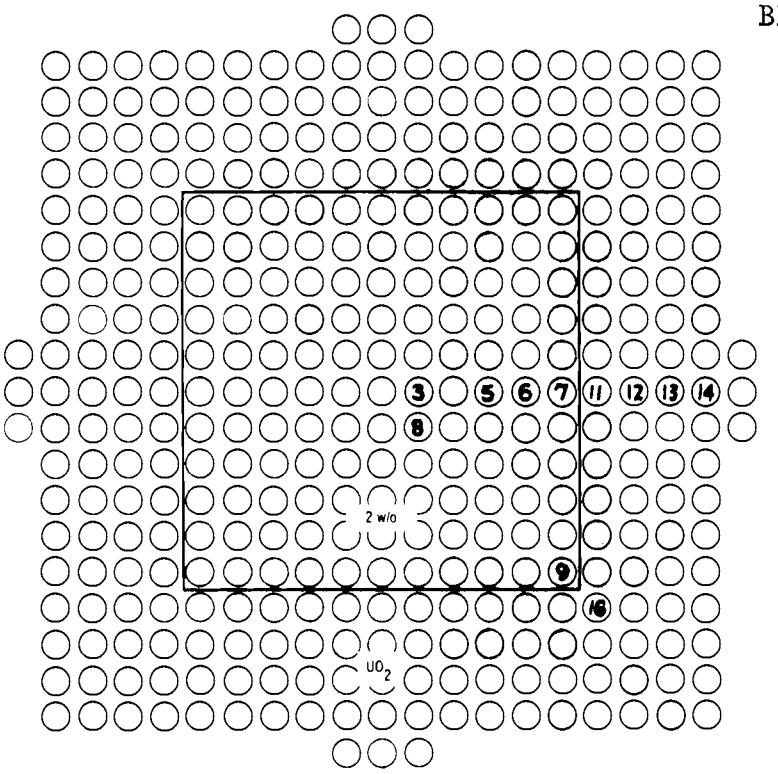

11x11, UO_2-2 WT% PuO_2 (8% ^{240}Pu) ELEMENT IN UO_2-2.35% ^{235}U

Experimental Power Distribution:

Position No.	Relative Power
UO_2-2 WT% PuO_2 Rods	
3	1.209
5	1.146
6	1.114
7	1.201
8	1.194
9	1.128
UO_2-2.35% ^{235}U Rods	
11	.832
12	.890
13	.840
14	.804
16	.726

FIGURE D-5

TABLE D-V. Experimental - Calculational Power Distribution Comparisons, 11 × 11, UO_2-2 wt% PuO_2 (8% ^{240}Pu) Element in UO_2-2.35% ^{235}U

Rod Location	Symmetry Points	Experimental Rod Power, Arbitrary Units	Case No. 57 St. RIBOT 4G - 4M Sets No. 1 and 3 Power	δ, %	Case No. 58 St. RIBOT 5G - 4M Sets No. 1 and 3 Power	δ, %	Case No. 59 RIBOT, M.H.(1) 4G - 4M Sets No. 15 and 34 Power	δ, %	Case No. 60 RIBOT, H.M.(1) 5G - 4M Sets No. 15 and 34 Power	δ, %
3	1	(1.192)	1.248	(+4.7)	1.256	(+5.6)	1.249	(+4.8)	1.253	(+5.1)
	2	1.227		+1.7		+2.4		+1.8		+2.1
	3	1.215		+2.8		+3.4		+2.8		+3.1
8	1	1.189	1.239	+4.2	1.247	+4.8	1.240	+4.3	1.244	+4.6
	2	1.205		+2.8		+3.5		+2.9		+3.3
	3	1.223		+1.3		+1.9		+1.4		+1.7
5	1	1.157	1.183	+2.3	1.189	+2.8	1.187	+2.6	1.189	+2.8
	2	1.158		+2.2		+2.7		+2.5		+2.7
	3	(1.133)		(+4.4)		(+5.0)		+4.7)		(+5.0)
6	1	1.118	1.159	+3.7	1.163	+4.0	1.165	+4.2	1.166	+4.3
	2	1.130		+2.6		+2.9		+3.1		+3.2
	3	1.127		+2.9		+3.2		+3.4		+3.5
7	1	1.227	1.267	+3.2	1.272	+3.7	1.254	+2.2	1.255	+2.3
	2	1.208		+4.9		+5.3		+3.8		+3.9
	3	1.202		+5.4		+5.8		+4.3		+4.4
9	1	(1.169)	1.201	(+2.8)	1.199	(+2.6)	1.179	(+0.8)	1.174	(+0.4)
	2	1.136		+5.7		+5.5		+3.8		+3.3
	3	1.141		+5.3		+5.1		+3.3		+2.9
Group Average δ, 15 points			(3.40 ± 1.40)%		(3.93 ± 1.44)%		(3.09 ± 0.87)%		(3.21 ± 0.85)%	
11	1	0.834	0.837	+0.3	0.838	+0.4	0.844	+1.3	0.845	+1.3
	2	0.837		0		+0.1		+0.9		+1.0
	3	0.824		+1.5		+1.7		+2.5		+2.6
12	1	0.885	0.887	+0.2	0.891	+0.7	0.886	+0.1	0.889	+0.5
	2	0.894		-0.8		-0.3		-0.9		-0.6
13	1	0.835	*0.840	+0.6	*0.840	+0.6	*0.840	+0.6	*0.840	+0.6
	2	0.843		-0.4		-0.4		-0.4		-0.4
	3	0.841		-0.2		-0.2		-0.2		-0.2
14	1	0.801	0.806	+0.6	0.804	+0.4	0.807	+0.7	0.805	+0.5
	2	0.805		+0.1		-0.1		+0.2		0
	3	0.807		-0.1		-0.4		0		-0.2
16	1	0.724	0.789	+0.7	0.729	+0.7	0.732	+1.1	0.731	+1.0
	2	0.723		+0.8		+0.8		+1.2		+1.1
	3	0.732		-0.4		-0.4		0		-0.1
Group Average δ, 14 points			(0.21 ± 0.56)%		(0.26 ± 0.61)%		(0.51 ± 0.86)%		(0.51 ± 0.84)%	
Loading Average δ, 29 points			(1.86 ± 1.94)%		(2.01 ± 2.04)%		(1.84 ± 1.57)%		(1.90 ± 1.60)%	
K_{eff}		1.0033	1.0028		1.0035		1.0013		1.0017	

1. Homogenized moderator cross sections, see text.

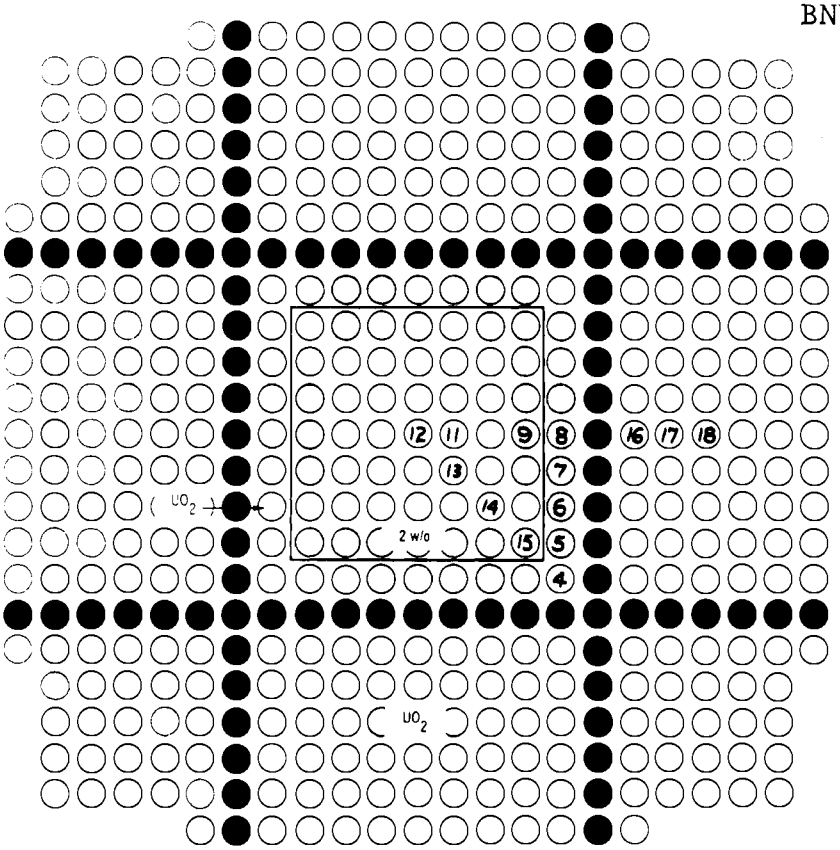

BASIC 9x9, COMPOSITE ELEMENT #2 IN UO_2-2.35% ^{235}U

Experimental Power Distribution:

Position No.	Relative Power
UO_2-2 WT% PuO_2 Rods	
12	.841
11	.810
9	1.080
13	.828
14	.896
15	1.235
UO_2-2.35% ^{235}U Rods	
4	1.223
5	1.016
6	.965
7	.966
8	.966
16	1.004
17	.774
18	.651

FIGURE D-6

TABLE D-VI. Experimental - Calculational Power Distribution Comparisons, Basis 9 × 9, Composite Element No. 2 in UO_2-2.35% ^{235}U

Rod Location	Symmetry Points	Experimental Rod Power, Arbitrary Units	Case No. 62 St. RIBOT 4G - 4M Sets No. 1 and 3		Case No. 63 St. RIBOT 5G - 4M Sets No. 1 and 3		Case No. 64 THERMOS - HRG 4G - 4M Sets No. 14 and 32	
			Power	δ, %	Power	δ, %	Power	δ, %
4	1	1.222	*1.224	+0.2	*1.224	+0.2	*1.224	+0.2
	2	1.218		+0.5		+0.5		+0.5
	3	1.231		-0.6		-0.6		-0.6
5	1	1.010	1.024	+1.4	1.008	-0.2	1.027	+1.7
	2	(0.990)		(+3.4)		(+1.8)		(+3.7)
	3	1.022		+0.2		-1.4		+0.5
6	1	0.961	0.969	+0.8	0.953	-0.8	0.979	+1.9
	2	0.970		-0.1		-1.7		+0.9
	3	0.965		+0.4		-1.2		+1.5
7	1	0.965	0.966	+0.1	0.950	-1.7	0.980	+1.5
	2	0.966		0		-1.7		+1.5
8	1	0.967	0.968	+0.1	0.953	-1.5	0.983	+1.7
	2	0.964		+0.4		-1.1		+2.0
	3	(1.000)		(-3.2)		(-4.7)		(-1.7)
Group Average δ, 12 points			(0.28 ± 0.49)%		(-0.93 ± 0.70)%		(1.11 ± 0.80)%	
9	1	1.087	1.153	+6.0	1.095	+0.7	1.118	+2.8
	2	1.092		+5.6		+0.3		+2.4
	3	(1.018)		(+13.3)		(+7.6)		(+9.8)
11	1	(0.816)	0.895	(+9.7)	0.856	(+4.9)	0.890	(+9.1)
	2	0.842		+6.3		+1.7		+5.7
	3	0.833		+7.4		+2.8		+6.8
12	1	0.848	0.894	+5.4	0.856	+0.9	0.889	+4.8
13	1	0.838	0.897	+7.0	0.856	+2.1	0.891	+6.3
	2	0.836		+7.3		+2.4		+6.6
	3	0.842		+6.5		+1.7		+5.8
	4	(0.823)		(+9.0)		(+4.0)		(+8.3)
14	1	0.907	0.961	+6.0	0.912	+0.6	0.944	+4.1
	2	0.900		+6.8		+0.1		+4.9
	3	(0.867)		(+10.8)		(+5.2)		(+8.9)
15	1	1.252	1.365	+9.0	1.286	+2.7	1.303	+4.1
	2	1.251		+9.1		+2.8		+4.2
	3	1.238		+10.3		+3.9		+5.3
	4	1.244		+9.7		+3.4		+4.7
Group Average δ, 14 points			(7.31 ± 1.59)%		(1.86 ± 1.20)%		(4.89 ± 1.32)%	
16	1	1.002	1.031	+2.9	1.016	+1.4	1.035	+3.3
	2	1.005		+2.6		+1.1		+3.0
	3	(1.031)		(0)		(-1.5)		(+0.7)
17	1	0.773	0.789	+2.1	0.756	-2.2	0.782	+1.2
	2	0.774		+1.9		-2.3		+1.0
	3	0.775		+1.8		-2.4		+0.9
18	1	0.654	0.662	+1.2	0.632	-3.4	0.657	+0.5
	2	0.647		+2.3		-2.3		+1.5
	3	0.652		+1.5		-3.1		+0.8
Group Average δ, 9 points			(2.04 ± 0.56)%		(-1.66 ± 1.84)%		(1.52 ± 1.02)%	
Loading Average δ, 35 points			(3.6 ± 3.36)%		(0.08 ± 2.00)%		(2.76 ± 2.13)%	
K_{eff}		1.0022	1.0042		1.0052		0.9967	

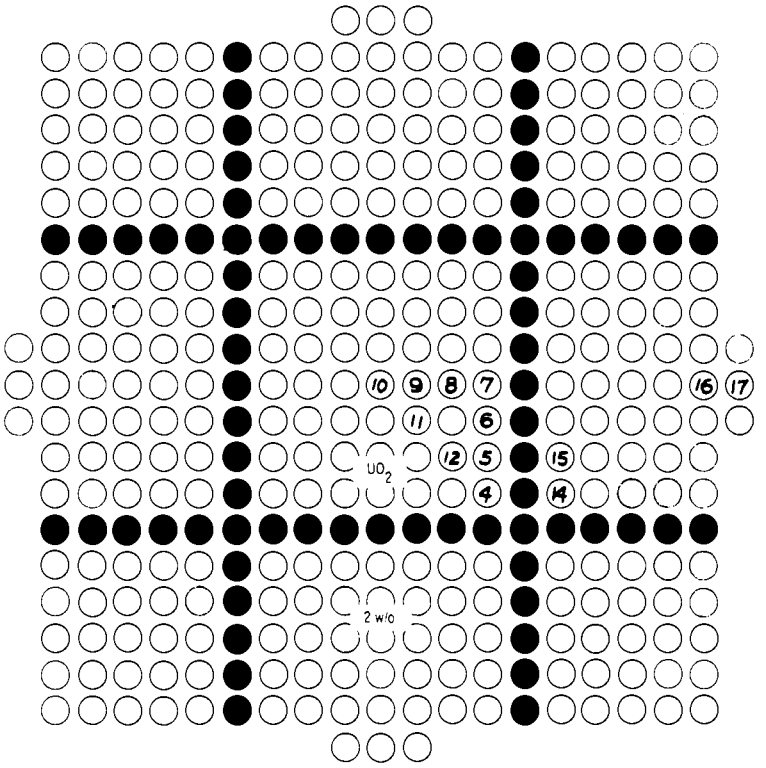

BASIC 7x7, UO_2-2.35% ^{235}U ELEMENT IN UO_2-2 WT% PuO_2 (8% ^{240}Pu)

Experimental Power Distribution:

Position No.	Relative Power
UO_2-2.35% ^{235}U Rods	
10	1.271
9	1.278
8	1.316
7	1.498
11	1.283
12	1.373
4	1.708
5	1.543
6	1.514
UO_2-2 WT% PuO_2 Rods	
14	1.982
15	1.653
16	.701
17	.949

FIGURE D-7

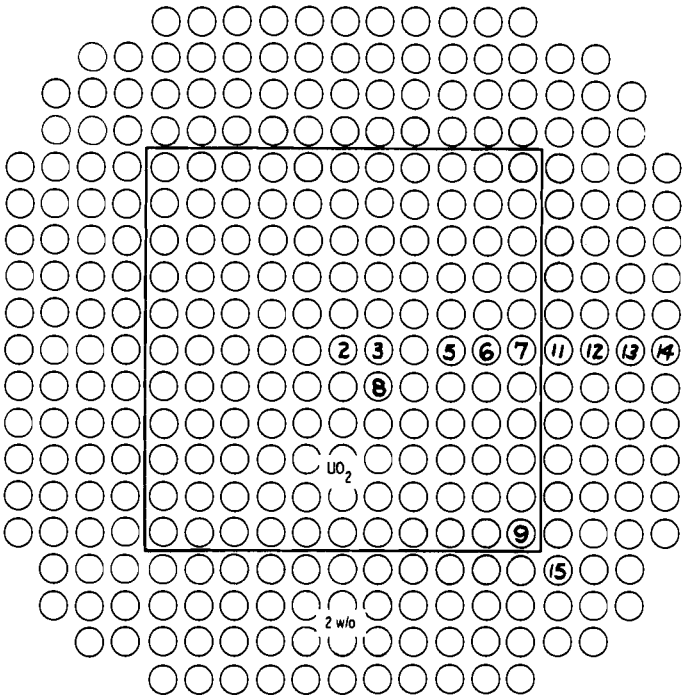

11x11, UO_2-2.35% ^{235}U ELEMENT IN UO_2-2 WT% PuO_2 (8% ^{240}Pu)

Experimental Power Distribution:

Position No.	Relative Power
UO_2-2.35% ^{235}U Rods	
2	2.562
3	2.532
5	2.329
6	2.127
7	1.748
8	2.502
9	1.251
UO_2-2 WT% PuO_2 Rods	
11	2.066
12	1.527
13	1.440
14	1.867
15	1.336

FIGURE D-8

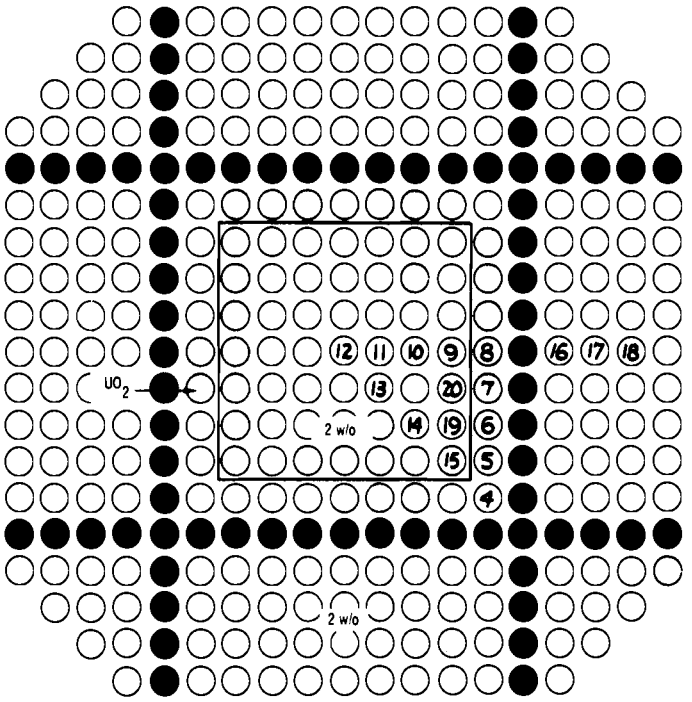

BASIC 9x9, COMPOSITE ELEMENT #2 IN UO_2-2 WT% PuO_2 (8% ^{240}Pu)

Experimental Power Distribution:

Position No.	Relative Power
UO_2-2.35% ^{235}U Rods	
4	1.212
5	1.030
6	1.004
7	1.003
8	1.003
UO_2-2 WT% PuO_2 Rods	
12	.933
11	.917
10	.956
9	1.180
13	.926
14	.983
15	1.376
19	1.170
20	1.178
16	1.185
17	.730
18	.630

FIGURE D-9

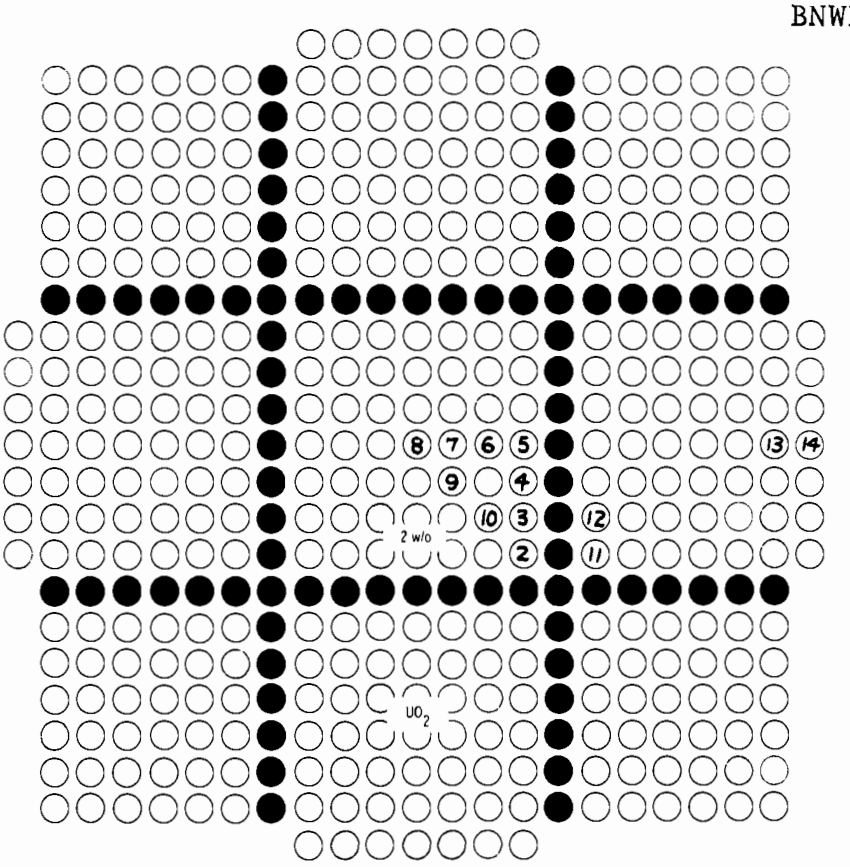

BASIC 7x7, UO_2-2 WT% PuO_2 (8% ^{240}Pu) ELEMENT IN UO_2-2.35% ^{235}U

Experimental Power Distribution:

Position No.	Relative Power
UO_2-2 WT% PuO_2 Rods	
8	.900
7	.935
6	1.007
5	1.434
9	.952
10	1.115
2	1.903
3	1.517
4	1.431
UO_2-2.35% ^{235}U Rods	
11	1.367
12	1.209
13	.569
14	.612

FIGURE D-10

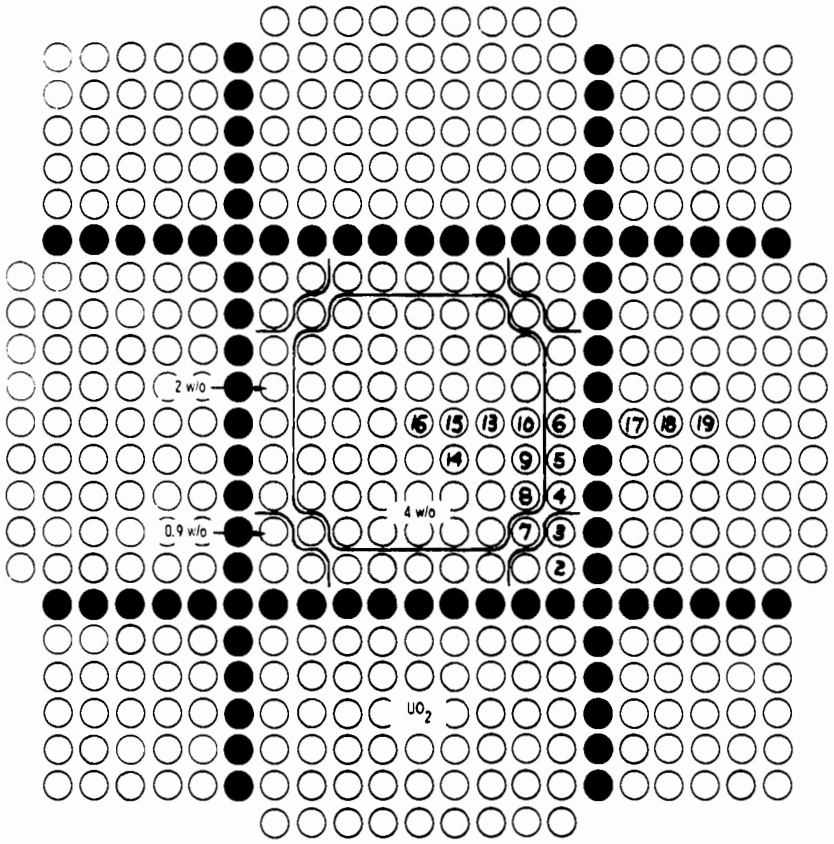

BASIC 9x9, COMPOSITE ELEMENT #1 IN UO_2-2.35% ^{235}U

Experimental Power Distribution:

Position No.	Relative Power
0.9 WT% PuO_2 Rods	
2	.840
3	.660
2.0 WT% PuO_2 Rods	
4	.938
5	.881
6	.891
7	.751
4.0 WT% PuO_2 Rods	
16	.874
15	.856
13	.871
10	.983
14	.867
8	1.065
9	.993
UO_2-2.35% ^{235}U Rods	
17	.578
18	.457
19	.388

FIGURE D-11

APPENDIX E

CONTROL BLADE WORTH MEASUREMENTS AND CALCULATIONS

P. Loizzo and N. Pacilio

APPENDIX E

CONTROL BLADE WORTH MEASUREMENTS AND CALCULATIONS

P. Loizzo and N. Pacilio

MATHEMATICAL FRAMEWORK

In order to give an operative definition to the parameter α, we start with the conventional one-point monoenergetic kinetic equations related to a fundamental space-mode and a unified delayed neutron group,

$$\dot{n}(t) = -\alpha n(t) + \lambda c(t)$$
$$\dot{c}(t) = \alpha_c n(t) - \lambda c(t) \qquad (1)$$

where the symbols indicate

$n(t)$	neutron density at time t
$c(t)$	delayed neutron precursor density at time t
$\alpha = \frac{1-k(1-\beta)}{\ell}$	Rossi-alpha or prompt-period reciprocal
k	effective multiplication factor
β	effective total fraction of delayed neutrons
ℓ	prompt neutron lifetime
$\alpha_c = \frac{\beta}{\ell}$	critical Rossi-alpha
λ	delayed neutron precursor time-decay constant.

The general solution of Equation (1) is given by

$$n(t) = Ae^{-\omega_1 t} + Be^{-\omega_2 t}$$

where the two decay constants are approximately given by

$$\omega_1 \approx \frac{\lambda(\alpha-\alpha_c)}{4\alpha} \text{ and } \omega_2 \approx \alpha$$

and are the stable period and the prompt period reciprocals. If the presence of delayed neutrons is neglected, i.e., if

λ is set equal to zero, Equation (1) degenerates into a first order differential equation, whose solution is

$$n(t) = Ce^{-\alpha t} \tag{2}$$

It indicates that for $\lambda = 0$, ω_2 (namely α) becomes the fundamental eigenvalue. This also means that, if a suitable time basis is chosen such that mostly prompt neutrons are observed, a time behavior like Equation (2) is expected for them. In fact, pulsed neutrons and reactor noise analysis experiments are based on the assumption that a fundamental space-mode and exponential time decay exists for the prompt neutron flux and is characterized by the parameter α.

If Equations (1) and (2) are generalized to a multigroup diffusion theory model, one obtains

$$\left\langle \frac{1}{v_i} \right\rangle \frac{\partial \phi_i}{\partial t} = D_i \Delta \phi_i - \left(\Sigma_a^i + \Sigma_r^i\right) \phi_i + (1-\beta)\chi_i \sum_j \nu \Sigma_f^j \phi_j + \sum_j \Sigma_r^{(j\to i)} \phi_j + \chi_i \lambda c \tag{1'}$$

$$\left\langle \frac{1}{v_i} \right\rangle \frac{\partial \phi_i}{\partial t} = D_i \Delta \phi_i - \left(\Sigma_a^i + \Sigma_r^i\right) \phi_i + (1-\beta)\chi_i \sum_j \nu \Sigma_f^j \phi_j + \sum_j \Sigma_r^{(j\to i)} \phi_j \tag{2'}$$

where i and j are energy-group subscripts.

The corresponding static equations obtained by setting $\dot{\phi} \equiv 0$ and replacing the terms containing c, are:

$$-D_i \Delta \phi_i + (\Sigma_a^i + \Sigma_r^i)\phi_i - \sum_j \Sigma_r^{(j\to i)} \phi_j = \frac{\chi_i}{k} \sum_j \nu \Sigma_f^j \phi_j \tag{1''}$$

$$-D_i \Delta \phi_i + (\Sigma_a^i + \Sigma_r^i)\phi_i - \sum_j \Sigma_r^{(j\to i)} \phi_j = \frac{\chi_i (1-\beta)}{k_p} \sum_j \nu \Sigma_f^j \phi_j \tag{2''}$$

The multiplication factor k and the prompt multiplication factor k_p are the required eigenvalues of Equations (1'') and (2''), respectively, and are usually obtained via iterative methods operating in multigroup code calculations.

The same procedure used to transform Equation (2') into Equation (2'') can be adopted to reduce the prompt neutron time behavior problem to a static problem. In fact, if the condition $\dot{\phi} = \alpha\phi_i$ is imposed in Equation (2'), one obtains

$$-D_i\Delta\psi_i + (\Sigma_a^i - \alpha\langle\frac{1}{\nu_i}\rangle + \Sigma_r^i)\psi_i - \sum_j \Sigma_r^{(j\to i)} \psi_j$$

$$= \chi_i(1-\beta)\sum_j \nu \Sigma_f^j \psi_j \qquad (3)$$

which has the same formalism of Equation (2''), only with a modified absorption given by

$$\Sigma_a^i = \Sigma_a^i - \alpha \langle\frac{1}{\nu_i}\rangle \qquad (4)$$

and k_p set equal to unity.

Thus, the static problem can be solved as usual and the value of α is derived as the fundamental eigenvalue of Equation (3).* A typical calculation procedure can be summarized as follows:

a) The static problem (determination of k) is solved and the converged fluxes are saved. This is made for critical and subcritical configurations obtained by inserting rods or by increasing the axial buckling.

b) The modified static problem (determination of α) is now solved by using the converged fluxes of Case (a) as starting values. Few iterations are needed for converging to $k_p = 1$ in critical and slightly subcritical assemblies; a greater number of iterations are required for more subcritical systems. This is due to the different physical meaning of the flux distribution in the calculation of k and α. This is also the reason why two different symbols, viz. ϕ_i and ψ_i have been adopted in Equations (2'') and (3) respectively.

---

* *Equation (3) has been obtained via a simplified heuristic procedure. However, the same equation can be obtained via a rigorous treatment.*[25]

In the first problem the flux profile is essentially the delayed neutron space distribution while in the second problem the prompt neutron distribution is obtained. The two profiles, rather differently shaped if the reactor is nonuniform, tend to be as much different as the degree of subcriticality involved. The wide discrepancy between the two flux shapes further clarifies the approach to the problem of calculating α, since it obviously excludes any perturbation-theory implication.

Results of calculations made for water reflected and moderated regular enriched UO_2 and UO_2-PuO_2 systems clearly show that while delayed neutrons (i.e., the actual power distribution) have the expected flux shape with pronounced peaks in the core and less accentuated peaks in the reflector, prompt neutrons have a rather damped distribution in the core and an extremely peaked profile in the reflector.

These phenomena are physically explicable looking at prompt and delayed neutron lifetimes in the different zones, in fact, while delayed neutrons live longer in the core than the reflector, the opposite occurs for prompt neutrons; a major fraction of the delayed neutron population is in the core and a major part of prompt neutron population is in the reflector at any instant of reactor life.

As a final point, one might inquire about the subcriticality limit beyond which α cannot either be calculated or observed. It must be recalled that, for reflected systems, a time-decay eigenvalue exists which is related to neutrons spending their entire lifetime in the reflector. Its value is approximately given (here the core-reflector reactivity coupling effect is neglected and the dependence of the reflector eigenvalue on reactivity is regarded as secondary effect and not discussed) by

$$\gamma = \left(\nu^{th} \Sigma_a^{th}\right) \text{ reflector} \qquad (5)$$

For very subcritical configurations, it may occur that α becomes larger than γ, i.e., that $\bar{\Sigma}_a^{th}$ of Equation (4) gets negative for the reflector. Since the immediate consequence is an extremely high flux profile (second eigenfunction) in the reflector, it comes out that EXTERMINATOR-2 converges to γ instead of to α. Additional analysis of this problem is needed.

CALCULATION MODEL

Calculations of k (static problem) and α (modified static problem) were executed via EXTERMINATOR-2. This code allows α to be calculated as a proportionality factor which multiplies the poison cross sections $1/v_i$ of each energy group. According to the code nomenclature, α is used as 'drive factor' of the eigenvalue problem which yields a value $k_p = 1$.

The parameters $1/v_i$ have been calculated by adopting the same averaging procedure[26] used for Σ_a^i, i.e.,

$$\left\langle \frac{1}{v_i} \right\rangle = \int_{E_1^i}^{E_2^i} \frac{1}{v} \phi(E)dE \Big/ \int_{E_1^i}^{E_2^i} \phi(E)dE \qquad (6)$$

where E_1^i and E_2^i are the lower and upper boundary of the i^{th} energy group. If a 1/E energy distribution is assumed for the fast groups, Equation (6) becomes

$$\left\langle \frac{1}{v_i} \right\rangle = \frac{2\sqrt{E_o}}{v_o \Delta u_i} \left(\frac{1}{\sqrt{E_1^i}} - \frac{1}{\sqrt{E_2^i}} \right) \qquad (6')$$

where $E_o = 0.0253$ eV, $v_o = 2200$ m/sec and Δu_i is the lethargy of the group i. For the thermal groups, $\langle 1/v_i \rangle$ can be calculated as an absorption cross section of a 1/v poison, whose value is normalized to $1/v_o$ at the conventional energy E_o. Thus, we obtain;

$$\left\langle \frac{1}{v_i} \right\rangle = \frac{\text{unit}_{(i)}}{v_o} \qquad (6'')$$

Several checks of the sensitivity of α on core and reflector parameters have been made, with special focus on the values of $1/v_i$. These quantities have been arbitrarily changed for some or all the energy groups of the core and of the reflector and the values of α derived. Results are given in Tables E-I and E-II. A major influence of the $1/v_i$ of Groups 4 and 5 in both core and reflector is noticeable in the corresponding values of α. The reference core is Configuration D, described in Figure 9 on page 20.

TABLE E-I. Sensitivity of α on $1/v_i$ in a 5-Group Model Calculation (variations on $1/v_i$ are always equal to -10% and are related to the group quoted in the table.)

Groups Varied			
Core $1/v_i$	Reflector $1/v_i$	α	α/α (Standard)
Standard	Standard	102.5	1.000
1,2,3	Standard	103.9	1.014
1,2,3	4,5	109.0	1.063
Standard	1,2,3,4,5	109.2	1.065

TABLE E-II. Sensitivity of α on $1/v_i$ in a 4-Group Model Calculation (variations on $1/v_i$ are always equal to -10% and related to the group quoted in the table.)

Groups Varied			
Core $1/v_i$	Reflector $1/v_i$	α	α/α(Standard)
Standard	Standard	104.1	1.000
Standard	1,2,3,4 (water gap only)	106.0	1.018
Standard	1,2,3,4	107.3	1.031
1,2,3,4	Standard	110.1	1.058

PHYSICAL MEANING AND ROLE OF THE ROSSI-ALPHA

A comparison between Equations (2'') and (3) leads to an immediate interpretation of the term α/v_i as the amount of poison which must be subtracted from the reactor to make it prompt-critical. The poison is considered as uniformly distributed in the whole system and is characterized by a 1/v cross section.[27,28]

Since a uniform poisoning experiment cannot be realized in practice, the theory-experiment check-up is actually based on comparing the time-decay constant α measured via a dynamic method, e.g., pulsed neutron or reactor-noise analysis techniques, with an absorption cross section α/v_i computed via a modified static calculation. Obviously the final comparison is only possible if the value of $1/v_i$ is assumed as a priori known.

It is worthy to note that theory-experiment comparisons of this type are extendable to highly subcritical systems unlike all other reactivity-based procedures.

Practically, the parameter α is at least as much expressive as k only with the difference that k is unity for all kinds of critical reactors, while α_c is not (but it expresses some reactor characteristics very well). On the other hand, α is experimentally observable, while k is not. A set of experiments based on α does not necessarily need a critical experiment, while one based on k consists only in a critical experiment.

One of the most discussed subjects in this specific field is that of the α versus reactivity relationship. According to the definition of α in the one-point monoenergetic diffusion theory model, one obtains

$$\alpha = \frac{1-k_p}{\ell} = \frac{1}{\ell}\frac{\beta-R}{1-R} = \frac{\beta}{\Lambda}(1-\$) \qquad (7)$$

where R is the reactivity, Λ the generation time and \$ the reactivity in dollar units. The linear α versus \$ behavior has been confirmed by a number of experiments, but evidence has also been observed of a breakdown of this relationship, prevalent for subcritical experiments in reflected systems.

Although the methods suggested here, i.e., measuring α and ignoring k, bypasses the question (in fact the troublesome concept of reactivity has never been introduced), an investigation on the subject has been made by some subcritical configurations and calculating both α and k for each of them.

Subcriticality has been obtained by different ways, i.e., by incrementing the axial buckling of a critical radial size reactor or by inserting thicker and thicker rods. The former approach has been adopted for calculations in UO_2 cores; (Configuration A has been chosen as reference core) results are shown in Table E-III.

TABLE E-III. Values of α and k Calculated for Different Subcritical Clean Cores (Configuration A is reference case)

B^2 Axial, cm^{-2}	K	\$, Dollars	Linearly Extrapolated α, sec^{-1}	Calculated α, sec^{-1}	Deviation, %
0.00089	1.00000	0.00	163.9(αc)	163.9	-
0.00219	0.95942	-5.54	1072	1019	-4.9
0.00349	0.92116	-11.20	2000	1806	-9.7
0.00479	0.88518	-16.98	2947	2520	-14.5
0.00609	0.85124	-22.87	3912	3163	-19.1

The linearly extrapolated value of α was obtained using the reactivity - alpha relationship, $\$ = (\alpha_c - \alpha)/\alpha_c$. The calculated value of α is shown to diverge from the reactivity relationship as the core is made more subcritical.

CONTROL-ROD STRUCTURE AND CHARACTERISTICS

The details of the boral blade (with and without wings) are shown in Figure E-1. The test cruciform blade* was constructed of stainless steel as were the spacers and the walls of the flat and cylindrical tubes. The test blade (not to scale) is shown in Figure E-2 and E-3. The different types of poison that were loaded into it are seen in Figure E-4 to E-6. Each wing of the blade in the figures is typical of what all four wings look like when the blade was loaded with that poison material.

The dimensions and specifications of the various materials used in the test cruciform blade are summarized below:

- Round tubes - 0.188 in. outer diameter
  35.25 in. long
  0.025 in. wall thickness
  Material - B_4C (16 g/tube)
  HfO_2 (27.3 g/tube)
  13 tubes/wing
- Flat tubes - 0.185 in. thick
  1.203 in. wide
  35.5 in. long
  0.028 in. wall thickness
  Material- B_4C (148.2 g/tube)
  HfO_2 (247.0 g/tube)
  B_4C-HfO_2 mixture (218.8 g/tube)
  54.7 g B_4C
  164.1 g HfO_2
  2 tubes/wing
- Thin hafnium metal bars - 0.090 in. thick
  1.141 in. wide
  35.5 in. long
  767.7 g/bar average
  2 bars/wing
- Thick hafnium metal bars - 0.155 in. thick
  1.163 in. wide
  35.5 in. long
  1330.7 g/bar average
  2 bars/wing

---

* *The test cruciform blade and control materials were provided by the Nuclear Energy Division of the General Electric Company, San Jose, California*

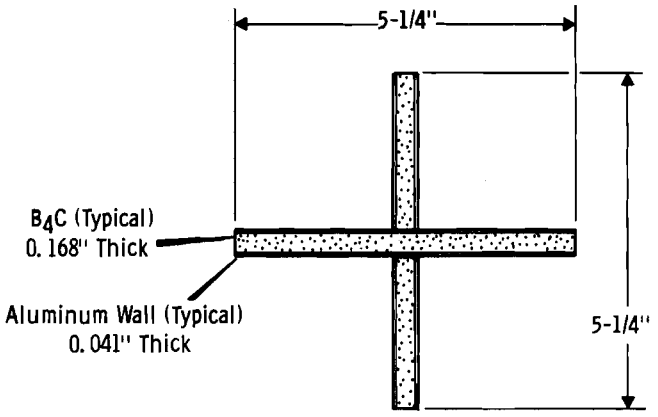

BORAL CONTROL BLADE WITH WING EXTENDERS

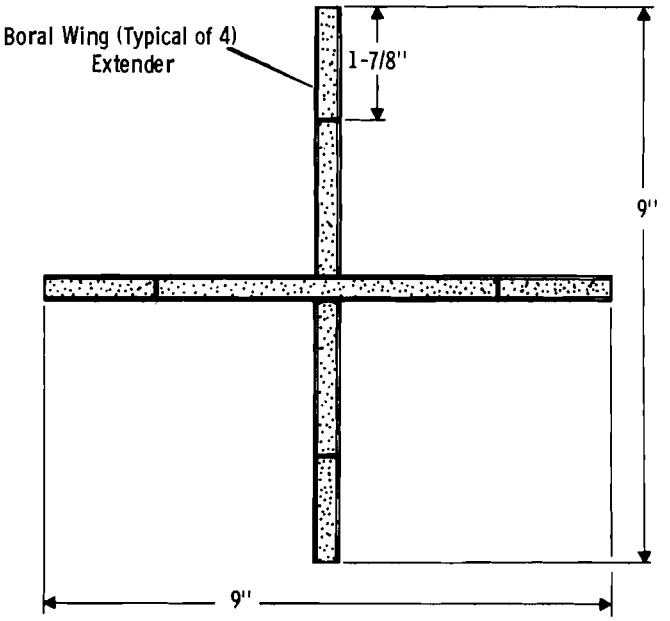

NOTE:

Aluminum wall thickness and B_4C thickness same for Wing Extenders as for Blade.

The Blade is 36" long and the Wing Extenders are 33" long and both are centered about the fuel when inserted.

FIGURE E-1. BORAL BLADE DETAIL

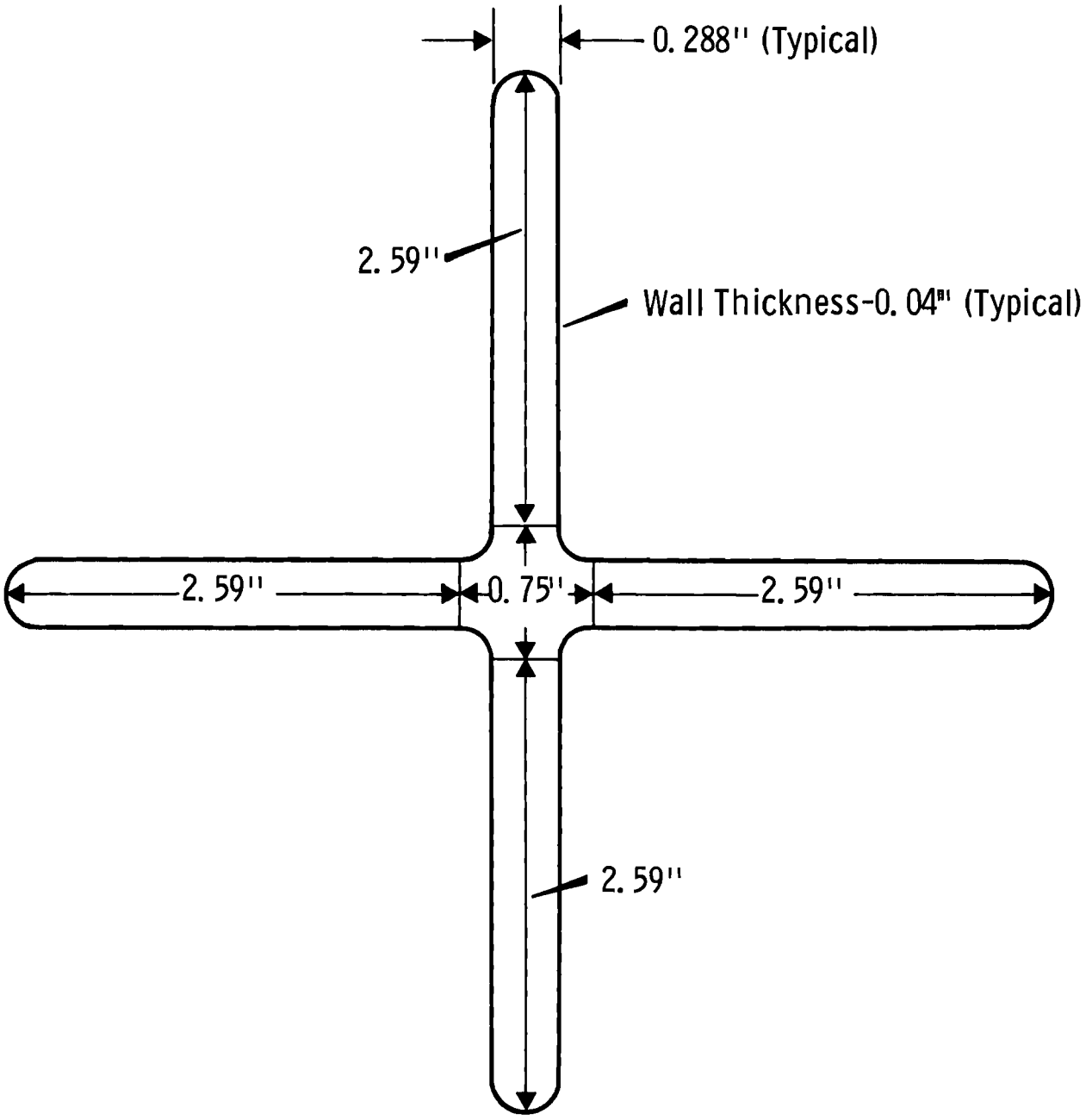

FIGURE E-2. TEST CRUCIFORM BLADE DETAILS

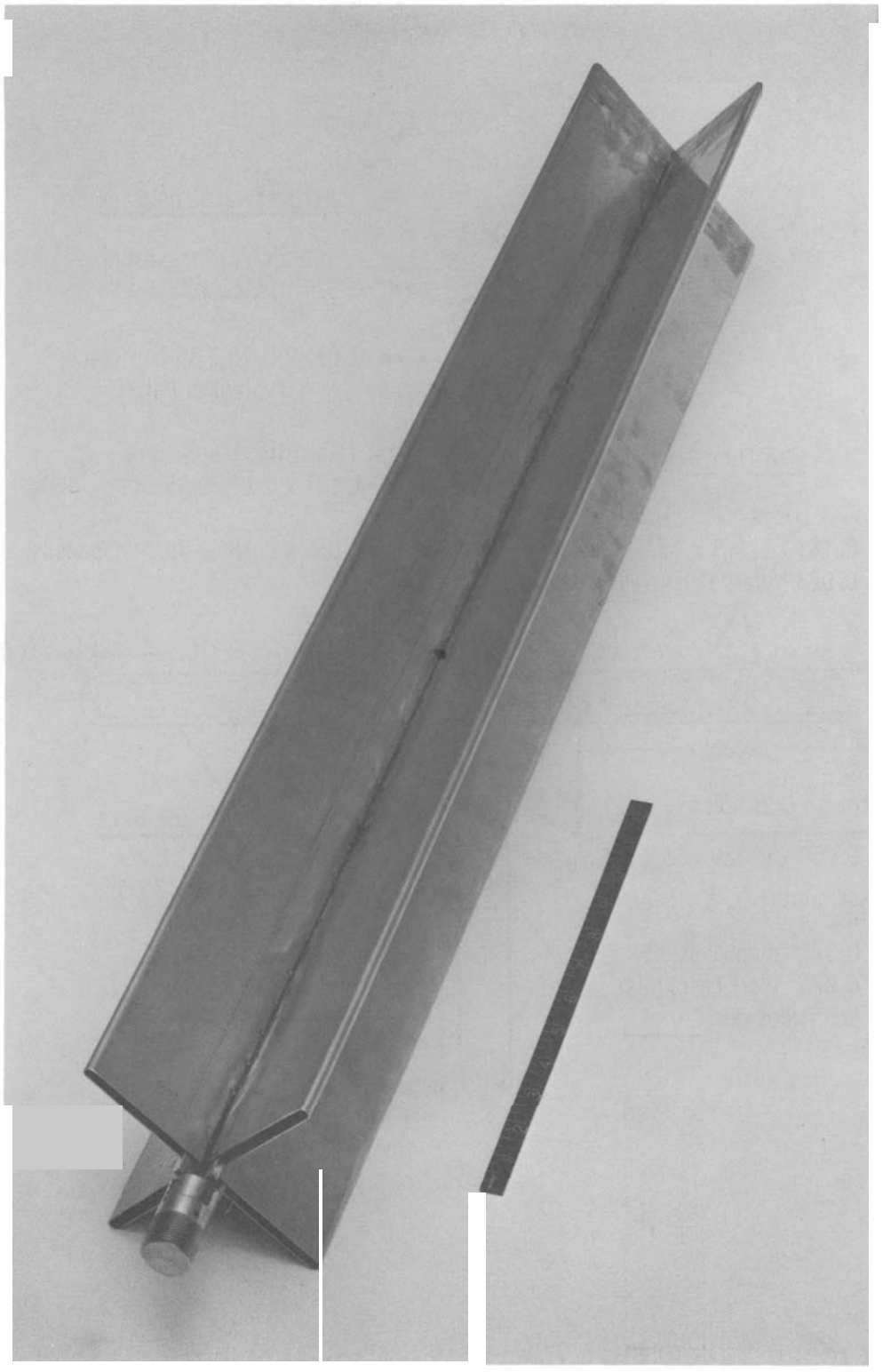

FIGURE E-3. TEST CRUCIFORM BLADE
PERSPECTIVE VIEW

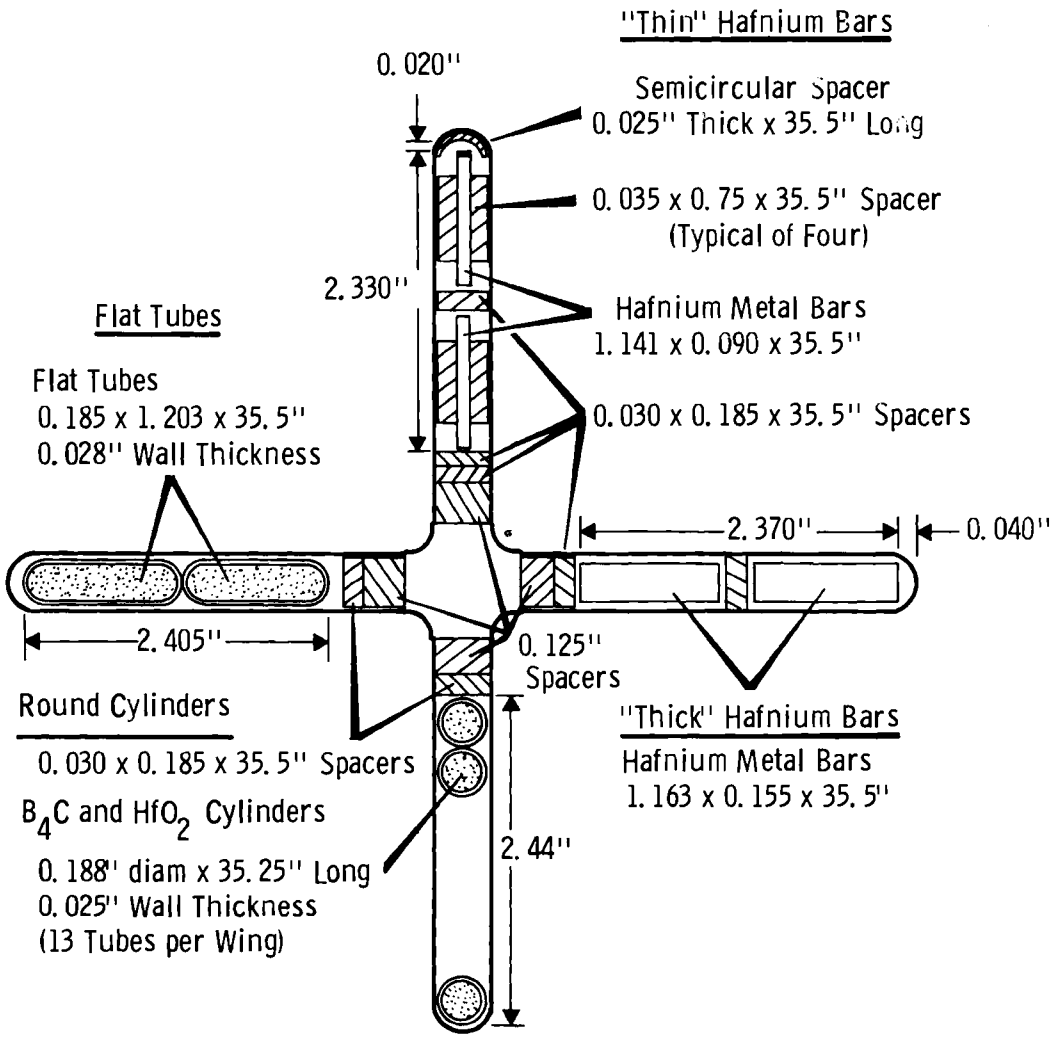

FIGURE E-4. TEST CRUCIFORM BLADE-LOADING DETAILS

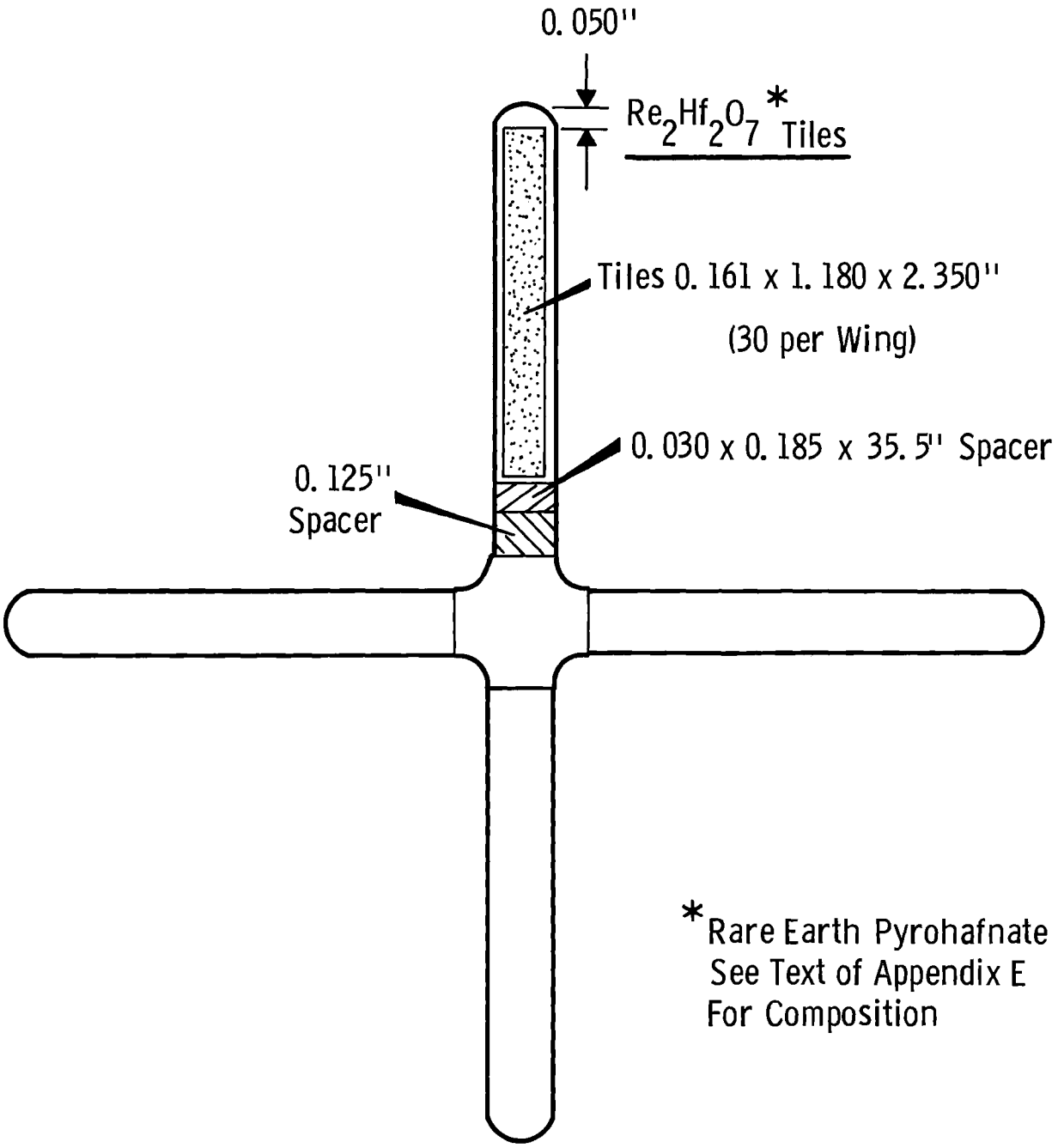

FIGURE E-5. TEST CRUCIFORM BLADE-LOADING DETAILS (CONTINUED)

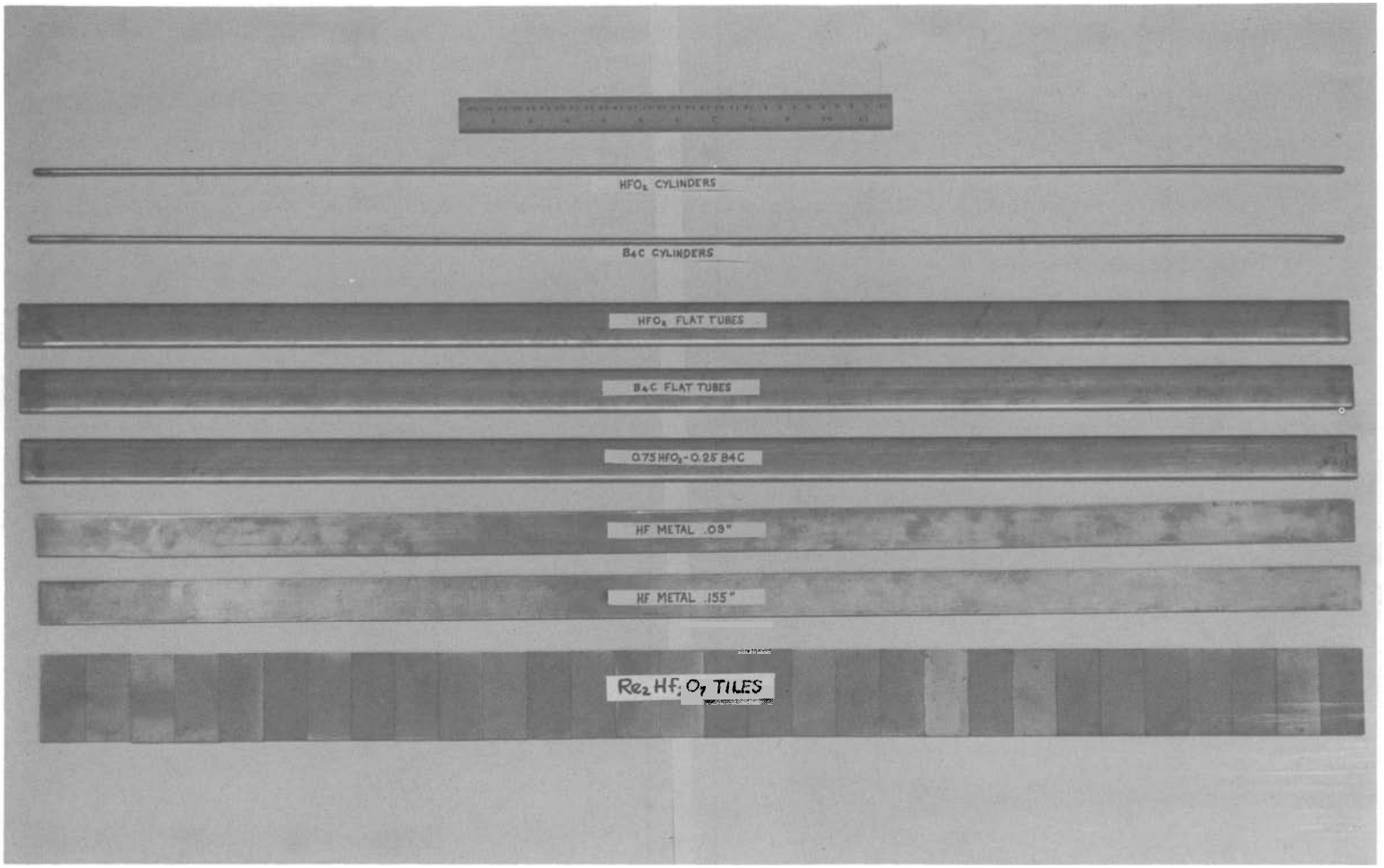

FIGURE E-6. TEST CRUCIFORM BLADE POISON MATERIAL PERSPECTIVE VIEW

- Rare earth pyrohafnate tiles- 0.161 in. thick
  1.180 in. wide
  2.350 in. long
  Material-$Re_2Hf_2O_7$
  Re = 60% dysprosium,
  20% helmium,
  20% erbium
  1682.1 g/30 tiles average
  30 tiles/wing

The specifications for the boral blade are summarized below:

- Details of blade are shown in Figure E-1
- Core material, 0.168 in. thick; Aluminum skin, 0.041 in. thick
- Core material is B_4C grit particles (20 to 200 mesh) dispersed in 1100 Aluminum
- The effective density of the core material is 2.484 $\pm$ 0.002 g/cm^3
- Core material is (34.9 $\pm$ 0.2) wt% B_4C and (65.1 $\pm$ 0.2) wt% Aluminum.

EXPERIMENTAL PROCEDURE, DATA REDUCTION AND MEASURING APPARATUS

The counting chain was of the ordinary type often used for monitoring and routine measurements in nuclear reactors. The only new elements were the location of the neutron detector, the adoption of a preselecting device for spotting the presence of spontaneous bursts of a desired minimum amplitude and the use of a multichannel scaler.

Two types of BF_3 proportional counters were used: their thermal neutron sensitivities were 7 cps/nv for critical and slightly subcritical systems and 45 cps/nv for more subcritical assemblies. They were always placed in an effective location, i.e. near the peak of the flux profile. Since the top-peak was in the water reflector for all systems, the preferential detector placement could be achieved with no need of special

in-core equipment. A digital preselector was adopted; a modification of a gated-scaler. The output coming from the counting chain was sampled during adjustable time increments (Usually smaller than or equal to the multiscaler channel width) and reset to zero at the end of each sampling. Since the mean counting rate could be separately obtained, the preselector could be set at the desired amplitude of positive fluctuations above the mean level. Its operation was that of triggering the multichannel scaler when the selected number of counts was obtained during the sampling interval. Upon triggering of the multichannel scaler, data was collected in the individual channels from initial triggering to the end of the sweep. The sweep duration was prefixed in terms of a selected number of channels. The operation was repeated a total of N sweeps (generally 10^4 times) to improve the measurement statistical significance and reach the desired precision. A delay line was used before feeding counts into the data register, in order to observe the rise as well as the decay of spontaneous bursts.

The data ensemble $\{n(\Delta t)\}$ was printed out and went through a three-stage treatment before being reduced to give the desired value of α. The raw data were elaborated according to the formula

$$n^*(\Delta t) = \frac{n(\Delta t)}{1 - \tau/\Delta t}$$

where τ is the memory-storage cycle-time, i.e., the dead time for channel advance and Δt is the channel width. For the equipment used, τ was equal to 34 microsec. Then, data had to be corrected because of the neutron counting chain dead time θ. The dead time formula was applied, i.e.,

$$n'(\Delta t) = \frac{n^*(\Delta t)}{1 - \frac{n^*(\Delta t)\,\theta}{N\Delta t}}$$

The ensemble $\{n'(\Delta t)\}$ is then fed into the program LEARN, whose fitting techniques are based upon second order Taylor expansion of the mean square misfit and utilize the standard minimization formulae to obtain convergence. Its output gave the best values of background and exponential amplitude and decay constant together with their standard deviations.

A block diagram of the measuring apparatus is given in Figure E-7. The single blocks of the system correspond to the following symbolism and purposes:

(DT)	BF_3 proportional counter, Reuter-Stokes models RSN-7A or RSN-45A
(PA)	Preamplifier, Canberra Instruments, Model 1410
(A)	Amplifier, Canberra Instruments, Model 1416
(D)	Discriminator, Canberra Instruments, Model 1430
(S_1, S_2, S_3)	Scalers, RIDL Model 49-43 (6 decades) gated by timers RIDL Model 54-8
(PS_1)	Preselector of the number of multiscaler channels to be swept (2 decades)
(PS_2)	Preselector of counting bursts (two decades, i.e. millisec and decimal fraction, for the sampling time interval, two decades for the number of counts in the sampling interval; a dial for the desired number of counts)
(O)	Timer, Wavetek Model 111
(MCS)	Multichannel time analyzer, Nuclear Data Model 180, used in multiscaler mode.
(DL)	Magnetostrictive delay line, Anderson, 8.5 millisec (constant delay)

Simply speaking, the measuring circuit selected neutron counting bursts of a desired minimum amplitude and analyzed their die-away on a suitable time basis. The pulses coming out from the DT-PA-A-D counting chain are fed into the preselector. If

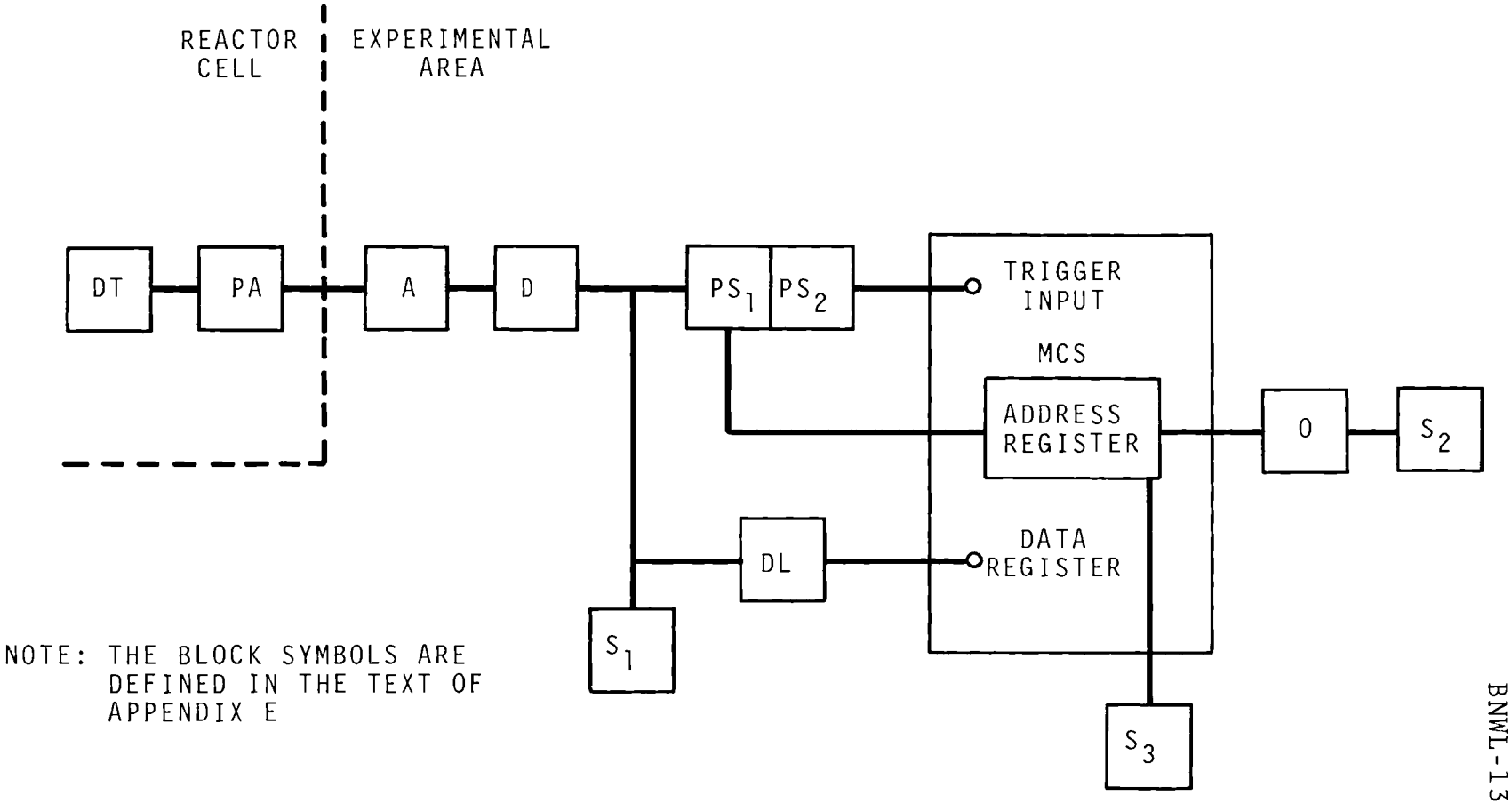

FIGURE E-7. BLOCK DIAGRAM OF THE ALPHA MEASURING APPARATUS

BNWL-1379

the number of pulses arriving in a given time interval, i.e., the sampling interval of the burst monitor, equals or exceed a preset value then a pulse is generated by PS_2 which triggers the multichannel scaler, i.e., makes it start the data collection.

The advance-channel function is triggered by the external frequency generator 0 and is stopped and reset as soon as the number of channels preset by PS_1 has been reached. A memory-storage cycle-time must be taken into account for every channel advancement since the first section of every channel will not accept counts, as it is gated during channel advance.

A delay line (DL) was used to allow the prehistory of the triggering burst to be observed.

Scalers (S) were connected at various points of the circuit in order to check the long-time-averaged counting rate (S_1), the stability of the channel dwell time generator (S_2) and to count the number of burst analysed i.e. number of sweeps (S_3).

Typical run-durations range from 1 hr for critical and near-critical measurements to 2 1/2 hr for far-subcritical measurements.

APPENDIX F

CROSS SECTIONS

P. Loizzo

APPENDIX F

CROSS SECTIONS

P. Loizzo

When 5 energy groups cross sections are given for Standard RIBOT, the Σ and D of the first three groups are the same as in the 4 group set; Σ_r^3 scatters 68% in Group 4 and 32% in Group 5; Σ_r^4 scatters to Group 5 and Σ_r^5 scatters to Group 4 (up scattering).

When Moderator Homogenized (M.H.) cross sections are given, both for 4 and 5 groups, the fast groups cross sections are identical to the corresponding Standard RIBOT cross sections.

UO_2-2 wt% PuO_2(8% ^{240}Pu) CROSS SECTIONS

Set 1 (Standard RIBOT 20 °C, ρ_{H_2O} = 1.0000 g/cm^3)

Group 4G	D	Σ_r	Σ_a	$\nu\Sigma_f$	Σ_f	$\langle 1/v \rangle$
1	1.64181	0.062688	0.002228	0.004419	0.001661	$7.304\ 10^{-10}$
2	0.84766	0.171036	0.0	0.0	0.0	$4.589\ 10^{-9}$
3	0.71117	0.086300	0.034048	0.016406	0.005911	$1.992\ 10^{-7}$
4	0.23106	–	0.162801	0.273316	0.096918	$3.215\ 10^{-6}$
5G						
4	0.40164	0.477618	0.198818	0.328539	0.114167	$1.2065\ 10^{-6}$
5	0.19574	0.005447	0.155343	0.261881	0.93347	$3.6309\ 10^{-6}$

Set 11 (Same as Set 1 except Group 3 constants decreased by 10%)

Group					
3	0.71117	0.07767	0.030643	0.014765	0.005320

Set 12 (HTH-^{239}Pu in thermal zone: Leonard-Westcott library)

Group	D	$\Sigma_r(g\to g+1)$	$\Sigma_r(g\to g+2)$	Σ_a	$\nu\Sigma_f$	Σ_f
1	1.726504	0.063747	0.001752	0.003094	0.006145	0.002666
2	0.851609	0.162317	0.000019	0.003927	0.001064	0.000389
3	0.611620	0.069757	–	0.028104	0.014369	0.005291
4	0.321300	–	–	0.145970	0.242300	0.086759

Set 13 (HTH-^{239}Pu in thermal zone: Schmidt's KFK 120 Library)

Group						
4	0.324800	–	–	0.144540	0.243510	0.086527

Set 14 (THERMOS/BATTELLE-HRG, Leonard-Westcott for ^{239}Pu)

Group	D	$\Sigma_r(g \to g+1)$	$\Sigma_r(g \to g+2)$	Σ_a	$\nu\Sigma_f$	Σ_f
1	1.35093	0.048647	0.000014	0.003360	0.004706	0.001717
2	0.67861	0.060344	0.023498	0.025290	0.012373	0.004493
3	0.68340	0.426885	–	0.044389	0.018218	0.006657
4	0.22221	–	–	0.146520	0.24410	0.087390

Set 15 (RIBOT M.H.)

4G

Group	D	Σ_r	Σ_a	$\nu\Sigma_f$	Σ_f
4	0.26353	–	0.143577	0.241043	0.085475

5G

4	0.46449	0.412992	0.171916	0.284084	0.098719
5	0.22101	0.004825	0.137580	0.231935	0.082672

Set 16 (Standard RIBOT, ρ_{H_2O} = 0.8067 g/cm^3)

4G

Group	D	Σ_r	Σ_a	$\nu\Sigma_f$	Σ_f
1	1.78320	0.052677	0.002228	0.004419	0.001661
2	0.94466	0.138335	0.0	0.0	0.0
3	0.81727	0.069899	0.033276	0.016259	0.005860
4	0.28266	–	0.161244	0.27369	0.096962

5G

4	0.46148	0.378157	0.193075	0.320055	0.111236
5	0.23790	0.004784	0.153275	0.262085	0.093388

Set 17 (Standard RIBOT ρ_{H_2O} = 0.9306 g/cm^3)

Group

4G	D	Σ_r	Σ_a	$\nu\Sigma_f$	Σ_f
1	1.68775	0.059508	0.002228	0.004419	0.001661
2	0.876243	0.160648	–	–	–
3	0.741758	0.081090	0.033828	0.016365	0.005897
4	0.245481	–	0.162366	0.273583	0.096987

5G

4	0.418852	0.445797	0.197249	0.326279	0.113386
5	0.207510	0.005242	0.154726	0.262041	0.093395

Set 18 (Standard RIBOT ρ_{H_2O} = 0.8796 g/cm^3)

Group	D	Σ_r	Σ_a	$\nu\Sigma_f$	Σ_f
4G					
1	1.72971	0.056453	0.002228	0.004419	0.001661
2	0.905583	0.150666	–	–	–
3	0.773736	0.076084	0.033595	0.016320	0.005881
4	0.260957	–	0.161904	0.273727	0.097011
5G					
4	0.436874	0.415417	0.195529	0.323747	0.112512
5	0.220147	0.005040	0.154104	0.262123	0.093415

Set 19 (Standard RIBOT ρ_{H_2O} = 0.7543 g/cm^3)

Group	D	Σ_r	Σ_a	$\nu\Sigma_f$	Σ_f
4G					
1	1.729710	0.056453	0.002228	0.004419	0.001661
2	0.905583	0.150666	–	–	–
3	0.773736	0.076084	0.033595	0.016320	0.005881
4	0.260957	–	0.161904	0.273727	0.097011
5G					
4	0.436874	0.415417	0.195529	0.323747	0.112512
5	0.220147	0.005040	0.154104	0.262123	0.093415

H_2O (20 °C, ρ = 1 g/cm^3) CROSS SECTIONS

Set 2

4G (Standard RIBOT)

Group	D	Σ_r	Σ_a	$\langle 1/\nu \rangle$
1	1.97115	0.093330	0.0	$7.304\ 10^{-10}$
2	0.88558	0.304850	0.0	$4.589\ 10^{-9}$
3	0.58765	0.152900	0.0013	$1.992\ 10^{-7}$
4	0.13950	–	0.0197	$4.025\ 10^{-6}$
5G				
4	0.39850	0.7954	0.00614	$1.255\ 10^{-6}$
5	0.13260	0.0040	0.001964	$4.025\ 10^{-6}$

Set 21 (HRG-THERMOS/BATTELLE

Group	D	$\Sigma_r(g\to g+1)$	$\Sigma_r(g\to g+2)$	Σ_a
1	1.58758	0.074081	0.000021	0.000252
2	0.60085	0.124025	0.049012	0.000575
3	0.58082	0.780099	–	0.003175
4	0.11997	–	–	0.019135

UO_2-2.35 wt% ^{235}U CROSS SECTION

Set 3 (Standard RIBOT, 20 °C, ρ_{H_2O} = 1.0000 g/cm^3)

4G

Group	D	Σ_r	Σ_a	$\nu\Sigma_f$	Σ_f	$\langle 1/\nu \rangle$
1	1.74900	0.068340	0.001643	0.003258	0.001225	$7.304\ 10^{-10}$
2	0.88451	0.198597	0.0	0.0	0.0	$4.589\ 10^{-9}$
3	0.70921	0.099906	0.020708	0.009530	0.003890	$1.992\ 10^{-7}$
4	0.21944	–	0.079590	0.118933	0.048544	$3.515\ 10^{-6}$

5G

4	0.50268	0.523819	0.028764	0.041886	0.017096	$1.244\ 10^{-6}$
5	0.18553	0.004647	0.085675	0.128157	0.052309	$3.786\ 10^{-6}$

Set 31 (HTH)

Group	D	$\Sigma_r(g\to g+1)$	$\Sigma_r(g\to g+2)$	Σ_a	$\nu\Sigma_f$	Σ_f
1	1.73443	0.069931	0.001991	0.002238	0.004243	0.001524
2	0.86029	0.189606	0.0	0.002804	0.000730	0.000300
3	0.59892	0.082294	–	0.020803	0.11188	0.004604
4	0.29818	–	–	0.074995	0.110680	0.045547

Set 32 (THERMOS/BATTELLE-HRG)

Group	D	$\Sigma_r(g\to g+1)$	$\Sigma_r(g\to g+2)$	Σ_a	$\nu\Sigma_f$	Σ_f
1	1.45497	0.054199	0.000015	0.002483	0.003396	0.001267
2	0.68912	0.074619	0.029219	0.019584	0.007912	0.003256
3	0.69201	0.511392	–	0.011901	0.013193	0.005429
4	0.18937	–	–	0.075658	0.111400	0.045843

Set 33 (Standard RIBOT ρ_{H_2O} = 0.8330 g/cm^3)

4G

Group	D	Σ_r	Σ_a	$\nu\Sigma_f$	Σ_f
1	1.91202	0.058305	0.001643	0.003258	0.001225
2	0.99096	0.165815	0.0	0.0	0.0
3	0.81498	0.0083464	0.020356	0.009499	0.003877
4	0.26522	–	0.76480	0.117284	0.047871

5G

4	0.58260	0.435885	0.028052	0.041822	0.001707
5	0.22114	0.004136	0.083205	0.127763	0.052148

Set 34 (RIBOT M. H. ρ_{H_2O} = 1.0000 g/cm^3)

Group	D	Σ_r	Σ_r	$\nu\Sigma_f$	Σ_f
4G					
4	0.22993	–	0.075154	0.112304	0.045838
5G					
4	0.51325	0.513034	0.028172	0.041023	0.016744
5	0.019730	0.004370	0.080566	0.120515	0.049190

Set 35 (Standard RIBOT, ρ_{H_2O} = 0.9676 g/cm^3)

Group	D	Σ_r	Σ_a	$\nu\Sigma_f$	Σ_f
4G					
1	1.798220	0.065163	0.001643	0.003259	0.001225
2	0.915650	0.188218	–	–	–
3	0.739595	0.094701	0.020607	0.009521	0.003886
4	0.232225	–	0.078651	0.118500	0.048367
5G					
4	0.525514	0.495952	0.028541	0.041870	0.017090
5	0.195537	0.004486	0.084920	0.127968	0.052280

Set 36 (Standard RIBOT, ρ_{H_2O} = 0.8953 g/cm^3)

Group	D	Σ_r	Σ_a	$\nu\Sigma_f$	Σ_f
4G					
1	1.84965	0.061986	0.001643	0.003258	0.001225
2	0.949062	0.177840	–	–	–
3	0.772703	0.089496	0.020497	0.009512	0.003882
4	0.24649	–	0.077673	0.117990	0.048159
5G					
4	0.550507	0.468111	0.028316	0.041870	0.017082
5	0.206645	0.004325	0.084920	0.128086	0.052252

Set 37 (Standard RIBOT, ρ_{H_2O} =0.7903 g/cm^3)

Group	D	Σ_r	Σ_a	$\nu\Sigma_f$	Σ_f
4G					
1	1.95901	0.055639	0.001643	0.003258	0.001225
2	1.02369	0.157104	–	–	–

Group	D	Σ_r	Σ_a	$\nu\Sigma_f$	Σ_f
3	0.848608	0.079095	0.020243	0.009490	0.003873
4	0.280532	—	0.075569	0.116683	0.047626
5G					
4	0.608267	0.412562	0.027858	0.041798	0.017060
5	0.232942	0.003998	0.082497	0.127558	0.052064

UO_2-4 wt% PuO_2 CROSS SECTIONS

Set 4 (Standard RIBOT)

Group	4G D	Σ_r	Σ_a	$\nu\Sigma_f$	Σ_f
1	1.65356	0.062598	0.002103	0.004172	0.001568
2	0.85123	0.171217	0.0	0.0	0.0
3	0.71352	0.086389	0.044070	0.025366	0.008938
4	0.22447	—	0.220917	0.379287	0.132513
5G					
4	0.36911	0.492433	0.263655	0.436788	0.151073
5	0.18690	0.006297	0.209815	0.364349	0.127691

Set 41 (THERMOS/BATTELLE-HRG)

Group	D	$\Sigma_r(g\to g+1)$	$\Sigma_r(g\to g+2)$	Σ_a	$\nu\Sigma_f$	Σ_f
1	1.36314	0.048770	0.000014	0.003409	0.005097	0.001843
2	0.67774	0.059774	0.023302	0.028494	0.018645	0.006605
3	0.67352	0.042402	—	0.077155	0.025625	0.009166
4	0.21493	—	—	0.189630	0.321320	0.113470

UO_2-9 wt% PuO_2 CROSS SECTIONS

Set 5 (Standard RIBOT)

Group	4G D	Σ_r	Σ_a	$\nu\Sigma_f$	Σ_f
1	1.64697	0.062874	0.002249	0.004460	0.001676
2	0.84792	0.171859	0.0	0.0	0.0
3	0.71028	0.086709	0.027020	0.007019	0.002503
4	0.23352	—	0.091732	0.131733	0.046974
5G					
4	0.45321	0.464505	0.112508	0.178659	0.061951
5	0.20465	0.004182	0.089001	0.125566	0.044440

Set 51 (THERMOS/BATTELLE-HRG)

Group	D	$\Sigma_r^{(g\to g+1)}$	$\Sigma_r(g\to g+2)$	Σ_a	$\nu\Sigma_f$	Σ_f
1	1.35433	0.049238	0.000014	0.003106	0.004088	0.001501
2	0.67971	0.062738	0.024441	0.021074	0.005477	0.001963
3	0.68850	0.436114	—	0.028661	0.007483	0.002706
4	0.22306	—	—	0.086449	0.123050	0.043815

UO_2-2 wt% PuO_2 (24% ^{240}Pu) CROSS SECTIONS

Set 6 (Standard RIBOT)

Group	D	Σ_r	Σ_a	$\nu\Sigma_f$	Σ_f
4G					
1	1.64547	0.062688	0.002229	0.004420	0.001661
2	0.84765	0.171036	0.0	0.0	0.0
3	0.71116	0.086300	0.036321	0.014780	0.005333
4	0.23325	—	0.149100	0.239169	0.085035
5G					
4	0.41489	0.472829	0.175135	0.283453	0.098516
5	0.19749	0.005250	0.143974	0.230450	0.082381

APPENDIX G

MISCELLANEOUS CALCULATIONS

APPENDIX G

MISCELLANEOUS CALCULATIONS

WATER DENSITY IN THE VOIDED ELEMENTS

The voids were simulated in a basic 9 × 9 element by inserting aluminum thimbles in the interstices between the fuel rods. The OD of the aluminum tubes was 5/16 in. and the tubes wall thickness was 0.020 in. It was assumed in the calculations that the aluminum was the same as a void. Therefore, we have the following results.

Water Density in the Voided Elements

	UO_2-PuO_2 Element, g/cm^3	UO_2 Element, g/cm^3
Corner rods (4) - 1/4 aluminum tube	0.9386	0.9476
Side rods (28) - 1/2 aluminum tube	0.8796	0.8953
Center rods (49) - 1 aluminum tube	0.7543	0.7903
Element weighted average	0.8067 g/cm^3	0.8345 g/cm^3

CALCULATIONS OF β_{eff}*

Two sets of MUFT-IV calculations were made, one assuming the source neutrons had a fission spectrum and the second assuming that the neutrons were born in Group 12 (498 keV <E> 638). Using the appropriate thermal constants (from RIBOT) and the same value for B^2 in the two corresponding MUFT-IV sets, for each configuration a multiplication factor was found for both prompt and delayed neutrons. Then,

$$\beta_{eff} = \beta_{core} \frac{k_{eff}\ (\text{delayed})}{k_{eff}\ (\text{prompt})}$$

* *M. Michelini of CNEN-Casaccia (Rome) performed the β_{eff} calculations.*

β_{core} was calculated in RIBOT as the weighted average of the β_i on the fissions from the various nuclides. In Table G-1 are shown the results, in different conditions, for the UO_2-2.35% ^{235}U the UO_2-2 wt% PuO_2(8% ^{240}Pu) cores.

TABLE G-1. Summary of β_{eff} Calculation

Core	$B^2(m^{-2})$	Case	k_{eff}	$\beta_{eff} \times 10^3$	Notes
UO_2-2 wt% PuO_2 (8% ^{240}Pu)	93.4	Prompt Delayed	1.032 1.176	3.74	Minimum Critical
	83	Prompt Delayed	1.019 1.148	3.62	Critical with Rods
UO_2-2.35% ^{235}U	85	Prompt Delayed	1.0106 1.152	7.64	Minimum Critical
	75	Prompt Delayed	1.007 1.123	7.47	Critical with Rods

CALCULATIONS OF THE TRANSPARENCIES OF POISON BLADES

Given a purely absorbing slab of thickness t, the extrapolation length, in the P_1 approximation, is given by:

$$d = 2.13\, D \frac{1 + 3\, E_4\, (t\, \Sigma_a)}{1 - 2\, E_3\, (t\, \Sigma_a)}$$

where $$E_n(x) = x^{n-1} \int_x^\infty \frac{e^{-y}}{y^n}\, dy$$

D is the diffusion coefficient of the outside medium

Σ_a is the absorption cross section in the slab

Hence, $$C = \frac{D}{d} = \frac{1 - 2\, E_3\, (t\, \Sigma_a)}{2.13\, [1 + 3\, E_4\, (t\, \Sigma_a)]} \qquad (1)$$

In the Hurwitz and Roe's formulation one assumes:

$$P = 2\, E_3\, (t\, \Sigma_a)$$

and $$C = \frac{1}{2.13} \frac{1-P}{1+P} = \frac{1 - 2\, E_3\, (t\, \Sigma_a)}{(2.13)[1+2\, E_3\, (t\, \Sigma_a)]} \qquad (2)$$

Equations (1) and (2) give a difference in C which amounts to a few percent. Therefore (2) was preferred because it is simpler than (1). In all the energy groups, the following equation was used:

$$P_g = \int P(E)\,\phi(E)\,dE \Big/ \int \phi(E)\,dE \simeq \frac{1}{\Delta u_g}\int P(u)\,du$$

where u is the neutron lethargy.

$$C_g = \frac{1}{2.13}\,\frac{1-P_g}{1+P_g}$$

Boral rod: active thickness = 0.147 in. = 0.3734 cm
Density of B_4C (assumed) = 2.34 g/cm^3 (94% TD)
$\sigma\alpha$ 1/u

$t \times \Sigma_a^o = 29.3$ Therefore $P_4 = P_5 = P_{th} = 0$; $C_4 = C_5 = C_{th} = 0.4695$

in the fast region $P_i = \frac{2}{\Delta u_i}\int E_3\,(\Sigma a\ t)\,du$ (see Table G-2)

Hafnium rod: thickness = 0.155 in. = 0.3937 cm, ρ = 13.3 g/cm^3

$t \times Hf = 1.767\ 10^{-2}$ atoms/cm^2; $\Sigma_a^o\ t = 1.855$

An HRG calculation was made to find the values of Σ_a in each 0.5 lethargy group. The integration was done by hand (see Table G-2).

Hafnium

Thermal Zone

Group	$t\ \Sigma_a$	C
4	0.44	0.181
5	1.51	0.375
th.	1.37	0.358

TABLE G-2. Calculations of Poison Blade "Reflectance" in the Fast Groups

		Fast Zone			
		Boron Rod		Hafnium Rod	
MUFT Group	HRG Group	Σt	P	Σt	P
54	66	5.7	0	0.42	0.50
53	65	4.9	0	3.53	0.01
52	64	4.3	0	3.53	0.01
51	63	3.8	0.01	0.29	0.65
50	62	3.3	0.01	2.37	0.04
49	61	2.9	0.02	2.66	0.04
48	60	2.6	0.03	0.20	0.70
47	59	2.3	0.05	0.79	0.28
46	58	2.0	0.06	1.08	0.20
45	57	1.8	0.08	3.0	0.02
44	56	1.6	0.10	1.62	0.10
43	55	1.4	0.13	0.53	0.42
42	54	1.23	0.16	0.28	0.65
41	53	1.08	0.20	0.28	0.64
40	52	0.95	0.23	0.36	0.55
39	51	0.84	0.27	0.43	0.49
38	50	0.75	0.30	0.36	0.55
37	49	0.66	0.34	0.54	0.42
36	48	0.58	0.39	0.41	0.51
35	47	0.51	0.44	0.26	0.64
34	46	0.45	0.48	0.28	0.65
33	45	0.40	0.52	0.23	0.67
32	43-4	0.33	0.58	0.18	0.72
31	41-2	0.26	0.64	0.13	0.80
30	39-40	0.20	0.70	0.08	0.88
29	37-8	0.16	0.75	0.06	0.90
28	35-6	0.12	0.81	0.04	0.92
27	33-4	0.09	0.84	0.04	0.92
26	31-2	0.07	0.87	0.04	0.92
25	29-30	0.06	0.89	0.04	0.92
24	27-8	0.04	0.92	0	1.
23	25-6	0.04	0.93	0	1.
22	23-4	0.03	0.95		
21	21-2	0.03	0.96		
20	20	0.02	0.97		
P_3		0.391	0.574		
C_3		0.205	0.127		
P_2		0.945	0.989		
C_2		0.013	0.003		

DISTRIBUTION

No. of Copies

OFFSITE

1 AEC Chicago Patent Group
G. H. Lee

8 AEC Division of Reactor Development and Technology
Director, RDT
Asst. Dir., Project Management
Chief, Water Projects Branch (2)
Asst. Dir., Reactor Technology
Chief, Reactor Physics Branch (2)
Asst. Dir., Reactor Technology

3 AEC Division of Technical Information Extension

1 Argonne National Laboratory
R. Avery

1 Atomic Energy of Canada Limited
M. Duret

1 Babcock and Wilcox
H. M. Jones

1 Bhabha Atomic Research Centre
Theoretical Physics Section/RED
Central Complex Bldg.
Trombay, Bombay-85, India
S. R. Dwivedi

1 Brookhaven National Laboratory
J. Chernick

1 Mr. H. B. Brooks
310 Power Bldg.
Chattanooga, Tennessee 37401

2 Combustion Engineering
R. Harding
S. Visner

No. of Copies

1 Commonwealth Edison Company
72 West Adams Street
Chicago, Ill.

A. Veras

1 Consumers Power Company
1945 W. Parnall Road
Jackson, Mich. 49201

G. J. Walke

31 CNEN - Centro Studi-Nucleaire
Casaccia, Rome, Italy

Ugo Farinelli (1)
Paolo Loizzo (25)
Renato Martinelli (3)
Nicalo Pacilio (2)

1 EBASCO Services

D. deBloisblanc

2 Edison Electric Institute
750 Third Avenue
New York, N. Y. 10017

John J. Kearney
George Watkins

2 E. I. du Pont deNemours & Company., Inc., SRL

G. Dessauer
H. Honeck

1 ENEL
Via G. B. Martini
(Pizaaz Verdi)
Rome, Italy

Mr. Paoletti Gualandi

3 General Electric Co., San Jose

D. L. Fischer
R. L. Crowther
F. R. Channon

1 General Electric Co., Vallecitos Atomic Lab.

T. M. Snyder

No. of Copies	
1	Idaho Nuclear Corporation R. M. Brugger
1	Japan Atomic Energy Institute Tokaimura, Ibarakiken, Japan Shojiro Matsuura, JPDR-TCA
1	Jersey Nuclear Enterprises Seattle, Washington R. L. Dickeman
1	Kerr-McGee Oklahoma City, Oklahoma Frank Pittman
1	Nuclear Materials and Equipment Corp. K. Puechl
1	NUKEM D-645, HANAU POSTFACH 869 Germany Mr. Wolgang K. L. Jager
1	Pakistan Institute of Nuclear Sci. & Tech. P. O. Nilore Rawalpindi, Pakistan M. A. Mannan
1	Philadelphia Electric Company 1000 Chestnut Street Philadelphia 5, PA. Mr. Wayne C. Astley
1	Power Reactor & Nuclear Fuel Development Corp. 9-13, 1- chome, Akasaka, Minato-ku, Tokyo, Japan Setsuo Kobayashi
1	S. C. K. - C. E. N. NOL-DONK Belguim Dr. H. Vanden Broeck BRL.

No. of Copies	
1	Tennessee Valley Authority 310 Power Building Chattanooga, Tennessee 37401 R. H. Davidson
1	United Nuclear Corporation J. R. Tomonto
3	Westinghouse Electric Corporation W. D. Leggett W. L. Orr J. B. Roll
1	AEC Chicago Patent Group R. K. Sharp (Richland)
4	RDT Assistant Director for Pacific Northwest Programs W. E. Fry P. G. Holsted (2) J. B. Kitchen
2	AEC Richland Operations Office H. A. House C. L. Robinson
3	Battelle Memorial Institute
2	Douglas United Nuclear C. D. Harrington G. C. Fullmer
5	WADCO Corp. WADCO Document Control
70	Battelle-Northwest F. W. Albaugh C. L. Bennett G. J. Busselman N. E. Carter D. E. Christensen F. G. Dawson E. C. Davis D. R. de Halas D. E. Deonigi J. B. Edgar (10)

No. of
Copies

Battelle-Northwest (Contd)

J. C. Fox
M. D. Freshley
G. L. Gelhaus
U. P. Jenquin
D. A. Kottwitz
J. W. Kutcher
J. H. Lauby
B. R. Leonard
R. C. Liikala
C. W. Lindenmeier
R. P. Matsen
D. F. Newman
D. R. Oden
W. D. Richmond
L. C. Schmid
R. I. Smith
W. P. Stinson
D. H. Thomsen
V. O. Uotinen
A. D. Vaughn
L. D. Williams (20)
W. C. Wolkenhauer
M. G. Zimmerman
BNW Legal (2)
Technical Information (5)
Technical Publications (2)